NORTH WEST SHELF
JOINT ENVIRONMENTAL
MANAGEMENT STUDY

Modelling circulation and connectivity on Australia's North West Shelf

NWSJEMS

TECHNICAL REPORT No. 6

• S. Condie • J. Andrewartha
• J. Mansbridge • J. Waring

June 2006

CSIRO

Government of Western Australia
Department of Environment

National Library of Australia Cataloguing-in-Publication data:

Modelling circulation and connectivity to Australia's North West Shelf.

Bibliography.
Includes index.
ISBN 1 921061 50 2 (pbk.).

1. Ocean circulation - Western Australia - North West Shelf. I. Condie, S. (Scott), 1963- . II. CSIRO. Marine and Atmospheric Research. North West Shelf Joint Environmental Management Study. III. Western Australia. (Series : Technical report (CSIRO. Marine and Atmospheric Research. North West Shelf Joint Environmental Management Study) ; no. 6).

551.462099413

Modelling circulation and connectivity on Australia's North West Shelf.

Bibliography.
Includes index.
ISBN 1 921061 51 0 (CD-ROM).

1. Ocean circulation - Western Australia - North West Shelf. I. Condie, S. (Scott), 1963- . II. CSIRO. Marine and Atmospheric Research. North West Shelf Joint Environmental Management Study. III. Western Australia. (Series : Technical report (CSIRO. Marine and Atmospheric Research. North West Shelf Joint Environmental Management Study) ; no. 6).

551.462099413

Modelling circulation and connectivity on Australia's North West Shelf.

Bibliography.
Includes index.
ISBN 1 921061 52 9 (pdf).

1. Ocean circulation - Western Australia - North West Shelf. I. Condie, S. (Scott), 1963- . II. CSIRO. Marine and Atmospheric Research. North West Shelf Joint Environmental Management Study. III. Western Australia. (Series : Technical report (CSIRO. Marine and Atmospheric Research. North West Shelf Joint Environmental Management Study) ; no. 6).

551.462099413

NORTH WEST SHELF JOINT ENVIRONMENTAL MANAGEMENT STUDY

Final report

North West Shelf Joint Environmental Management Study Final Report.

List of technical reports

NWSJEMS Technical Report No. 1
Review of research and data relevant to marine environmental management of Australia's North West Shelf.
A. Heyward, A. Revill and C. Sherwood

NWSJEMS Technical Report No. 2
Bibliography of research and data relevant to marine environmental management of Australia's North West Shelf.
P. Jernakoff, L. Scott, A. Heyward, A. Revill and C. Sherwood

NWSJEMS Technical Report No. 3
Summary of international conventions, Commonwealth and State legislation and other instruments affecting marine resource allocation, use, conservation and environmental protection on the North West Shelf of Australia.
D. Gordon

NWSJEMS Technical Report No. 4
Information access and inquiry.
P. Brodie and M. Fuller

NWSJEMS Technical Report No. 5
Data warehouse and metadata holdings relevant to Australia's North West Shelf.
P. Brodie, M. Fuller, T. Rees and L. Wilkes

NWSJEMS Technical Report No. 6
Modelling circulation and connectivity on Australia's North West Shelf.
S. Condie, J. Andrewartha, J. Mansbridge and J. Waring

NWSJEMS Technical Report No. 7
Modelling suspended sediment transport on Australia's North West Shelf.
N. Margvelashvili, J. Andrewartha, S. Condie, M. Herzfeld, J. Parslow, P. Sakov and J. Waring

NWSJEMS Technical Report No. 8
Biogeochemical modelling on Australia's North West Shelf.
M. Herzfeld, J. Parslow, P. Sakov and J. Andrewartha

NWSJEMS Technical Report No. 9
Trophic webs and modelling of Australia's North West Shelf.
C. Bulman

NWSJEMS Technical Report No. 10
The spatial distribution of commercial fishery production on Australia's North West Shelf.
F. Althaus, K. Woolley, X. He, P. Stephenson and R. Little

NWSJEMS Technical Report No. 11
Benthic habitat dynamics and models on Australia's North West Shelf.
E. Fulton, B. Hatfield, F. Althaus and K. Sainsbury

NWSJEMS Technical Report No. 12
Ecosystem characterisation of Australia's North West Shelf.
V. Lyne, M. Fuller, P. Last, A. Butler, M. Martin and R. Scott

NWSJEMS Technical Report No. 13
Contaminants on Australia's North West Shelf: sources, impacts, pathways and effects.
C. Fandry, A. Revill, K. Wenziker, K. McAlpine, S. Apte, R. Masini and K. Hillman

NWSJEMS Technical Report No. 14
Management strategy evaluation results and discussion for Australia's North West Shelf.
R. Little, E. Fulton, R. Gray, D. Hayes, V. Lyne, R. Scott, K. Sainsbury and D. McDonald

NWSJEMS Technical Report No. 15
Management strategy evaluation specification for Australia's North West Shelf.
E. Fulton, K. Sainsbury, D. Hayes, V. Lyne, R. Little, M. Fuller, S. Condie, R. Gray, R. Scott, H. Webb, B. Hatfield, M. Martin, and D. McDonald

NWSJEMS Technical Report No. 16
Ecosystem model specification within an agent based framework.
R. Gray, E. Fulton, R. Little and R. Scott

NWSJEMS Technical Report No. 17
Management strategy evaluations for multiple use management of Australia's North West Shelf – Visualisation software and user guide.
B. Hatfield, L. Thomas and R. Scott

NWSJEMS Technical Report No. 18
Background quality for coastal marine waters of the North West Shelf, Western Australia.
K. Wenziker, K. McAlpine, S. Apte, R.Masini

CONTENTS

ACRONYMS

ACOM	Australian Community Ocean Model
AFMA	Australian Fisheries Management Authority
AFZ	Australian Fishing Zone
AGSO	Australian Geological Survey Organisation now Geoscience Australia
AHC	Australian Heritage Commission
AIMS	Australian Institute of Marine Science
AMSA	Australian Maritime Safety Authority
ANCA	Australian Nature Conservation Agency
ANZECC	Australian and New Zealand Environment and Conservation Council
ANZLIC	Australian and New Zealand Land Information Council
APPEA	Australian Petroleum, Production and Exploration Association
AQIA	Australian Quarantine Inspection Service
ARMCANZ	Agricultural Resources Management council of Australia and New Zealand
ASIC	Australian Seafood Industry Council
ASDD	Australian Spatial Data Directory
CAAB	Codes for Australian Aquatic Biota
CAES	Catch and Effort Statistics
CALM	Department of Conservation and Land Management (WA Government)
CAMBA	China Australia Migratory Birds Agreement
CDF	Common data format
CITIES	Convention on International Trade in Endangered Species
CTD	conductivity-temperature-depth
CMAR	CSIRO Marine and Atmospheric Research
CMR	CSIRO Marine Research
COAG	Council of Australian Governments
ConnIe	Connectivity Interface
CPUE	Catch per unit effort
CSIRO	Commonwealth Science and Industrial Research Organisation
DCA	detrended correspondence analysis
DIC	Dissolved inorganic carbon
DISR	Department of Industry, Science and Resources (Commonwealth)
DEP	Department of Environmental Protection (WA Government)
DOM	Dissolved organic matter
DPIE	Department of Primary Industries and Energy
DRD	Department of Resources Development (WA Government)
EA	Environment Australia
EEZ	Exclusive Economic Zone
EIA	Environmental Impact Assessment
EPA	Environmental Protection Agency
EPP	Environmental Protection Policy
ENSO	El Nino Southern Oscillation
EQC	Environmental Quality Criteria (Western Australia)
EQO	Environmental Quality Objective (Western Australia)
ESD	Ecologically Sustainable Development
FRDC	Fisheries Research and Development Corporation
FRMA	Fish Resources Management Act
GA	Geoscience Australia formerly AGSO
GESAMP	Joint Group of Experts on Scientific Aspects of Environmental Protection
GIS	Geographic Information System
ICESD	Intergovernmental Committee on Ecologically Sustainable Development
ICS	International Chamber of Shipping
IOC	International Oceanographic Commission
IGAE	Intergovernmental Agreement on the Environment
ICOMOS	International Council for Monuments and Sites

IMO	International Maritime Organisation
IPCC	Intergovernmental Panel on Climate Change
IUNC	International Union for Conservation of Nature and Natural Resources
IWC	International Whaling Commission
JAMBA	Japan Australian Migratory Birds Agreement
LNG	Liquified natural gas
MarLIN	Marine Laboratories Information Network
MARPOL	International Convention for the Prevention of Pollution from Ships
MECO	Model of Estuaries and Coastal Oceans
MOU	Memorandum of Understanding
MPAs	Marine Protected Areas
MEMS	Marine Environmental Management Study
MSE	Management Strategy Evaluation
NCEP - NCAR	National Centre for Environmental Prediction – National Centre for Atmospheric Research
NEPC	National Environmental Protection Council
NEPM	National Environment Protection Measures
NGOs	Non government organisations
NRSMPA	National Representative System of Marine Protected Areas
NWQMS	National Water Quality Management Strategy
NWS	North West Shelf
NWSJEMS	North West Shelf Joint Environmental Management Study
NWSMEMS	North West Shelf Marine Environmental Management Study
ICIMF	Oil Company International Marine Forum
OCS	Offshore Constitutional Settlement
PFW	Produced formation water
P(SL)A	Petroleum (Submerged Lands) Act
PSU	Practical salinity units
SeaWIFS	Sea-viewing Wide Field-of-view Sensor
SOI	Southern Oscillation Index
SMCWS	Southern Metropolitan Coastal Waters Study (Western Australia)
TBT	Tributyl Tin
UNCED	United Nations Conference on Environment and Development
UNCLOS	United Nations Convention of the Law of the Sea
UNEP	United Nations Environment Program
UNESCO	United Nations Environment, Social and Cultural Organisation
UNFCCC	United Nations Framework Convention on Climate Change
WADEP	Western Australian Department of Environmental Protection
WADME	Western Australian Department of Minerals and Energy
WAEPA	Western Australian Environmental Protection Authority
WALIS	Western Australian Land Information System
WAPC	Western Australian Planning Commission
WHC	World Heritage Commission
WOD	World Ocean Database
www	world wide web

TECHNICAL SUMMARY

Ocean circulation on the North West Shelf (NWS) influences nearly all aspects of the ecosystem, including sediment transport and turbidity patterns, primary production in the water column and bottom sediments, and recruitment patterns for organisms with pelagic phases in their life cycles. Current patterns are also of direct interest to most industries operating on the NWS, particularly those associated with fisheries, shipping, and offshore structures and operations.

This study is the first attempt to describe the water circulation and transport patterns across the region on time scales from hours to years, and space scales from 10 km over the entire shelf to one kilometre in a selected focus area around the Dampier Archipelago. It has also provided a framework for embedded models describing processes such as sediment transport, nutrient cycling, and primary and secondary production (described in accompanying reports).

A series of nested circulation models have been developed with forcing by realistic winds, tides, and large-scale regional circulation. The simulations cover a period of more than six years, allowing the tidal, seasonal, and interannual characteristics to be investigated, as well as the response to episodic events such as tropical cyclones. Connectivity patterns throughout the shelf have also been characterised by forcing a particle transport model by the modelled circulation.

Model results demonstrate that the instantaneous current patterns are strongly dominated by the barotropic tide and its spring neap cycle. However, longer-term transports over the inner and mid shelf were mainly controlled by wind-driven flow, which followed the seasonal switch from summer monsoon winds to southeasterly trades in winter. Over the outer shelf and slope the large-scale regional circulation, provided by the global model, had a major influence.

Results were shown to be relatively insensitive to adjustable model parameters and sub-model structures. However, model performance was strongly dependent on the quality of the forcing fields. For example, the prediction of low frequency inner shelf currents was improved substantially when the relatively coarse resolution global winds where replaced by locally observed winds in the Dampier model. Lower skill in predicting low frequency currents on the outer shelf can be largely attributed to errors in the global circulation model.

Results from the connectivity modelling have been summarised in statistical form and can be accessed through a web-based user-interface developed as part of the project and referred to as the Connectivity Interface or *ConnIe* (http://www.per.marine.csiro.au/connie). This tool is expected to find applications in areas such as larval dispersion and recruitment studies, and the development of scenarios and risk assessments for contaminant dispersion.

1. INTRODUCTION

The North West Shelf Joint Environmental Management Study (NWSJEMS) was aimed at developing the science-based methods required to support integrated regional planning and management of the NWS marine environment and resources. A major component of the study was ecological modelling, which included characterisation of the circulation and connectivity patterns on the NWS. This report describes the spatial and temporal characteristics of the NWS circulation and connectivity based on results from hydrodynamic models of the region applied at a range of scales.

Circulation on the NWS strongly influences nearly all aspects of the ecosystem, particularly turbidity and sediment transport patterns, primary and secondary production in the water column and sediments, and recruitment patterns for species with pelagic phases in their life cycles. Current patterns are also of direct interest to most industries operating on the NWS, particularly those associated with shipping, offshore structures and offshore operations, and fisheries. They control the dispersion of contaminants, influence the trajectories of surface vessels, and impact fixed structures through both direct mechanical stresses and scouring at the seabed. The influence of the circulation on sediments and other biogeochemical components is described in accompanying reports, while the focus here is on the currents and connectivity patterns themselves.

The objectives of this component of the study were first to describe the oceanic circulation in the region on time scales from hours to years, and space scales from 10 km over the entire shelf to one kilometre in a selected focus area around the Dampier Archipelago. Second, to provide a transport framework for embedded models dealing with sediment movements, nutrient cycling, and production (described in accompanying reports). Third, to provide a comprehensive description of connectivity patterns across the region on the basis of the predicted circulation patterns.

Chapter 2 provides a brief review of previous studies related to circulation on the NWS. In Chapter 3, the hydrodynamic model will be described, including its assumptions, inputs and outputs. Chapter 4 will focus on sensitivity of the circulation to model parameters and validation against available field data. Chapter 5 will provide examples of current fields and summarise the results in the form of seasonal and interannual statistics. Chapter 6 will describe particle trajectories estimated from the modelled currents and the associated connectivity patterns, which have been captured within a web-based interrogation tool. Conclusions of the study are presented in Chapter 7.

2. BACKGROUND

The NWS is a tropical arid region with maximum daily summertime temperatures around 36°C and minimum daily wintertime temperatures around 13°C. The mean annual rainfall is typically only 300 mm, most of which falls over summer and autumn (Lough, 1998). However, extreme downpours can occur under tropical cyclone conditions, which usually impact the study area a few times per year. Terrestrial runoff into the marine environment similarly shows strong peaks during cyclones, but is generally very low. During summer, prevailing winds are from the northwest and southwest, swinging around to dry southeasterlies over winter. However, in coastal areas local sea breezes (generated by the temperature difference between land and sea) often dominate the daily patterns. Under extreme cyclone conditions winds can reach 180 km/hr, with 17 m ocean waves and ocean currents exceeding 3 m s^{-1}.

Circulation on the NWS is influenced by the broader scale circulation of the Indonesian Throughflow to the north (Cresswell et al. 1993; Meyers et al. 1995) and Leeuwin Current to the west (Godfrey & Ridgway, 1985; Batteen et al. 1992). These flows carry warm low salinity water southwestward along the outer NWS from February to June (Holloway & Nye, 1985; Holloway, 1995). However, strong winds from the southwest cause intermittent reversals of these currents over the remainder of the year, with occasional weak upwelling of cold deep water onto the shelf. The region is also impacted by El Nino Southern Oscillation (ENSO) cycles, with weakened Indonesian Throughflow (Meyers, 1996) and a lower incidence of tropical cyclones under El Nino conditions.

Daily current patterns on the NWS tend to be strongly dominated by tidal motions, with semidiurnal flows up to 1 m s^{-1} and tidal ranges up to 6 m on the Pilbara coast and 10 m on the Kimberly coast (Holloway, 1983). Wind forced currents only become dominant around the neap tide, when the cross shelf momentum balance is geostrophic and the dominant sub-inertial motions are continental shelf waves (Webster, 1985; Holloway & Nye, 1985). The tidal currents are predominantly in the cross shelf direction, except around Barrow Island and the Monte Bello Islands where they are orientated closer to the east-west direction.

The combination of large tides and strong stratification also generates large internal tides over the upper slope (Craig, 1988). A shock forms on the leading face of the internal tide and propagates onshore as it dissipates over the outer shelf (Holloway, 1984, 1987; Holloway et al. 1997). This dissipation is also expected to greatly enhance vertical mixing rates. The amplitude of the internal waves can be as large as 100 m near the shelf break and the associated currents comparable to the barotropic tide, with evidence of significant bottom intensification (Holloway, 1985; Holloway et al. 2001).

A number of models of the barotropic and internal tides have been developed previously for the NWS, ranging from solutions of a simplified wave equation (Holloway et al. 1997) to cross shelf two-dimensional solutions (Holloway, 1996) and full three-dimensional solutions of the primitive equations (Holloway, 2001). The approach adopted in the last of these studies is most similar to that used in NWSJEMS. It utilised a numerical grid with a horizontal resolution of 4 km, designed to resolve the internal tide wavelength ranging from around 70 km in water 500 m deep to 7 km in water 50 m deep (Holloway, 2001). However, it was acknowledged that smaller length-

scales associated with bathymetry and nonlinear effects may be important. Model forcing was restricted to a single tidal constituent for each run (M_2 and S_2). The relatively high resolution also limited model runs to four days. This was sufficient for internal waves to develop and propagate across the domain, revealing that nearly all the energy is dissipated over the upper slope and outer shelf.

During the summer period tropical cyclones can generate major short-term fluctuations in current patterns and coastal sea levels and are likely to have significant impacts on sediment distributions and other aspects of the benthic habitat. The circulation response on the NWS has been investigated using both depth-integrated models (Fandry & Steedman, 1994; Phillips & Luettich, 2000) and three-dimensional models (Hearn & Holloway, 1990) forced by cyclones with realistic tracks and idealised wind and pressure fields (Holland, 1980). Fandry and Steedman (1994) also derived simple empirical formulae for upper bounds on the maximum current (alongshore) and maximum surge height.

3. CIRCULATION MODEL DESCRIPTION

The model used to compute the circulation on the NWS was developed within CSIRO Marine Research and is referred to as MECO (Model for Estuaries and Coastal Oceans). It is a general purpose finite difference hydrodynamic model applicable to scales ranging from estuaries to ocean basins. It has found previous applications in systems such as the Derwent and Huon Estuaries in Tasmania, Gippsland Lakes, Port Phillip Bay (Walker, 1999), Bass Strait, the Great Australian Bight and south-eastern Australia (Bruce et al. 2001), and the Gulf of Carpentaria (Condie et al. 1999).

Inputs required by the model included forcing due to wind, atmospheric pressure gradients, and open boundary conditions such as temperature, salinity, and sea level. Wind-wave forcing could also be specified in terms of its enhancement of bottom friction in shallow water (Grant & Madsen, 1979). Surface heat and freshwater water fluxes can also be applied if reliable estimates are available, although this was not the case on the NWS. Outputs from MECO included three-dimensional distributions of velocity, temperature, salinity, density, passive tracers, mixing coefficients and sea level.

A comprehensive description of the theory underlying the model is provided in the MECO Scientific Manual (Herzfeld et al. 2002), and therefore only a very brief technical description will be provided here. MECO is based on the three dimensional equations of momentum, continuity and conservation of heat and salt, employing the hydrostatic and Boussinesq assumptions. The equations of motion were discretised on a finite difference stencil corresponding to the Arakawa C grid. The model used a curvilinear orthogonal grid in the horizontal and fixed ‘z’ coordinates in the vertical. It allowed for wetting and drying of surface cells, and so was capable of handling sea level changes associated with large tidal ranges.

The model had a free surface and used mode splitting to separate the two-dimensional mode from the three-dimensional mode. This allowed fast moving gravity waves to be solved on a short time-step and slower moving internal waves on a longer time-step, thereby greatly enhancing the computational efficiency. Explicit time-stepping was used throughout except for the vertical diffusion scheme which was implicit so as to guarantee unconditional stability in regions of high vertical resolution.

A Laplacian diffusion scheme was employed in the horizontal on geopotential surfaces, while the Mellor-Yamada level 2.0 scheme was most commonly used to parameterise vertical diffusion. Bottom friction was represented by a quadratic law with a bottom roughness of 0.002 m and a minimum drag coefficient of 0.003. A second-order centred scheme was usually adopted for advection of momentum and the Van Leer (1979) higher-order upwind scheme for advection of tracers, such as temperature and salinity.

3.1 Model implementations for the NWS

After testing a variety of grids, the model was finally implemented on three nested grids, designed to capture the dynamics over a range of spatial scales (figure 3.1.1). Each of these was a rotated latitude-longitude grid and could be described as follows:

1. A large regional model with horizontal resolution of approximately 10 km, extending from Cape Cuvier (south of Coral Bay) to the Bonaparte Archipelago and well beyond the shelf break. This will be referred to as the *Northwest model*.
2. A smaller regional model with horizontal resolution of approximately 5 km, extending from Ningaloo to Port Hedland and beyond the shelf break. This will be referred to as the *Pilbara model*.
3. A localised coastal model with horizontal resolution of approximately 1 km, covering the waters around the Dampier Archipelago to depths of almost 50 m. This will be referred to as the *Dampier model*.

The vertical resolution for the Northwest model expanded from 3 m near the surface to a maximum of 200 m at its maximum depth of 1200 m. The Pilbara model used the same vertical structure down to its maximum depth of 300 m. Truncating the depths of these two models had little effect on the circulation, but significantly improved computational times. The Dampier model used finer vertical resolution, expanding from 1 m near the surface to 5 m at depths below 45 m. In each case, the bathymetry was prescribed by spatially averaging a 30 second (0.9 km) product provided by Geoscience Australia onto the model grid (figure 3.1.1).

The Northwest and Pilbara models were forced at the surface by wind fields from the NCEP-NCAR 40-year re-analysis data set (Kalnay et al. 1996, figure 3.1.2). These fields had a 12 hourly time-step and a spatial resolution of 1.8°, which were linearly interpolated onto the model time-step and model grid. The interpolated product generally showed good agreement with locally measured winds at sub-diurnal frequencies (figure 3.1.3 and table 3.1.1). However, smaller scale processes, such as the daily sea breeze and occasional tropical cyclones, are more poorly resolved. The Dampier model was therefore forced using observed winds from Legendre Island. The high correlation with the NCEP-NCAR product at sub-diurnal frequencies (figure 3.1.3 and table 3.1.1) helped ensure a smooth nesting from the Pilbara to the Dampier model, despite the change in wind fields. More realistic tropical cyclone winds based on the model of Holland (1980) were also imbedded in NCEP-NCAR winds for detailed study of cyclone impacts.

Surface wave forcing was included in the Pilbara model so as to improve estimates of bottom friction. Wave characteristics on the NWS were modelled using a simple empirical formulation (U.S. Army Coastal Engineering Research Center, 1984) as described by Condie and Andrewartha (2002). This model assumed a fully developed sea state and required only the wind speed, fetch, and water depth as inputs. The near-bottom wave orbital velocity, direction, and frequency calculated by the wave model were used by the bottom boundary layer module to calculate bottom shear stresses using the Grant and Madsen (1979) scheme (figure 3.1.4).

Temperature and salinity fields around the lateral boundaries of the Northwest model were interpolated from a global circulation model known as the Australian Community Ocean Model (ACOM; Schiller et al. 2000). In the absence of reliable surface fluxes, interior temperatures and salinities were modified by relaxing them towards ACOM values with a 10 day relaxation time scale. Sea levels on the boundaries were also taken from ACOM output, with the addition of tidal constituents derived from tide gauge observations around the Cape Cuvier and Bonaparte Archipelago areas in combination with global tidal model estimates along the offshore boundaries (Eanes & Bettadpur,

1995). Boundary conditions for the Pilbara model were provided by a similar nesting strategy, this time using temperature, salinity, and sea level outputs directly from the Northwest model. Boundary conditions for the Dampier model were similarly taken from the Pilbara model output.

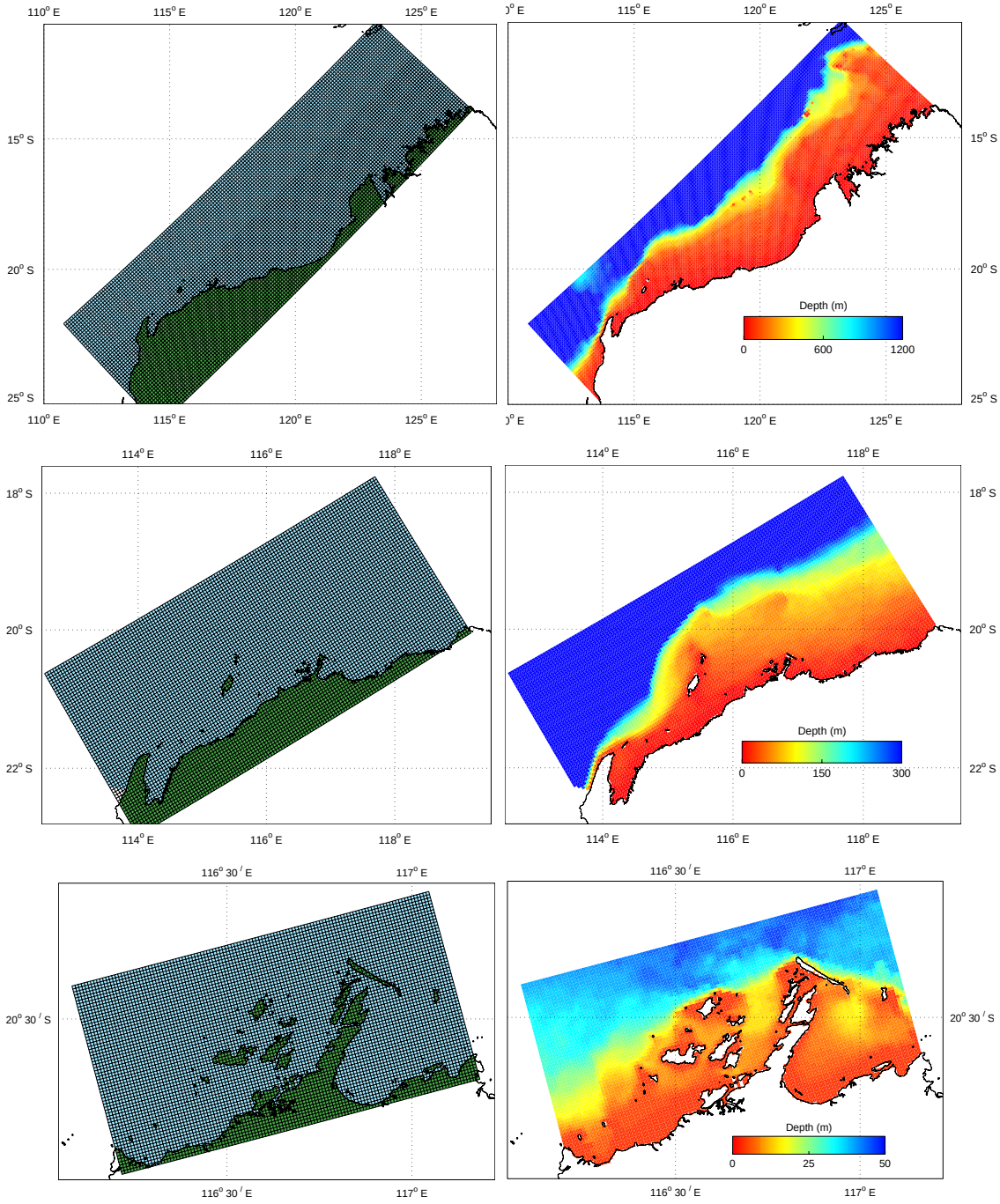

Figure 3.1.1: Model grids (left) and model bathymetry (right) for the Northwest model (top), the Pilbara model (centre), and the Dampier model (bottom). In each case, the model bathymetry was derived by averaging the Geoscience Australia product within each model grid cell.

All of the grids were rotated so as to provide the required spatial coverage and reasonable alignment with the bathymetry and coastline. Consequently, none of the grids were geographically aligned (figure 3.1.1). Outputs were therefore horizontally interpolated onto the boundary cells of the next sized grid. These outputs were saved at hourly increments, so as to provide adequate resolution of the barotropic tides. While higher frequency motions associated with internal tides were not retained by the nesting, these features tend to be dissipated before reaching inner shelf regions such as the Dampier Archipelago.

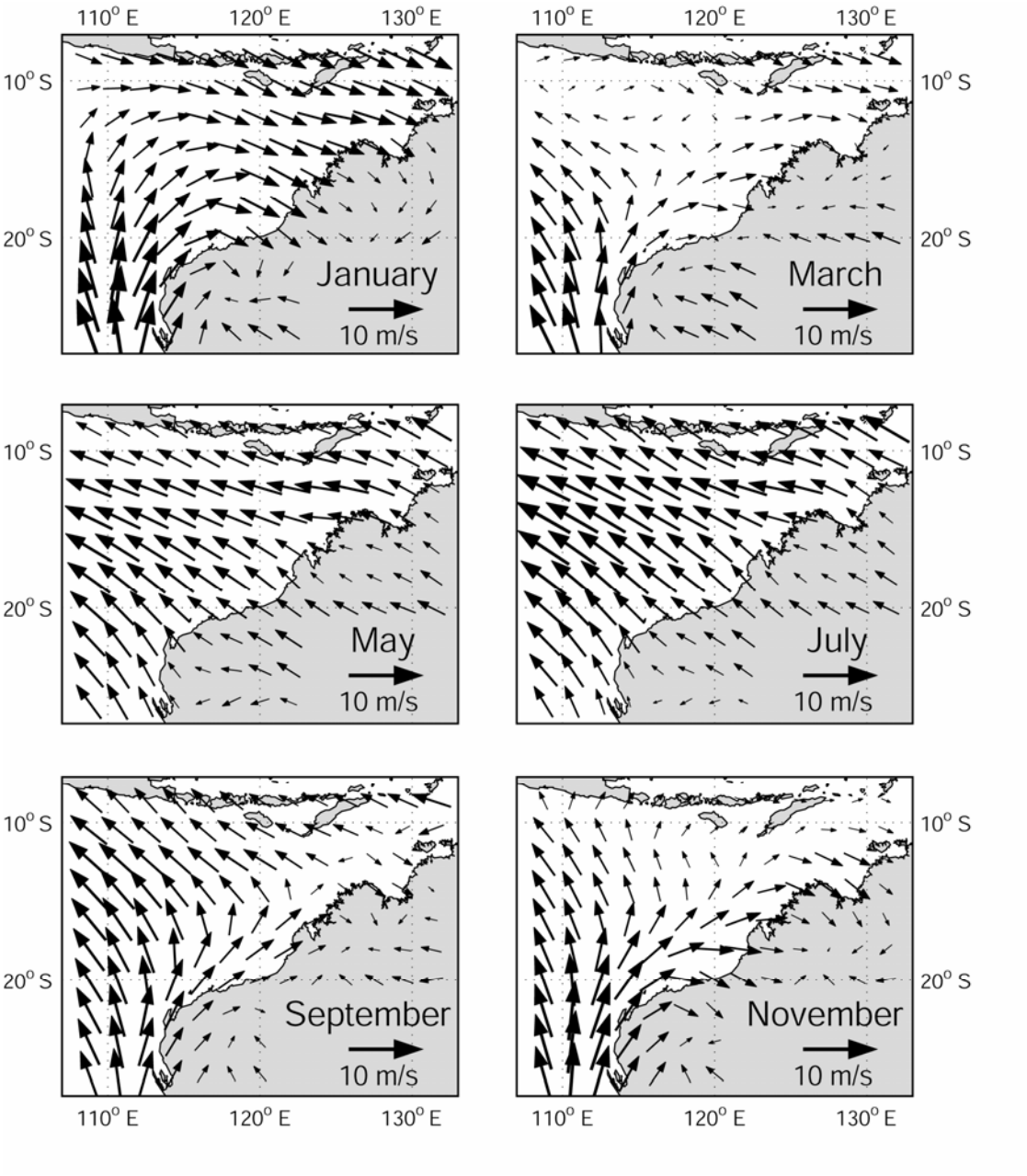

Figure 3.1.2: Seasonally averaged winds on the NWS at a height of 10 m above mean sea level during January, March, May, July, September, and November. These fields were calculated by vector averaging the 12 hourly outputs of the NCEP-NCAR re-analysis dataset across the years 1982 to 1999. They show the prevailing cycle of southeasterly trade winds over winter, switching to southwesterlies over summer as the trades are displaced to the south by equatorial westerlies.

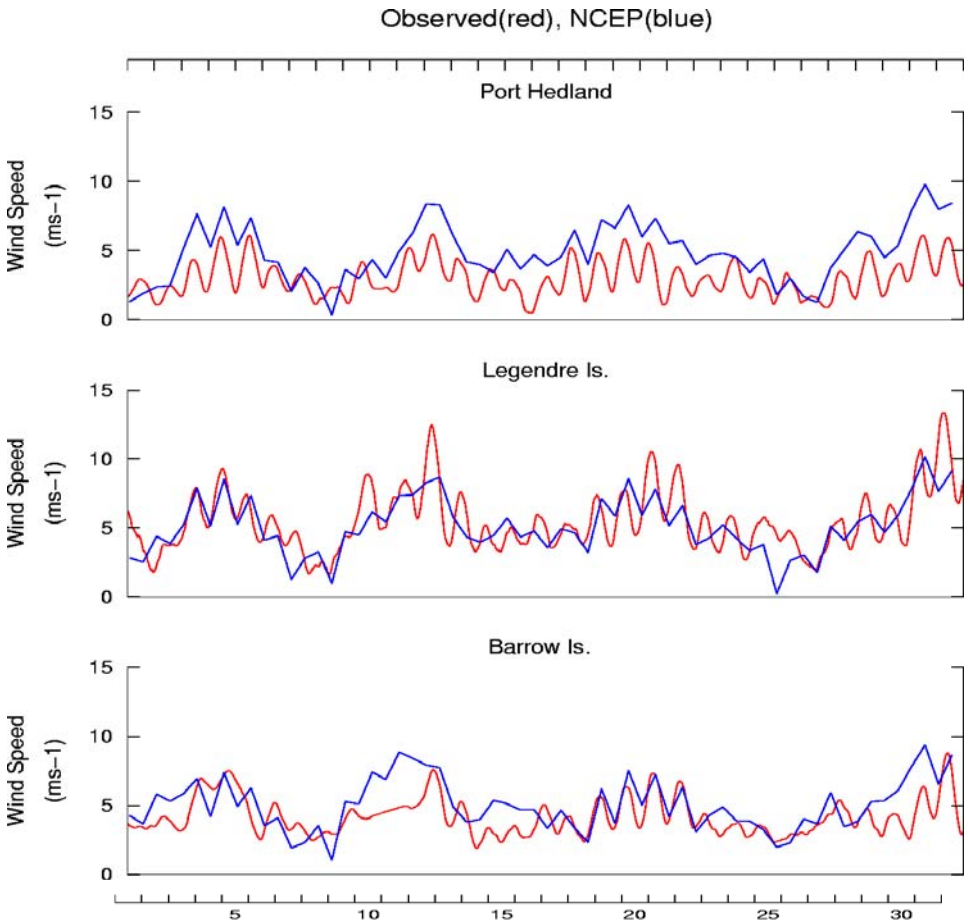

Figure 3.1.3: Time series comparisons between the interpolated NCEP-NCAR winds (blue lines) and locally observed winds (red lines) for June 1994. The NCEP-NCAR winds were used to force the Northwest and Pilbara models, while locally measured winds at Legendre Island were used to force the Dampier model.

Table 3.1.1: Comparison of wind speed statistics based on observations from meteorological stations and the NCEP-NCAR data set over the period 1991 to 1997. The statistics from the North Rankin platform are based only on the four month period of December 1984 to March 1985. Note the improved correlation at sub-diurnal frequencies, particularly at the coastal stations where the sea breeze has a major impact.

Location	Observed mean wind speed ($m\ s^{-1}$)	NCEP mean wind speed ($m\ s^{-1}$)	Correlation coefficient (12 hr av.)	Correlation coefficient (1d av.)	Correlation coefficient (3d av.)
Barrow Is.	5.14	5.02	0.52	0.61	0.64
Legendre Is.	6.27	4.81	0.69	0.77	0.82
Port Hedland	3.95	4.46	0.42	0.62	0.63
North Rankin	4.94	5.28	0.72	0.76	0.79

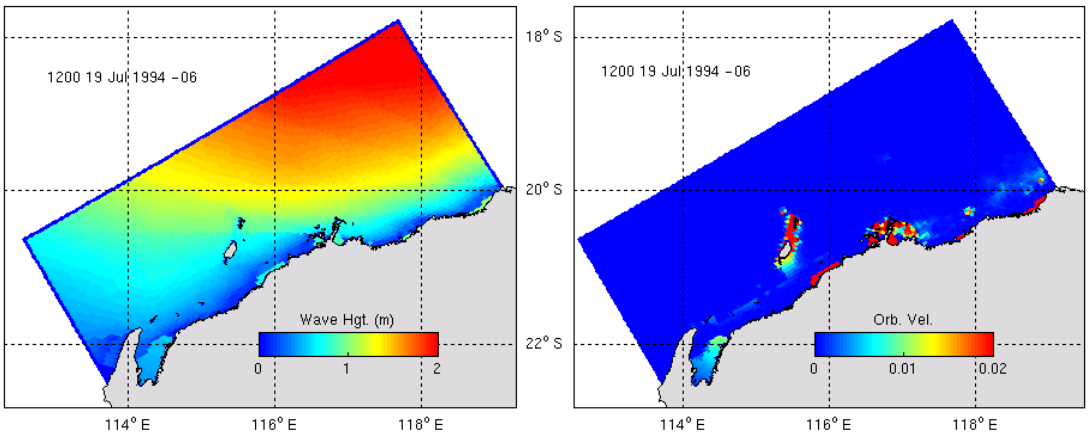

Figure 3.1.4: Example of significant wave-height (left) and bottom orbital velocity (right) for July 1994 from the simple wave model (Condie & Andrewartha, 2002).

3.2 Model runs and outputs

The Northwest model was used to simulate the circulation for a total of six years in the 1990s, while the Pilbara and Dampier models where run for two of these years (figure 3.2.1). All three models were also run over part of 1982, during which current meter data sets were available from both offshore and nearshore sites for model validation (section 4).

Since each of the models had the potential to generate unmanageably large quantities of output, fields were saved selectively so as to resolve the most significant processes at appropriate temporal and spatial scales. The final selection is summarised in Table 3.2.1. While the results will not be described in detail until section 5, sample outputs of sea level and surface currents are shown here from the global ACOM model and the three nested models (figure 3.2.2). As expected, fields generated at the three nested scales show consistent patterns, but each level of nesting reveals finer scale features in the current structure.

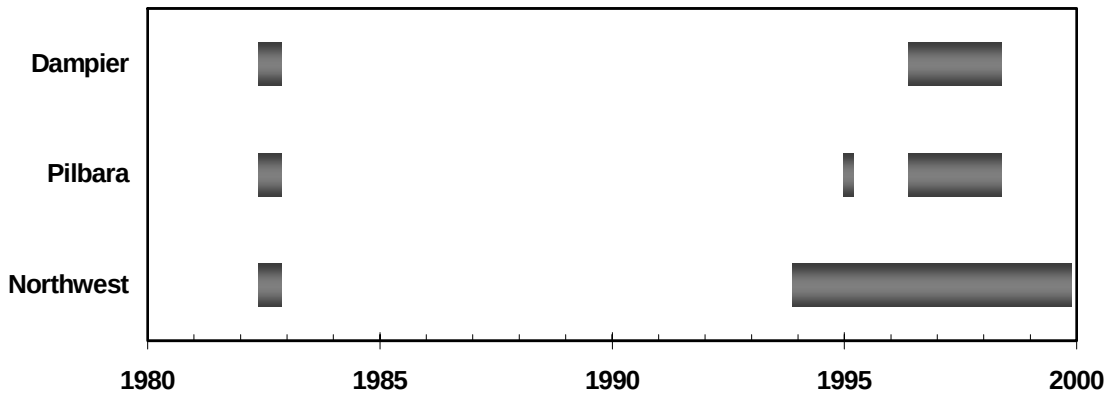

Figure 3.2.1: Duration of runs for each of the three models. The 1982 runs were for model validation, the short run of the Pilbara model in 1995 corresponded to Tropical Cyclone Bobby, and the long runs in the 1990s were production runs for investigating tidal, seasonal, and interannual variability.

Table 3.2.1: Gridded outputs saved from the three nested circulation models.

Quantity	Temporal Resolution	
	Hourly	10 daily
Sea level	X	
3-D temperature		X
Surface temperature	X	
3-D salinity		X
Surface salinity	X	
3-D currents		X
Surface currents	X	
Depth averaged currents	X	
Bottom stress	X	
3-D vertical viscosity		X
3-D vertical diffusivity		X

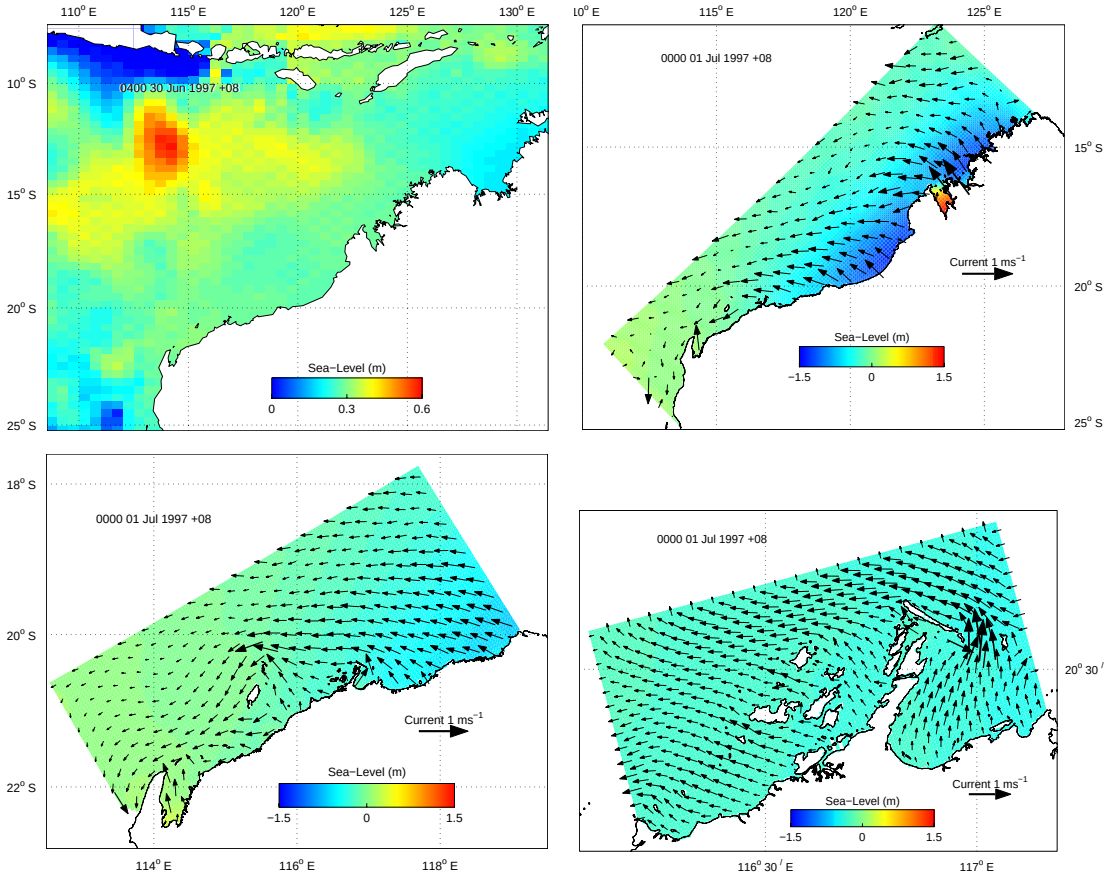

Figure 3.2.2: Sample outputs of sub-tidal sea level from ACOM and total sea level and current vectors (sub sampled) from the three nested models at a depth of 1.5 m on 1 July 1997.

4. MODEL SENSITIVITY AND VALIDATION

The models included a relatively large number of input parameters and an understanding of their influence on the model response provided one measure of uncertainty. However, there were additional uncertainties associated with both the model structure (e.g. parameterisations of sub-grid scale processes) and model forcing (e.g. winds and lateral boundary conditions), which could only be quantified through comparisons with field observations. The main observations used for this purpose were:

1. sea level measurements routinely collected at coastal stations using tide gauges,
2. temperature and salinity profiles collected during scientific voyages, and
3. current meter time series collected by moored instruments.

4.1 Sensitivity analysis

Model runs were conducted for the period May to August 1982 to test the model sensitivity to a range of parameters and sub-model structures. Sensitivity was quantified by comparing variations from the standard run with the variability within the standard run at an inner shelf site near the Dampier Archipelago and the outer shelf site of North Rankin (figure 4.1.1, table 4.1.1). Similar comparisons were made between available observations and the standard run as a benchmark for these statistics (last row in table 4.1.1).

Replacing the second-order centred momentum scheme with a first-order upwind scheme is known to increase numerical diffusion of temperature and salinity. However, because tidal mixing generally prevented the formation of sharp frontal features, the model was relatively insensitive to this change (table 4.1.1). The second-order scheme was stable for horizontal viscosities above 1000 $m^2 s^{-1}$, and showed sensitivity only in outer shelf salinity up to the standard run value of 2000 $m^2 s^{-1}$. The outer shelf currents were also affected when viscosities were increased to 5000 $m^2 s^{-1}$. Changes in horizontal diffusivity had little impact over the range 50 to 200 $m^2 s^{-1}$, with larger values likely to be less realistic.

The Mellor-Yamada level 2.0 (MY2) vertical mixing scheme (Mellor & Yamada, 1982) was used for the standard runs, where the only routinely adjusted parameter is the surface roughness length. Surface currents on the inner shelf were quite sensitive to this parameter when it fell below the standard run value of 2.0 m (table 4.1.1), although there was little effect at depths greater than a few metres. The sensitivity run was unstable using a roughness length of 0.2 m, with values as high as 1.0 m being unstable during other run periods. When the Mellor-Yamada scheme was replaced by the Csanady (1982) scheme, including modifications to account for stratification (Bowden & Hamilton, 1975), there were moderate changes to the currents on both the inner and outer shelf.

The vertical structure of the model grid influenced the model results in a number of ways (table 4.1.1). Not surprisingly, the minimum depth set for the water column changed the currents on the inner shelf. The maximum depth at which the model was truncated changed the currents on both the inner and outer shelf, with some influence on outer shelf salinities also evident. While increasing the maximum depth from 1200 to

2000 m had little effect, reducing it to 500 m had a significant impact on both sea level and current speed (figure 4.1.1). Reducing the number of vertical cells had only a small impact, while changing the minimum fractional height of the bottom cell had virtually no effect even on the bottom stress distributions (not shown).

Temperature and salinity in the interior of the model were modified by relaxation towards interpolated values from the global model as described in section 3.1. It was therefore not surprising that halving or doubling the relaxation time scale had an impact on these fields on both the inner and outer shelf (table 4.1.1). In particular, shorter relaxation times tended to smear gradients developing through advection of heat or salt (figure 4.1.1).

The overall conclusion of the analysis is that the model circulation was largely insensitive to the tunable model parameters and sub-model structures, provided parameter values were within a physically feasible range and did not violate model stability. Certainly differences between the model runs were less than the differences between the model runs and observations (table 4.1.1). There was no attempt to formally optimise the parameter values. However, in instances where some sensitivity was evident, the preferred parameter value was usually self-evident. For example, the Mellor-Yamada vertical mixing scheme adopted in the standard run is more sophisticated than the Csanady scheme and has undergone far more rigorous testing in other systems. It was also clear that truncating the model at 1200 m was more realistic that 500 m, and this was supported by comparisons with observed sea level (section 4.2). Conversely, improvements in extending the model to 2000 m were negligible, while the associated computational costs were substantial.

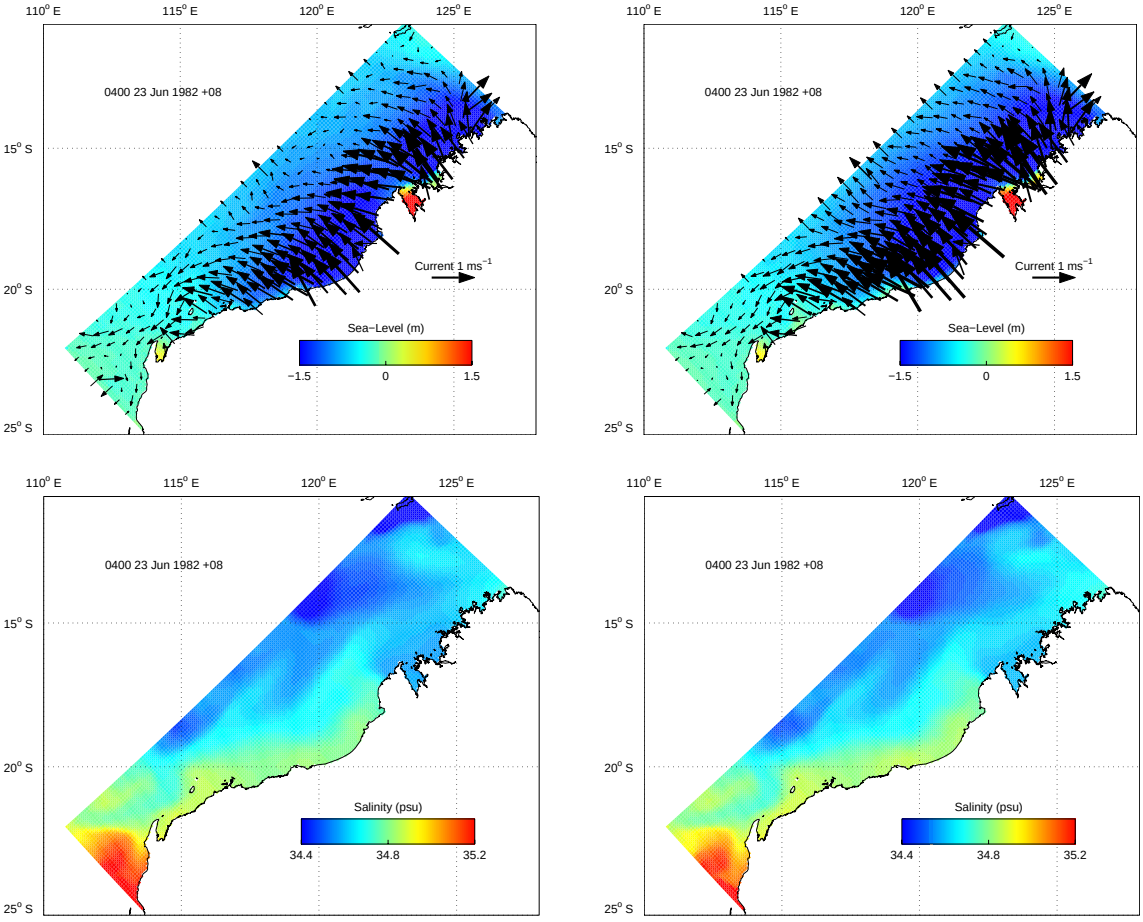

Figure 4.1.1: Outputs from the Northwest model showing current vectors overlain on sea level (upper) and salinity (lower) for the standard run (left) and runs in which the maximum model depth was reduced from 1 200 m to 500 m (upper right) and the relaxation time scale for salinity was increased from 10 to 20 days (lower right).

Table 4.1.1: Ratio of standard deviation from the standard run to standard deviation within the standard run for sea level, current speed, temperature, and salinity. The first value in each cell is for a coastal site near Dampier and the second value is for the North Rankin site (both for a depth of 1.5 m). Equivalent ratios comparing available observations (for a depth of 20 m at North Rankin) with the standard run over the same period are shown in the last row. Ratios greater than 0.1 are shown in bold.

Parameter/ sub-model	Unit	Standard run	Alternate values	Sea level	Current speed	Temperature	Salinity
Momentum scheme	-	2nd order centred	1st order upwind	0.004 0.014	0.019 0.037	0.000 0.003	0.003 0.050
Horizontal viscosity	m^2s^{-1}	2000 (1000 unstable)	1500	0.003 0.017	0.014 0.047	0.000 0.003	0.006 **0.l28**
			5000	0.018 0.010	0.071 **0.133**	0.001 0.013	0.015 **0.188**
Horizontal diffusivity	m^2s^{-1}	100	50	0.000 0.002	0.001 0.014	0.001 0.001	0.015 0.021
			200	0.000 0.002	0.001 0.013	0.002 0.001	0.031 0.034
Surface roughness length (MY2 scheme)	m	2.0 (0.2 unstable)	0.5	0.009 0.003	**0.327** **0.387**	0.001 0.056	0.019 0.003
			4.0	0.003 0.002	0.063 0.076	0.000 0.001	0.006 0.016
Vertical mixing scheme	-	MY2 scheme	Csanady scheme	0.014 0.029	**0.209** **0.186**	0.002 0.010	0.040 0.099
Minimum depth	m	9	20	0.095 0.013	**0.399** 0.084	0.002 0.001	0.045 0.016
Maximum depth	m	1200	500	**0.295** **0.162**	**0.617** **0.470**	0.003 0.010	0.041 **0.204**
			2000	0.035 0.025	**0.426** **0.130**	0.002 0.004	0.026 **0.100**
Vertical cells		52	26	0.012 0.021	0.070 0.097	0.001 0.096	0.010 0.005
Minimum fractional cell height	-	0.1	0.075	0.000 0.002	0.001 0.011	0.000 0.001	0.000 0.011
			0.2	0.000 0.003	0.001 0.011	0.000 0.001	0.000 0.010
Temperature and salinity assimilation time scale	days	10	5	0.003 0.010	0.002 0.048	**0.155** **0.152**	**0.213** **0.519**
			20	0.006 0.015	0.003 0.074	**0.231** **0.210**	**0.235** **0.843**
Wind waves	-	included	excluded	0.007 0.002	0.044 0.013	0.025 0.006	0.055 0.007
Relative to observations				**0.155** -	- **0.984**	- **1.008**	- -

4.2 Comparisons with observed sea level

Sea level measurements were available from coastal stations located at major ports and two offshore facilities on the NWS (figure 4.2.1). The tidal component clearly dominated the sea level signal and there was generally good agreement in the phase and amplitude at all the stations, with the model slightly overestimating amplitudes at Port Hedland and Barrow Island, and sometimes underestimating the amplitude of the flood tide at Exmouth (figure 4.2.2). Correlations improved and errors decreased substantially as the coastal sea level signal propagated to the southwest and the dependency on the northeast boundary condition diminished (table 4.2.1). Because the length scales associated with the tidal motions were much larger than any of the grid resolutions, all three models provided very similar estimates at Dampier (figure 4.2.3), where they explained around 96% of the observed variability ($r^2 = 0.96$) and rms errors were around 0.2 m (table 4.2.2).

The low frequency (sub-tidal) component of the sea level signal also exhibited only minor difference between the three models (figure 4.2.4, table 4.2.2). While there was a tendency for the model to underestimate sea levels during late summer and overestimate it during early autumn, the annual downward trend observed during 1997 was represented. The models also captured much of the variability associated with the continental shelf wave response to synoptic weather systems (period ~ 11 days; Webster, 1985), although at Broome amplitudes were overestimated and there were significant phase differences (figure 4.2.4). The discrepancies at Broome were again largely associated with errors in the ACOM sea level at the northeast boundary. Comparisons improved as the coastal sea level signal propagated to the southwest and wind forcing over the interior of the Northwest model exerted a greater influence (table 4.2.1).

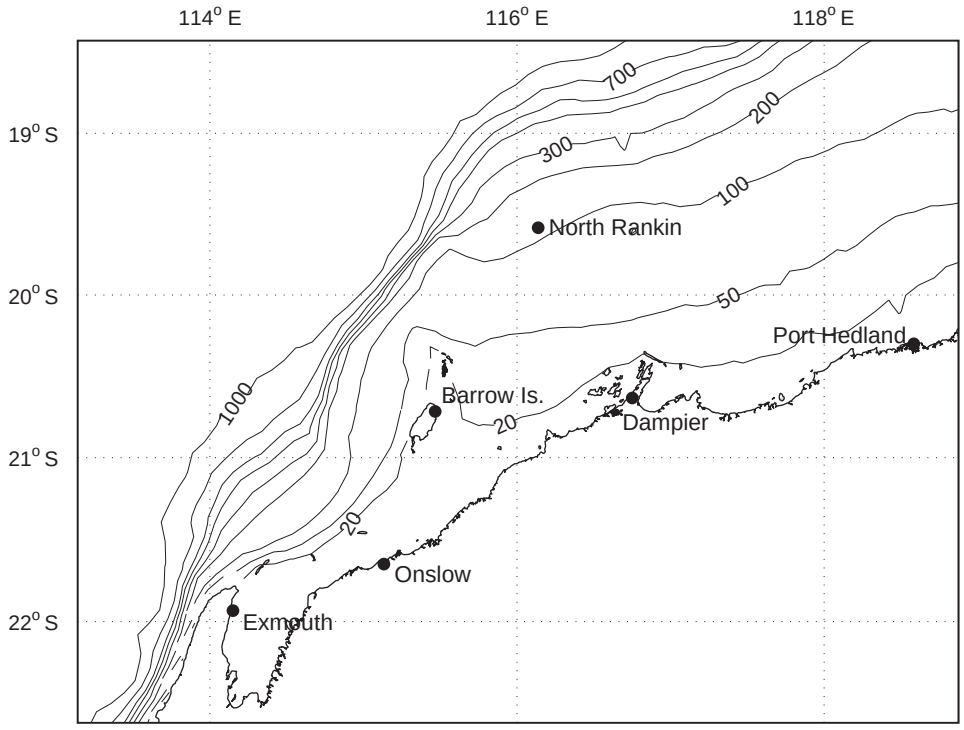

Figure 4.2.1: Location of tide gauges in the Pilbara region used to validate model sea level estimates.

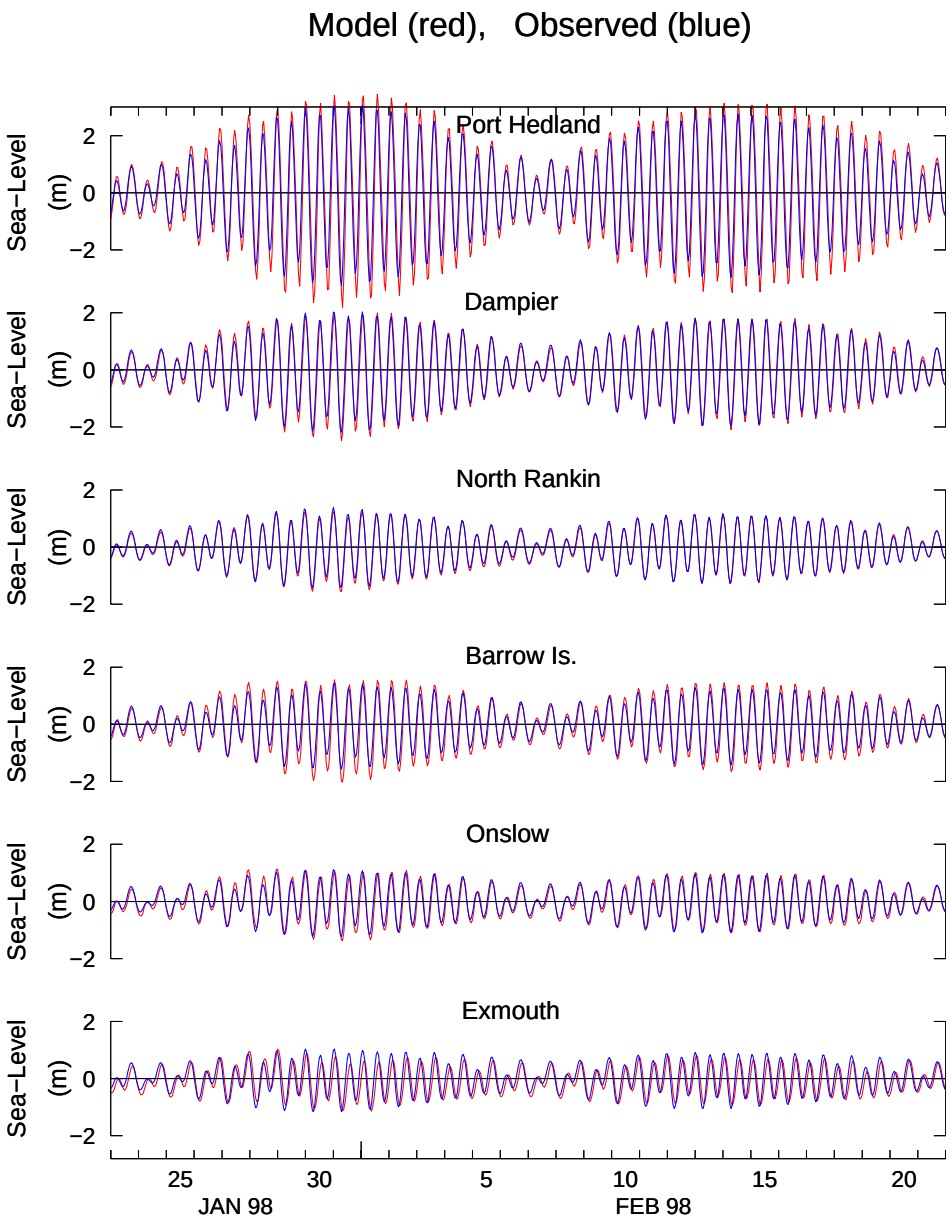

Figure 4.2.2: Comparison of observed sea level (blue lines) with corresponding time series from the Pilbara model (red lines) at six stations during January and February 1998.

Table 4.2.1: Statistical comparisons between the observed sea level and outputs from the Northwest model based on the data from the period July 1996 to December 1997.

		Broome	Port Hedland	Dampier	Onslow
Correlation coefficient r	Total signal	0.870	0.956	0.981	0.950
	Low freq.	0.234	0.793	0.804	0.772
rms error (m)	Total signal	1.20	0.50	0.19	0.18
	Low freq.	0.11	0.040	0.042	0.050

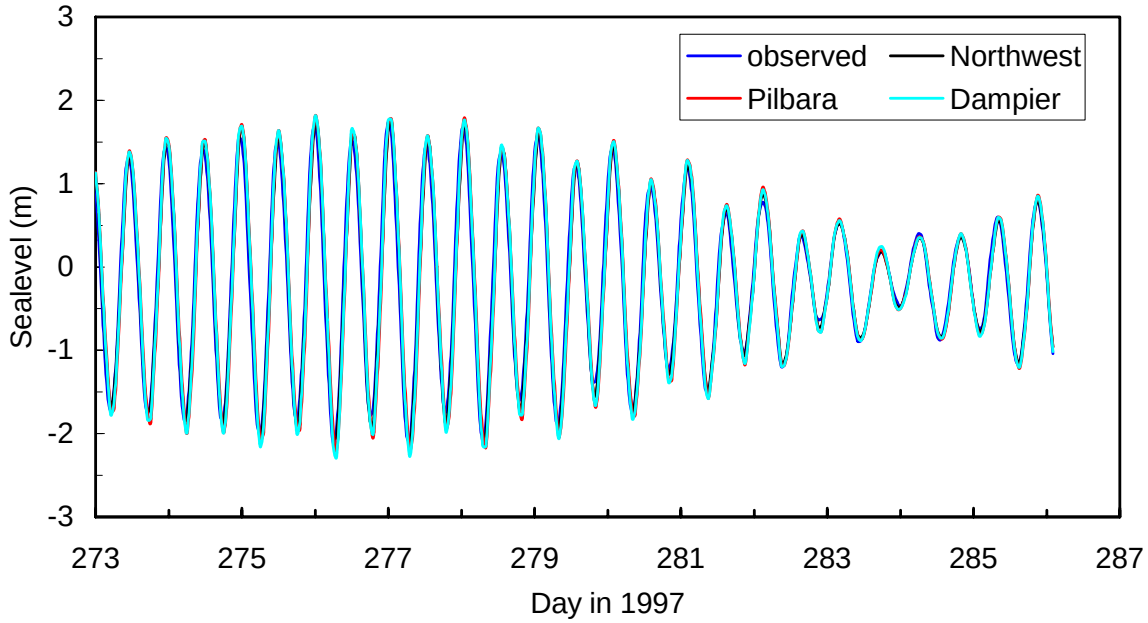

Figure 4.2.3: Comparison of observed sea level at Dampier during 1997 with corresponding time series from the Northwest, Pilbara, and Dampier models.

Table 4.2.2: Statistical comparisons between the observed sea level at Dampier and outputs from the Northwest, Pilbara, and Dampier models based on the data from the period July 1996 to December 1997.

		Northwest model	Pilbara model	Dampier model
Correlation coefficient r	Total signal	0.981	0.967	0.978
	Low frequency	0.804	0.800	0.803
rms error (m)	Total signal	0.19	0.27	0.22
	Low frequency	0.042	0.041	0.041

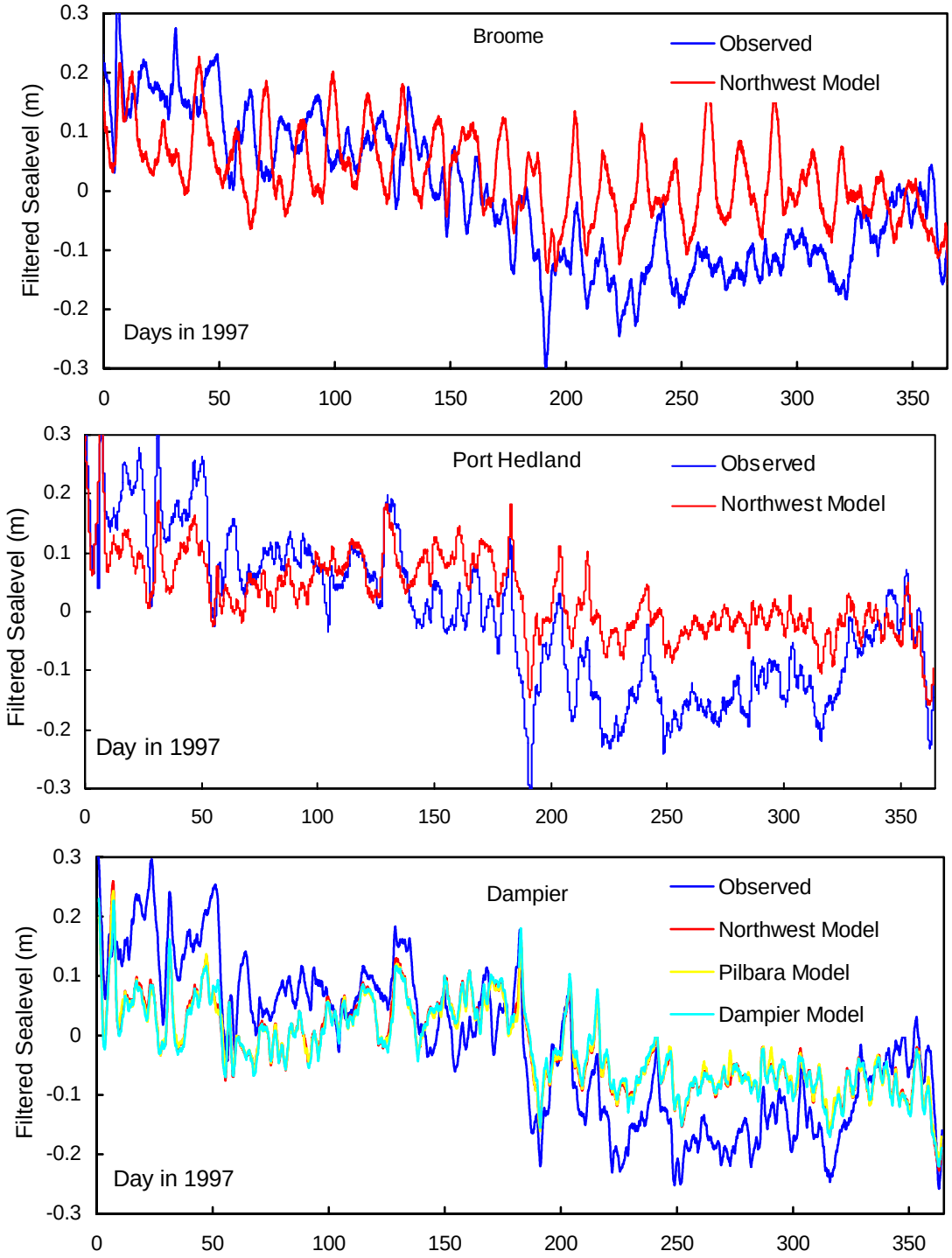

Figure 4.2.4: Comparison of observed low frequency sea level during 1997 with corresponding time series from the Northwest model at Broome (top), Port Hedland (centre), and Dampier (bottom). The Dampier case also includes outputs from the Pilbara and Dampier models.

4.3 Comparisons with observed temperature and salinity

Significant quantities of quality controlled hydrographic data were available from past research voyages on the NWS. These have been compared with outputs from the Northwest and Pilbara models. Since the Northwest model relied on the temperature

and salinity fields from the global ACOM model for both lateral boundary conditions and interior relaxation, the comparisons are as much a test of the ACOM outputs as of the nested models. Comparisons between the observations and models will begin with a relatively detailed analysis of the Pilbara model outputs during November 1996 (the only period in which the Pilbara runs overlap with available hydrographic data). They will then be extended across other seasons and years for the Northwest model.

Comparisons between individual profiles of observed and modelled temperature and salinity suggest that many of the significant features have been captured by the models, such as the vertical temperature gradients within the thermocline and the depth of the subsurface salinity maxima (figures 4.3.1 and 4.3.2). In most instances, the depth of the surface mixed layer was also adequately represented, although there were cases where it was overestimated by up to a factor of two (e.g. profile from 2/11/1996 12:05 in figure 4.3.1). There was also a tendency to underestimate vertical salinity gradients, suggesting that vertical diffusion rates in the model may have been excessive. These findings were consistent across the Pilbara and Northwest models.

More comprehensive comparisons of the temperature and salinity fields have been provided by plotting model outputs against observations at selected depths, as well as mean differences and rms errors as a function of depth (figure 4.3.3). These statistics reveal that while the model usually provided relatively accurate estimates of surface temperatures, high values tended to be underestimated. Below 50 m the model began to overestimate temperatures and this trend increased to shelf break depths of around 200 m, where the rms error peaked at 3.7°C. Errors then diminished monotonically with depth to less than 1°C below 700 m. While salinity errors peaked near the surface, there were no consistent trends except over a layer from around 300 to 800 m depth, where values were typically overestimated by 0.15 practical salinity units (PSU) (figure 4.3.3). The rms errors varied around 0.2 PSU over the upper 600 m, falling below 0.1 PSU at depths greater than 800 m.

The discrepancies between modelled and observed fields generally showed little seasonality. However, during the cooler months there was a clear tendency towards overestimating temperatures in shallow water and, in some instances, overestimating salinities (figure 4.3.4). Discrepancies were smaller further offshore, both near the surface (11 m) and below the mixed layer (50 m). However, they increased at depth (>100 m) over the outer shelf, where both temperature and salinity were overestimated (figure 4.3.4).

Significant differences between the model and observations might be attributable to the relatively coarse resolution of the ACOM output fields (to which the Northwest model was relaxed). Firstly, the large coastal cells in ACOM were each characterised by a mean depth, which was larger than the real values found close the coast. One consequence is that surface heat losses would have produced a smaller drop in water column temperatures than would have been the case with more realistic bathymetry. Secondly, neither ACOM nor the Northwest model was expected to resolve the nonlinear internal wave motions over the upper slope and outer shelf. Instead the models relied on sub-grid-scale parameterisations to determine the vertical mixing rates, which were likely to have significant errors in the energetic environment of the outer NWS. The temperature and salinity profiles described previously suggest that mixing was overestimated by the models (figures 4.3.1 and 4.3.2).

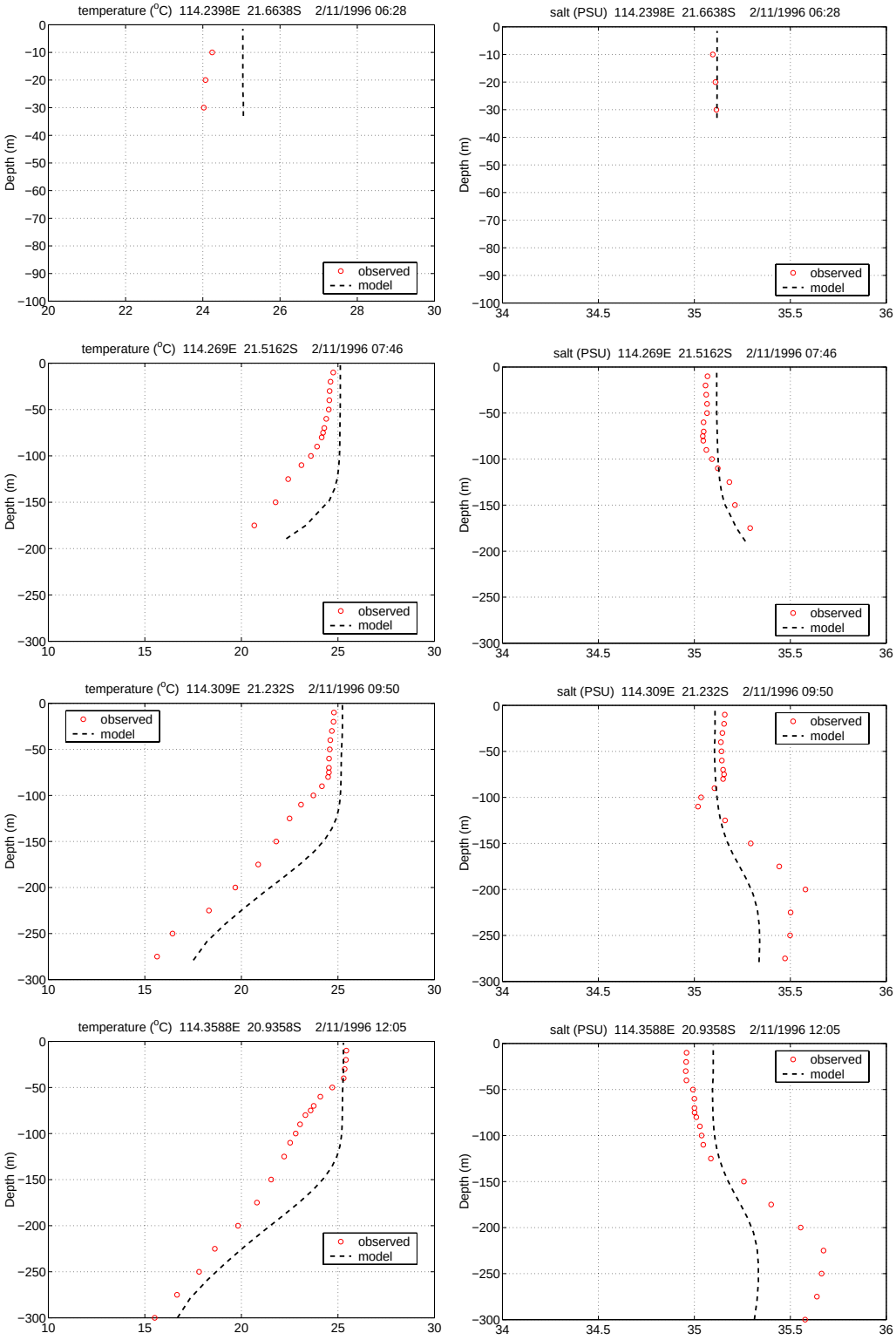

Figure 4.3.1: Examples of observed verses modelled temperature profiles (left) and salinity profiles (right) following a section NNE from North West Cape undertaken during November 1996. All model results are from the Pilbara model.

For processes such as water column primary productivity, the absolute temperature and salinity values are less important than their vertical distributions and associated surface mixed layer depths. Mixed layer depth can be estimated in a variety of ways based on temperature, salinity, or density fields, combined with threshold criteria (e.g. Brainerd & Gregg, 1995). Using a very simple method based only on temperature profiles yielded mixed layer depths in the range of 10 to 150 m for both the Northwest model and observations (figure 4.3.5). While the model showed significant variability in skill in relation to mixed layer depth, estimates were usually within a factor of two and the errors did not show any systematic spatial trend (figure 4.3.5).

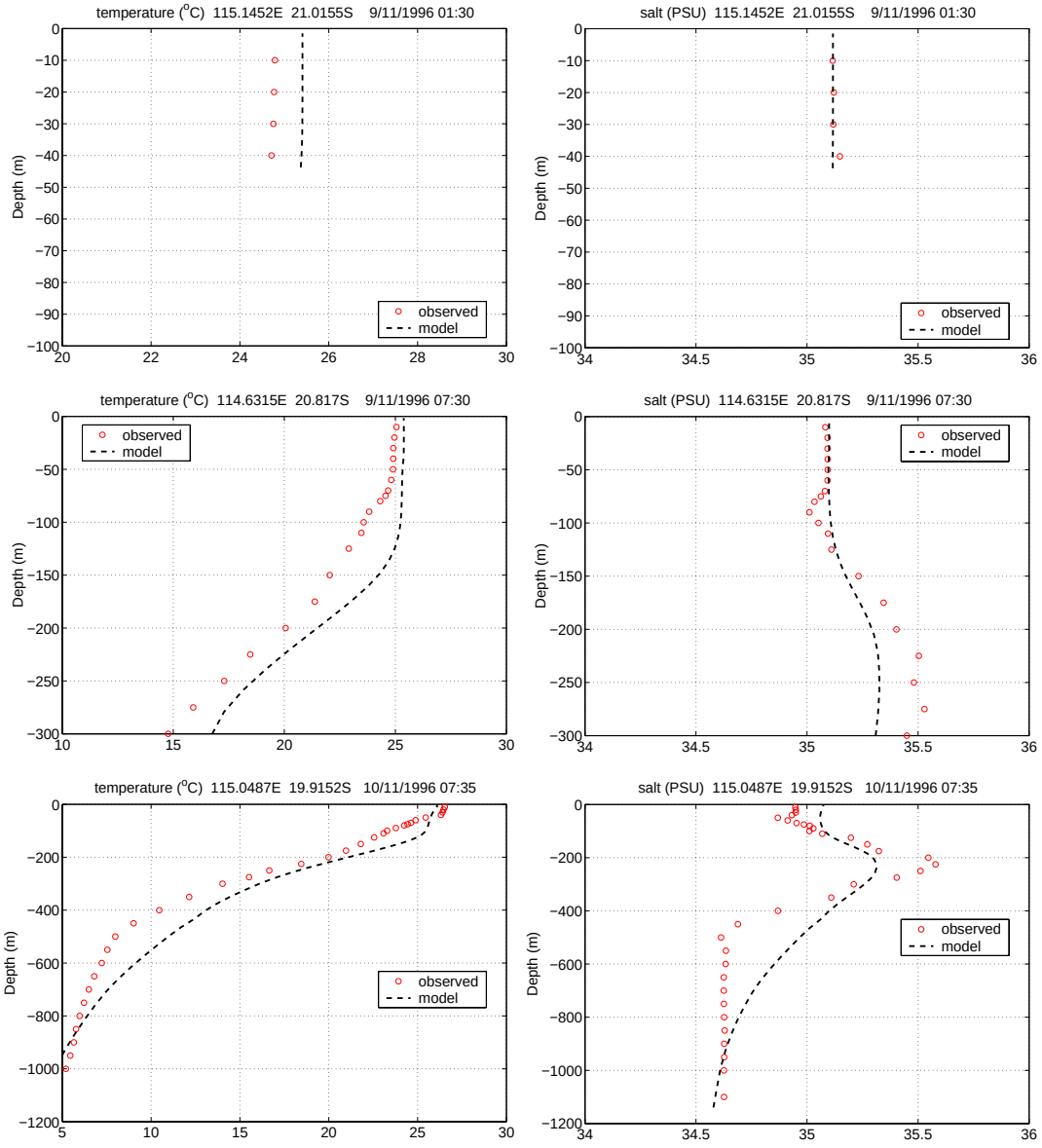

Figure 4.3.2: Examples of observed verses modelled temperature (left) and salinity (right) profiles taken north of Onslow during November 1996. The first two casts are compared to the Pilbara model (top and centre), while the last is from deeper water and is compared with the Northwest model (bottom).

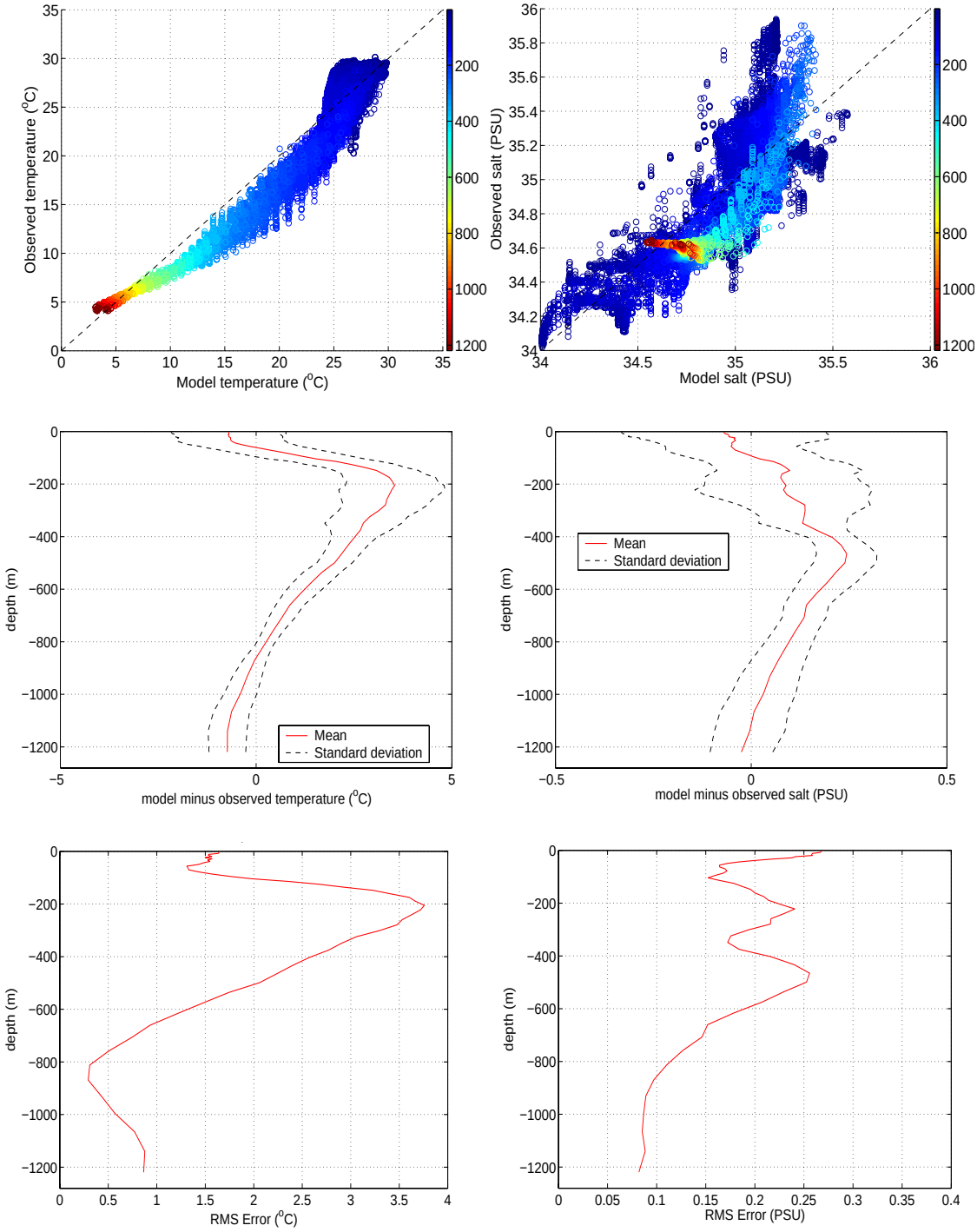

Figure 4.3.3: Upper panels show observed temperatures (left) and salinities (right) verses the Northwest model estimates interpolated to the same time and location, with colour coding indicating depth in metres. Centre panels show the corresponding mean difference between model and observations as a function of depth and the lower panels show the corresponding rms error. The observations consist of all available hydrographic casts from the modelling period of 1994 to 1999 (862 casts).

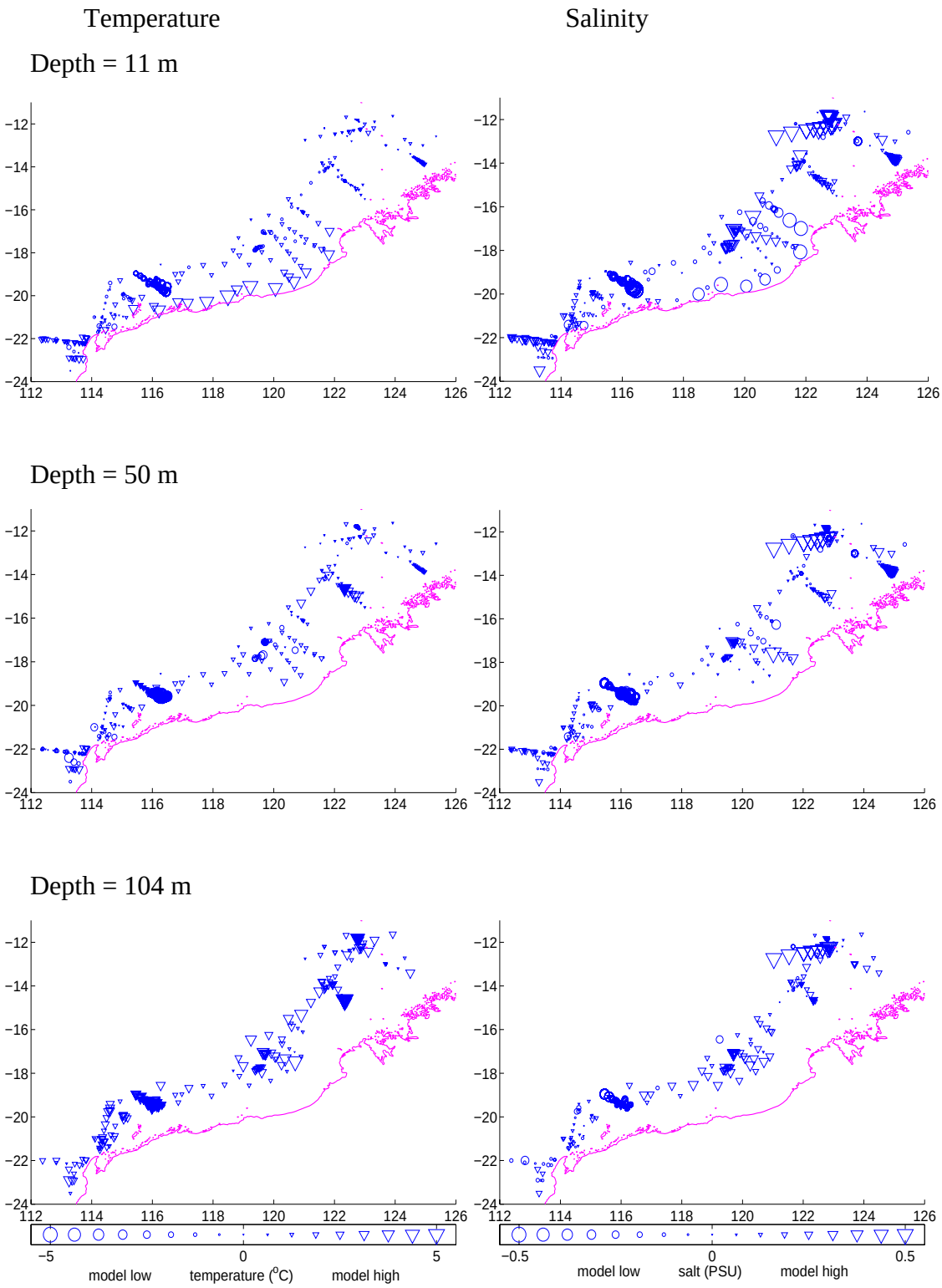

Figure 4.3.4: Difference between observed and modelled temperature (left) and salinity (right) at depths of 11 m (top), 50 m (centre), and 104 m (bottom). These results are based on the Northwest model and all available observations during the period 1994 to 1999 (862 casts).

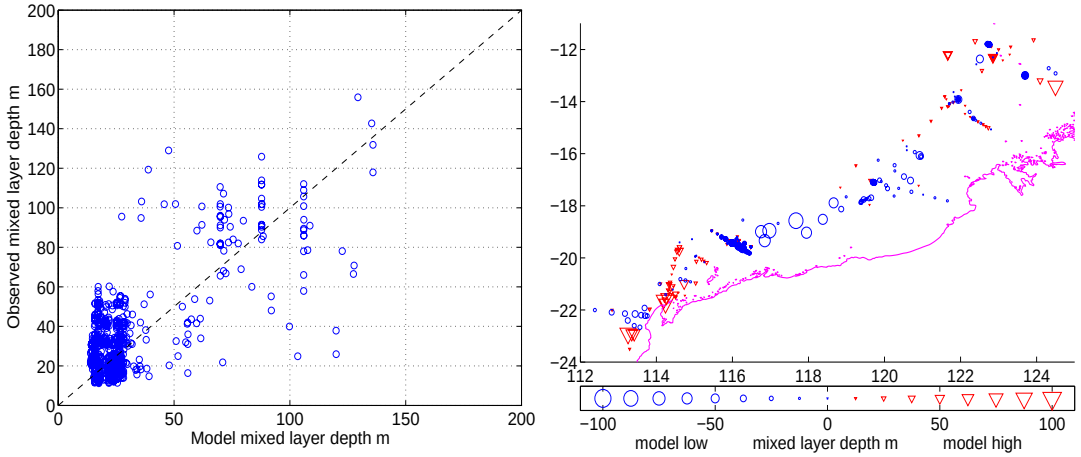

Figure 4.3.5: Observed verses modelled mixed layer depth (left) and difference between observed and modelled mixed layer depth (right). These results are based on the Northwest model and all available observations during the period 1994 to 1999 (862 casts). The mixed layer depth was defined as the depth where the observed temperature was 0.2°C below the observed near surface value. This criteria was reduced to 0.1°C for the model because of the smoother nature of the vertical profiles (e.g. figure 4.3.2).

4.4 Comparisons with observed currents

There have been significant quantities of current meter data collected on the NWS over a number of decades, mainly in response to the needs of the oil and gas industries. These records consist mainly of short time series scattered across the major oil and gas reserves and related offshore facilities. Many are also commercially sensitive and not readily accessible for scientific purposes. Comparisons have therefore focused on data provide by the WADEP from coastal sites around the Dampier Archipelago (figure 4.4.1) and data provided by Woodside Energy through WNI from the outer shelf at the North Rankin platform (figure 4.2.1). The period of the comparisons was mostly limited to the second half of 1982, when both current meter data and model forcing data sets were available.

Currents from the Dampier model were generally aligned with the observed flow, but showed less directional variability particularly during the neap period when the tidal component was less dominant (figures 4.4.2 and 4.4.3). Both observations and model results indicated that current direction was highly variable at site DA8, perhaps determined by its position in the wake of the Malus Islands during the outgoing tide (figure 3.2.2). Model current speeds exhibited similar trends to the observations, but commonly overestimated peak values by up to 50% (figures 4.4.2 and 4.4.3). DA8 again differed from the other three sites in that model current speeds were similar and sometimes less than those observed. The Dampier model explained 50 to 90% of the variability, with the exception of DA10 where this figure fell to around 15% (table 4.4.1). Rms errors in the current components were between 0.02 and 0.06 m s^{-1} (table 4.4.1), except for the northward component at DA7 (0.12 m s^{-1}) and the eastward component at DA10 (0.19 m s^{-1}). Both of these sites were located very close to islands and discrepancies were most likely associated with poorly resolved bathymetric features, such as the small island immediately east of DA10 (figure 4.4.1).

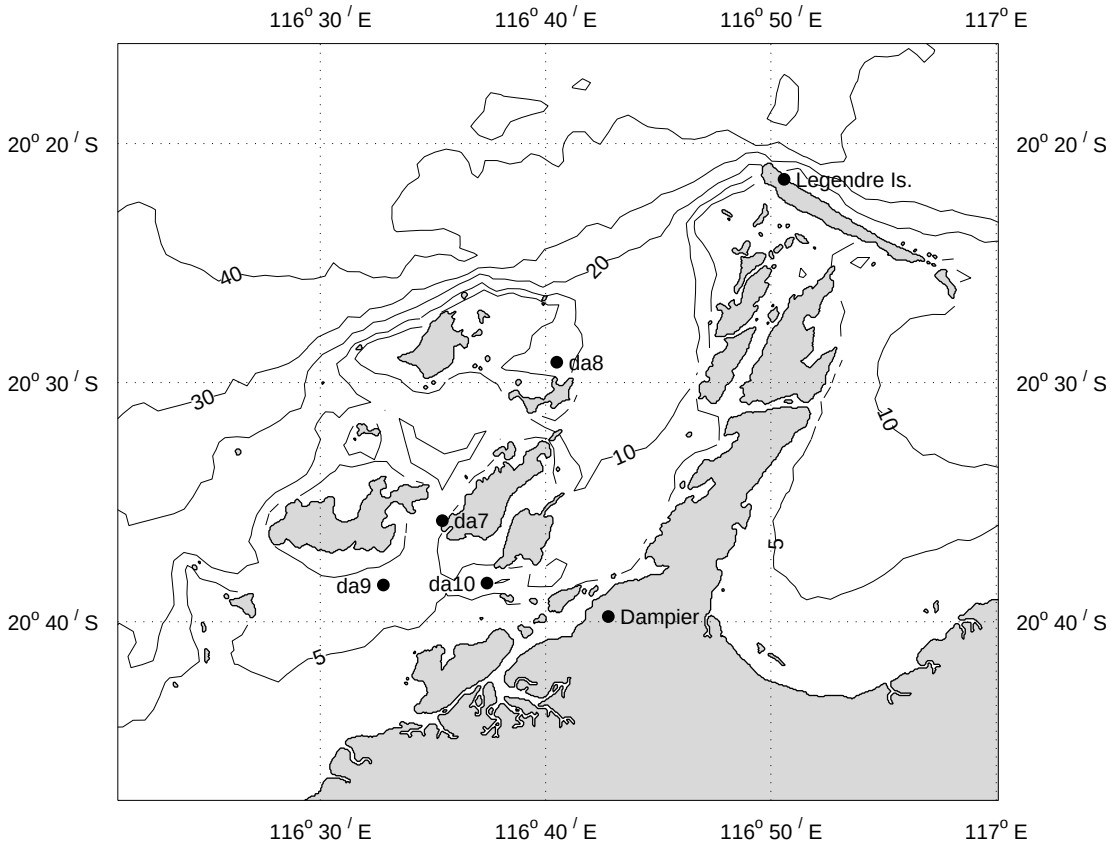

Figure 4.4.1: Map showing the sites of current meter moorings deployed in 1982 around the Dampier Archipelago (Mills et al. 1986), the location of the meteorological station on Legendre Island used to provide winds for the Dampier model, and the local bathymetry.

At the North Rankin site on the outer shelf (figure 4.2.1) the Pilbara model reproduced the current direction and speed relatively well in near surface waters (figure 4.4.4), with rms errors around 0.09 m s^{-1} (table 4.2.1). However, the observations had a more complex vertical structure, which was not captured by the model. This was most evident at the current meter closest to the seafloor (120 m), where observations revealed significant bottom intensification (<0.5 m s^{-1}), while model currents continued to decrease towards the bottom (<0.2 m s^{-1} and rms errors around 0.05 m s^{-1}). The model explained almost 50% of the variance in both current components at 20 m, but at 120 m this fell to 21% for the northward component (approximately cross shelf).

Low frequency currents from the Dampier model were in good qualitative agreement with observations (figures 4.4.5 and 4.4.6) and explained 50 to 75% of the variability in the dominant flow direction (table 4.4.2). Rms errors were usually less than 0.02 m s^{-1}, but reached twice this value for the northward component at DA7 (table 4.4.2). Here the model captured short-term periods (~ 1 week) of enhanced southward flow, but underestimated the mean flow to the northeast.

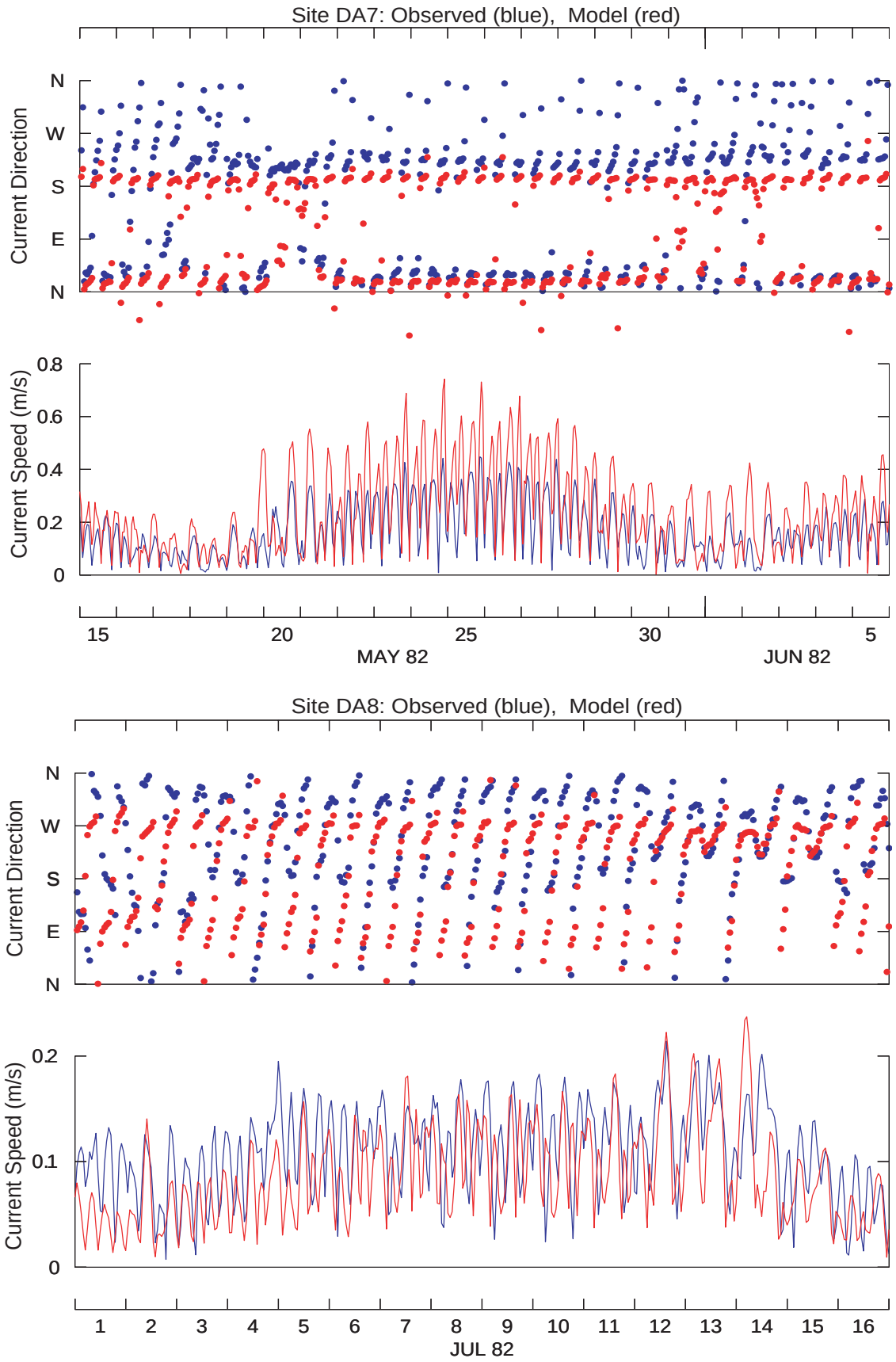

Figure 4.4.2: Observed (blue) verses modelled (red) current direction and current speed at sites DA7 (upper) and DA8 (lower) based on current meter measurements from 1982 (Mills et al. 1986).

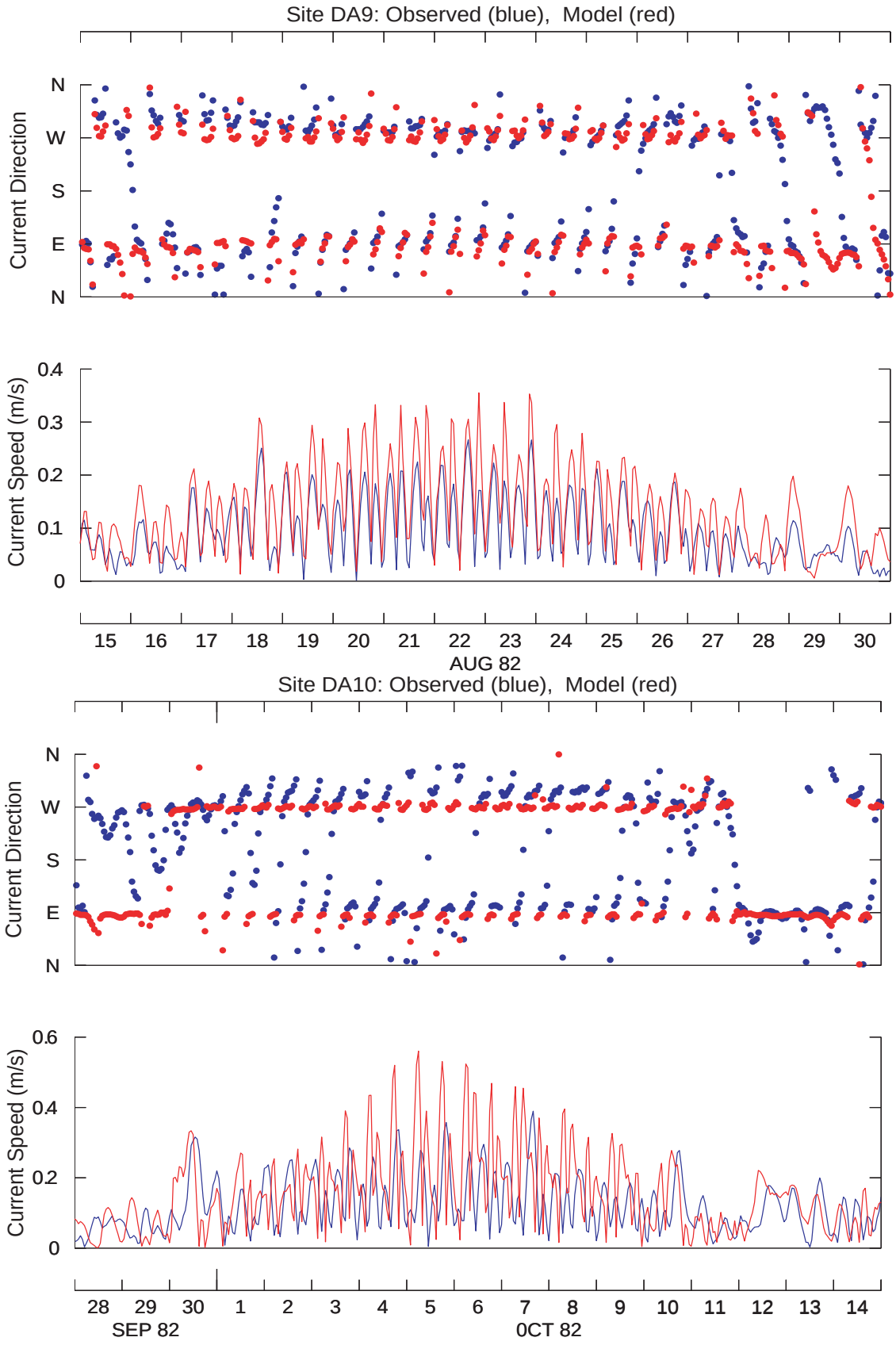

Figure 4.4.3: Observed (blue) verses modelled (red) current direction and current speed at sites DA9 (upper) and DA10 (lower) based on current meter measurements from 1982 (Mills et al. 1986).

Table 4.4.1: Statistical comparisons between the observed currents at sites DA7, DA8, DA9, and DA10 with outputs from the Dampier model based on the data from 1982 (Mills et al. 1986), and between the observed currents at North Rankin (NR) with outputs from the Pilbara model.

Mooring Code		**DA7**	**DA8**	**DA9**	**DA10**	**NR**	**NR**
Mooring depth (m)		13.0	10.0	10.5	7.0	20	120
Water depth (m)		15.0	12.0	12.5	9.0	125	125
Correlation coefficient	Eastward current	0.93	0.77	0.95	0.39	0.69	0.67
	Northward current	0.91	0.72	0.21	0.36	0.64	0.46
	Current speed	0.80	0.50	0.86	0.09	0.38	0.16
rms error ($m\ s^{-1}$)	Eastward current	0.029	0.058	0.051	0.19	0.11	0.077
	Northward current	0.12	0.021	0.028	0.012	0.092	0.028
	Current speed	0.092	0.004	0.040	0.120	0.089	0.051

Further insight can be obtained by examining how comparisons with observations changed when the Dampier model was forced by NCEP-NCAR re-analysis winds rather than winds measured locally at Legendre Island (figure 3.1.3). There was no major change in the raw current comparisons, with correlation coefficients typically falling by only around 10% and rms errors remaining largely unchanged. This result reflected the dominance of the tidal signal over the wind-driven signal at these frequencies. However, the use of the NCEP-NCAR winds significantly degraded the low frequency component of the currents. Most of the variability on time scales less than a week was lost (figures 4.4.6 and 4.4.7), with correlation coefficients for the dominant current component at DA10 falling from 0.82 to 0.47. There was a corresponding increase in the rms error from 0.032 m s^{-1} to 0.037 m s^{-1}. These results confirm the need for accurate winds in the coastal environment, so as to capture local variability and resolve high frequency processes such as the sea breeze.

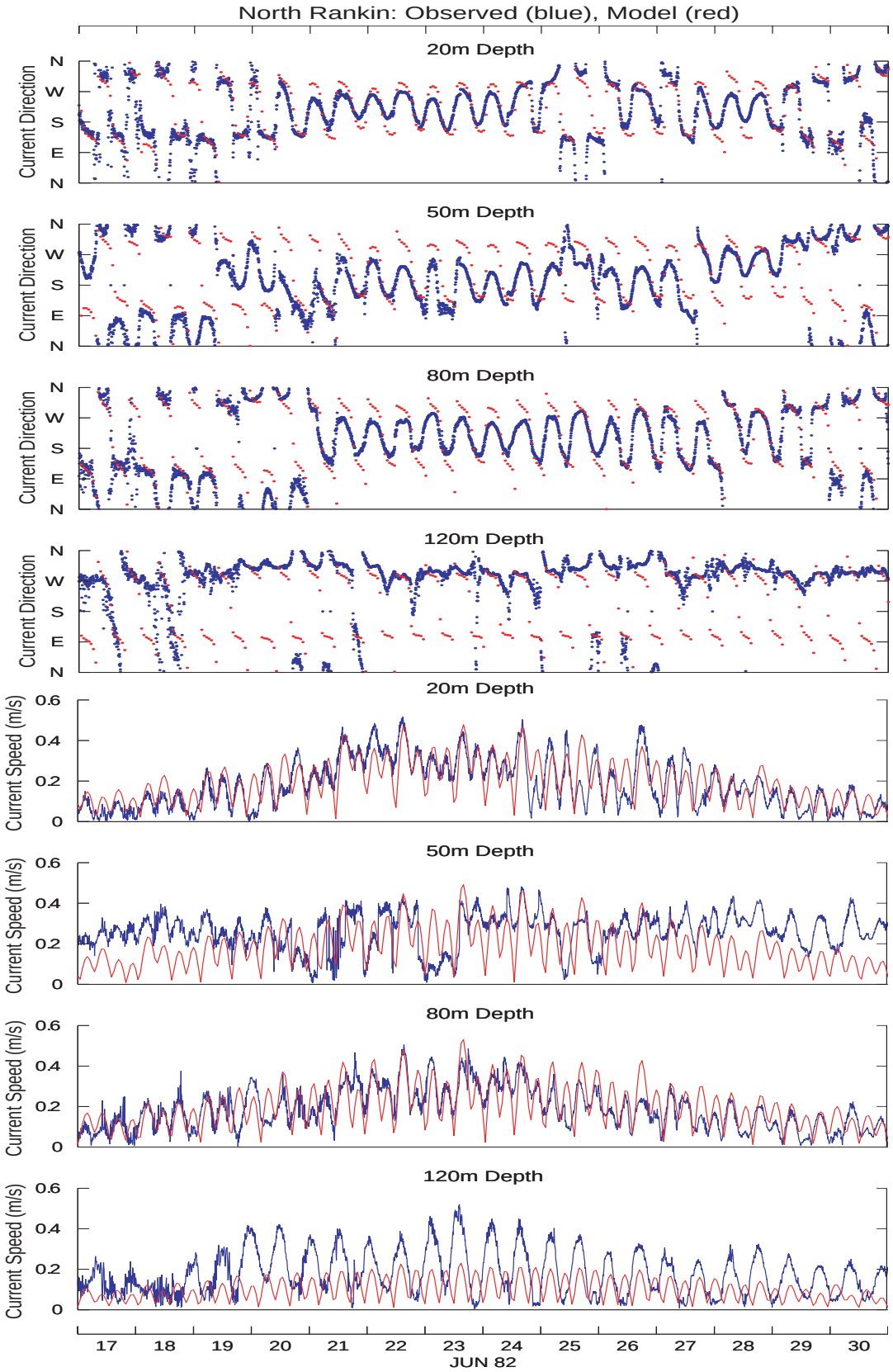

Figure 4.4.4: Observed (blue) verses modelled (red) current direction (upper) and current speed (lower) at the North Rankin platform (data kindly provided by Woodside Energy through WNI).

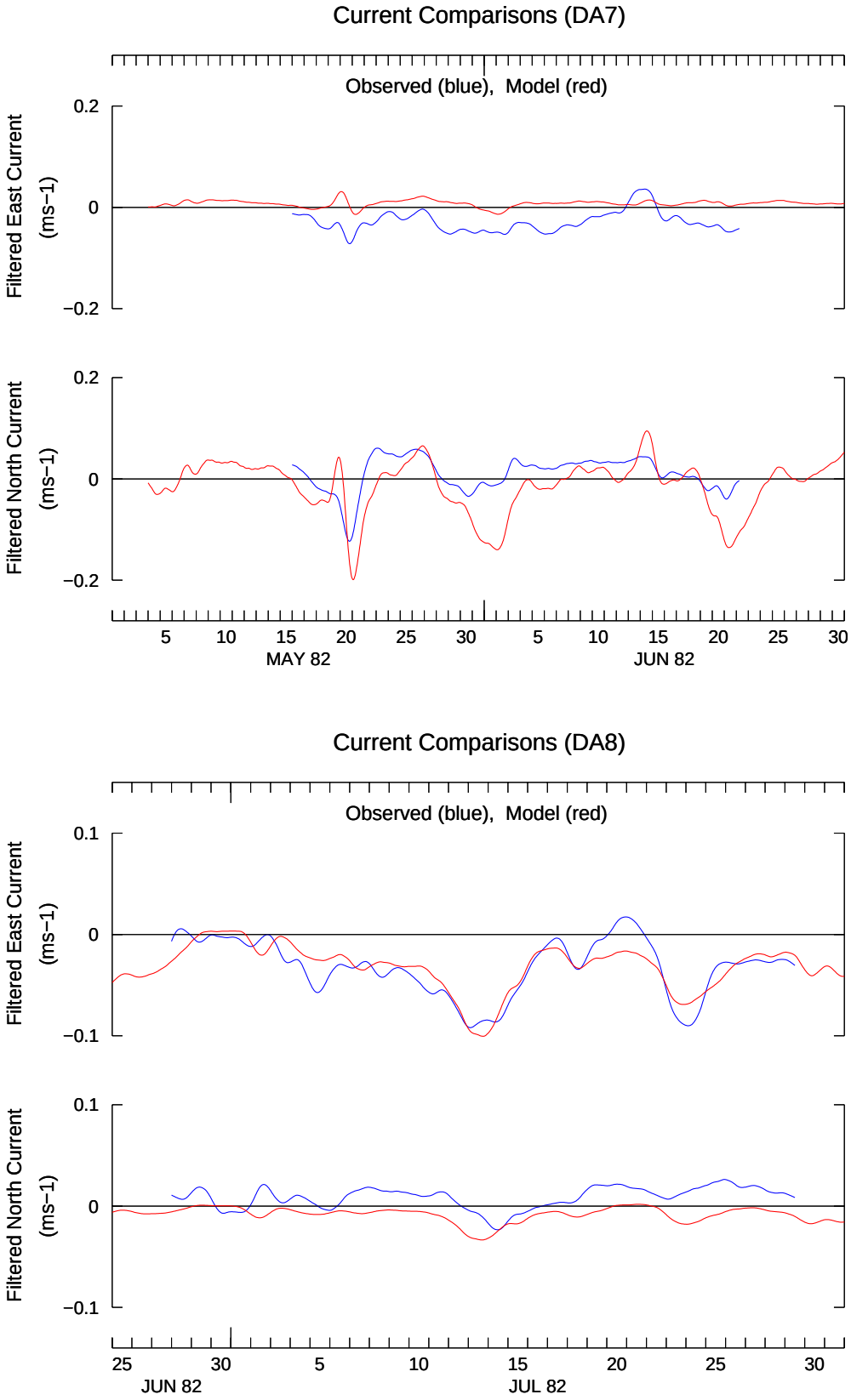

Figure 4.4.5: Observed (blue) verses modelled (red) low frequency current components at sites DA7 (upper) and DA8 (lower) based on current meter measurements from 1982 (Mills et al. 1986).

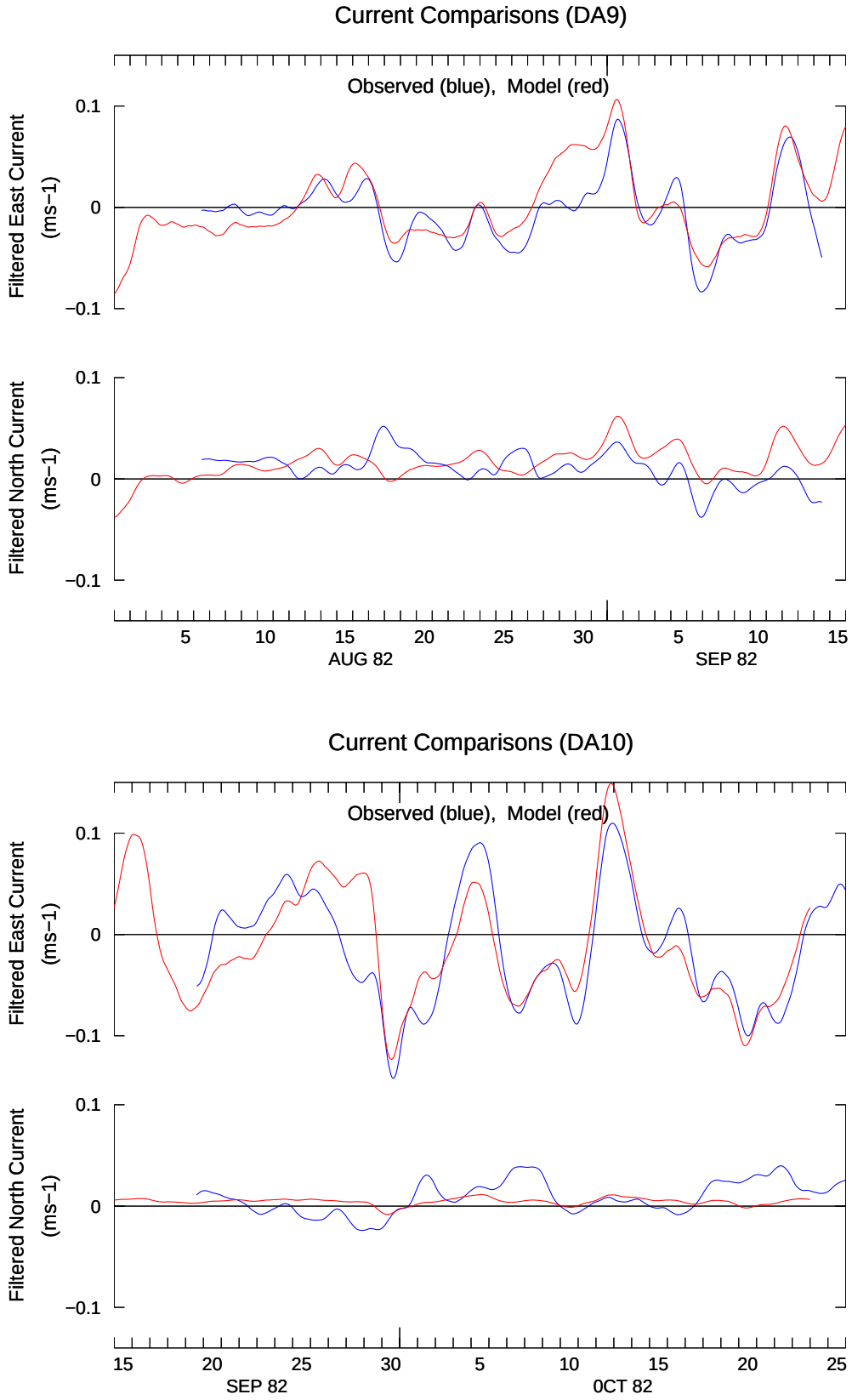

Figure 4.4.6: Observed (blue) verses modelled (red) low frequency current components at sites DA9 (upper) and DA10 (lower) based on current meter measurements from 1982 (Mills et al. 1986).

Table 4.4.2: Statistical comparisons between the observed low frequency currents at sites DA7, DA8, DA9, and DA10 with outputs from the Dampier model based on the data from 1982 (Mills et al. 1986), and between the observed low frequency currents at North Rankin (NR) with outputs from the Pilbara model.

Mooring Code		DA7	DA8	DA9	DA10	NR	NR
Mooring depth (m)		13.0	10.0	10.5	7.0	20	120
Water depth (m)		15.0	12.0	12.5	9.0	125	125
Correlation coefficient	Eastward current	0.29	0.87	0.84	0.82	0.45	0.30
	Northward current	0.70	0.52	0.11	0.14	0.49	0.28
	Current speed	0.52	0.92	0.49	0.72	0.40	-0.08
rms error ($m\ s^{-1}$)	Eastward current	0.0073	0.012	0.020	0.032	0.028	0.010
	Northward current	0.041	0.0065	0.013	0.0035	0.024	0.004
	Current speed	0.036	0.0096	0.019	0.021	0.032	0.006

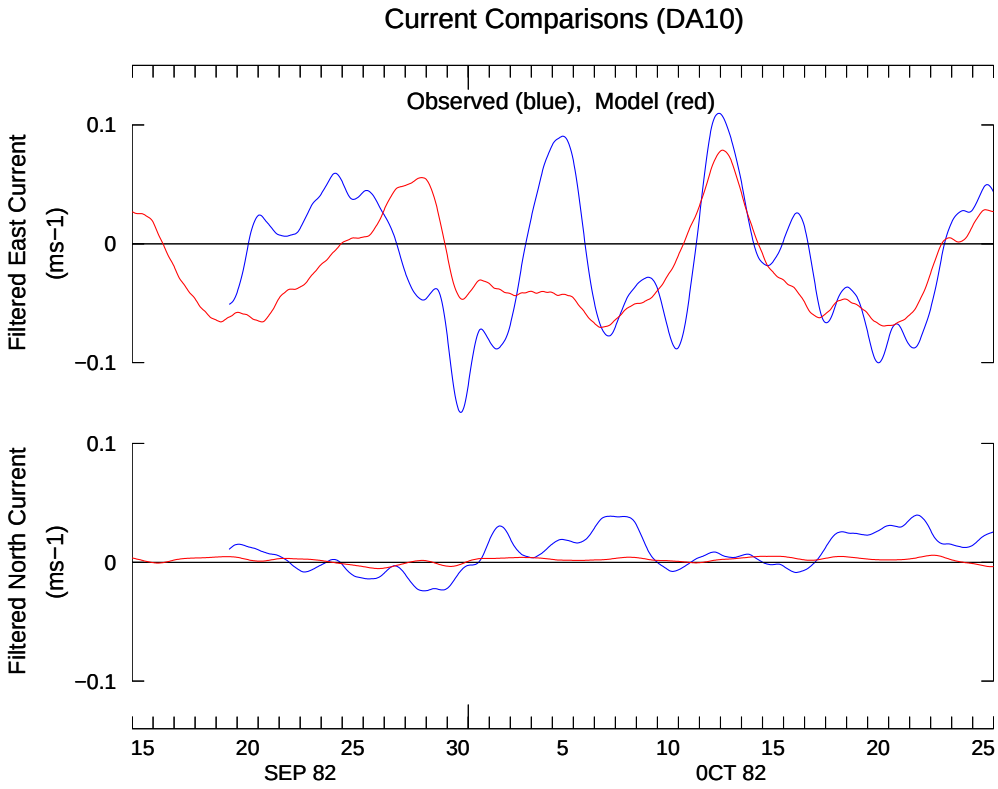

Figure 4.4.7: Observed (blue) verses modelled (red) low frequency current components at site DA10 (lower), when the Dampier model is forced by the NCEP-NCAR winds (rather than the Legendre Island winds used in figure 4.4.6).

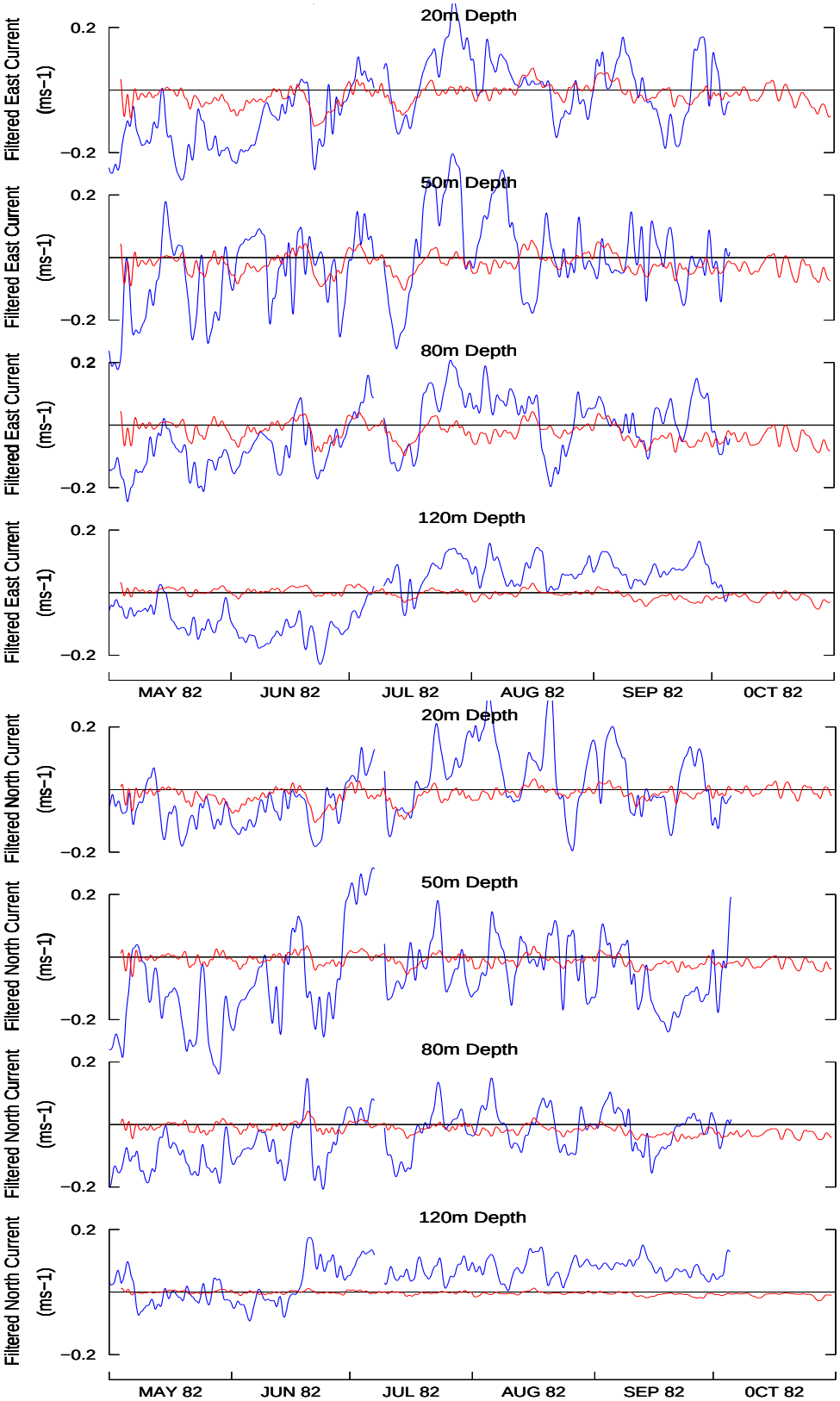

Figure 4.4.8: Observed (blue) verses modelled (red) low frequency easterly currents (upper) and northerly currents (lower) at the North Rankin platform (data kindly provided by Woodside Energy through WNI).

5. DESCRIPTION OF THE CIRCULATION FIELDS

The description of the model circulation fields begins with the semi-diurnal tide, which usually dominates the instantaneous flow patterns on the NWS. However, transport and dispersion over longer time scales of days to months are largely determined by seasonal patterns, which are described here in terms of monthly averaged fields. The flow on the NWS also varies on interannual time scales and this is considered at the scale of the Northwest model. Tropical cyclones represent major episodic events on the NWS, and will be investigated through a detailed analysis of Tropical Cyclone Bobby as it crossed the NWS in February 1995.

5.1 Tides

Semi-diurnal tidal currents are the dominant motions on the NWS. The model currents were mainly orientated in the cross shelf direction, except around Barrow Island and the Monte Bello Islands, where they were more east-west orientated (figure 5.1.1). The strength of the currents and associated tidal ranges increased to the northeast, peaking around King Sound. Close to the coast, current patterns were increasingly influenced by the local bathymetry and coastline geometry (figures 5.1.2 and 5.1.3). Peak currents occurred during the ebb tide and showed similar distributions to those just described (figure 5.1.4). They were orientated almost directly offshore over the northern Pilbara and Kimberly shelf, where peak speeds were in the range of 1 to 1.5 m s^{-1}, except in King Sound where they approached 3 m s^{-1}. Further offshore and over the southern Pilbara the peak currents were significantly weaker and orientated to the north. However, the presence of islands and related bathymetric features sometimes caused substantial local acceleration of currents, such as occurred around the eastern tip of Legendre Island (figure 5.1.4).

The shear generated by the tidal motions over bathymetry resulted in vertical mixing and the formation of relatively deep bottom mixed layers (~20 m). In shallow water the surface mixed layer and bottom mixed layer connected and mixing extended over the entire water column. Around spring tide well mixed conditions typically extend to the 50 m isobath (figures 5.1.2 and 5.1.3), retreating inside the 30 m isobath during the neap (figure 5.1.2). In shallow regions, such as the Monte Bellows, the entrainment of deeper water produced cool surface temperature anomalies (figure 5.1.2). However, it is perhaps the vertical mixing fields themselves that provide the clearest indication of the model's spring neap mixing cycle with strong peaks in vertical diffusivity evident over the spring tide (figure 5.1.5).

There was significant dissipation of the current energy near the sea bed and the associated bottom stresses were high compared to most shelf regions. There was significant temporal and spatial variability in the stress fields, down to quite small scales (figures 5.1.6 and 5.1.7). However, peak stresses generally occurred in topographic channels and around headlands. Notable 'hotspots' on the Pilbara shelf included the waters off Northwest Cape, south and north of Barrow Island extending across to the Monte Bellos, east of Legendre Island, and Nichol Bay (figure 5.1.8). These distributions have important implications for resuspension and transport of sediments and possibly the distribution of benthic species. Detailed investigations of these links are described in accompanying NWSJEMS reports on sediment transport (Margvelashvili et al. 2006) and benthic habitats (Fulton et al. 2006a).

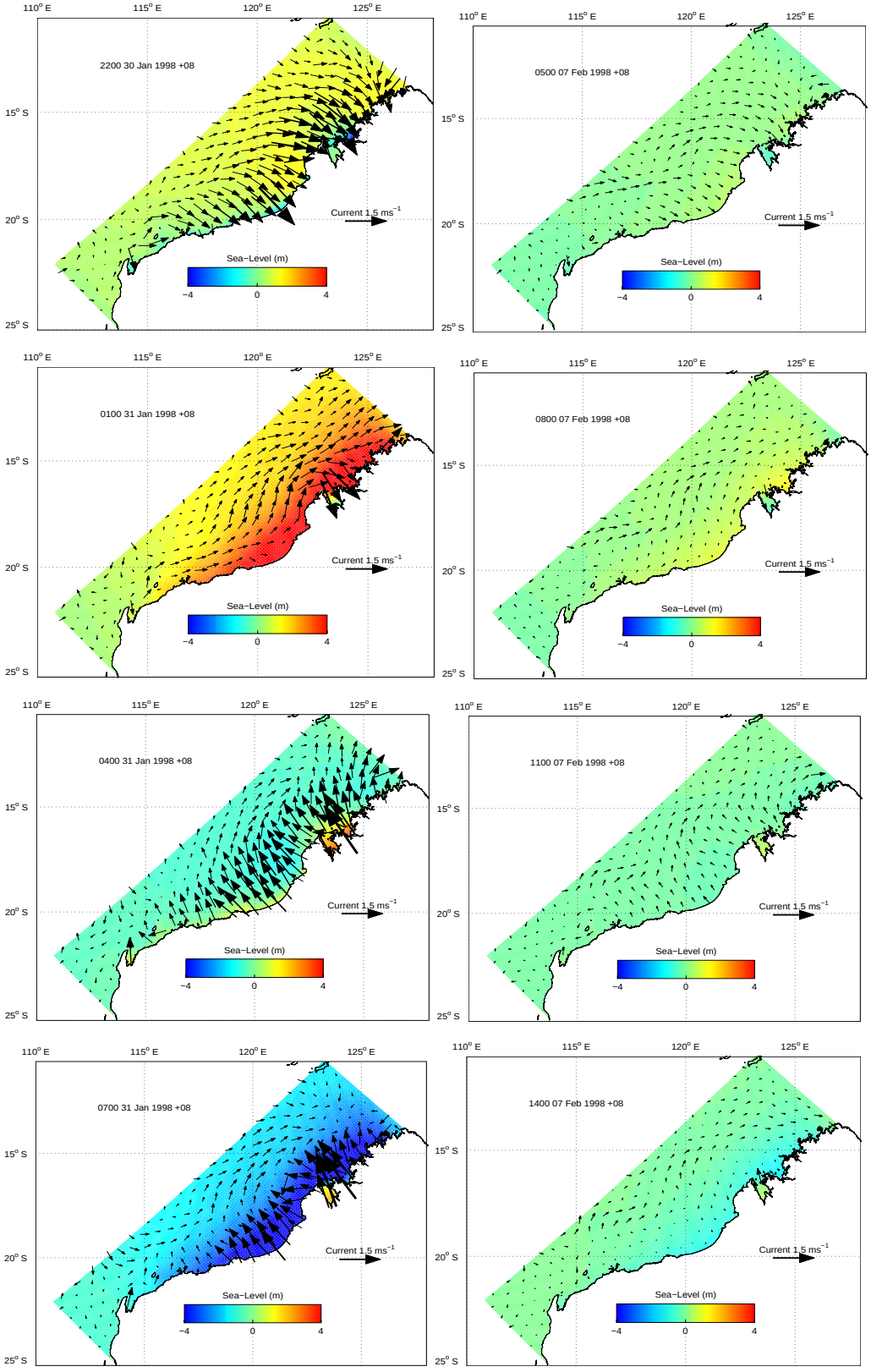

Figure 5.1.1: Current vectors in the top model cell (depth = 1.5 m) overlain on sea level close to spring tide (left) and neap tide (right) from the Northwest model. Plots in each column are at three hour intervals and from top to bottom correspond approximately to mid-flood tide, high tide, mid-ebb tide, and low tide.

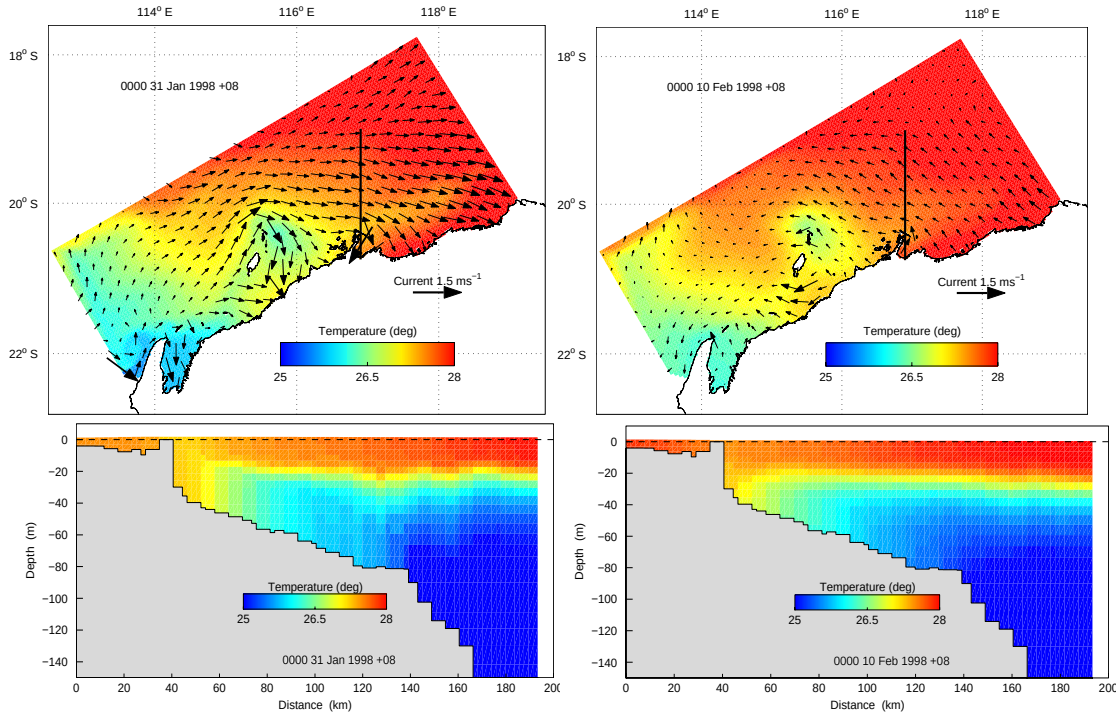

Figure 5.1.2: Upper panels show current vectors in the top model cell (depth = 1.5 m) overlain on temperature close to spring tide (left) and neap tide (right) from the Pilbara model. Lower panels show the corresponding vertical sections of temperature following a northerly line from Karratha (also marked on the upper panels).

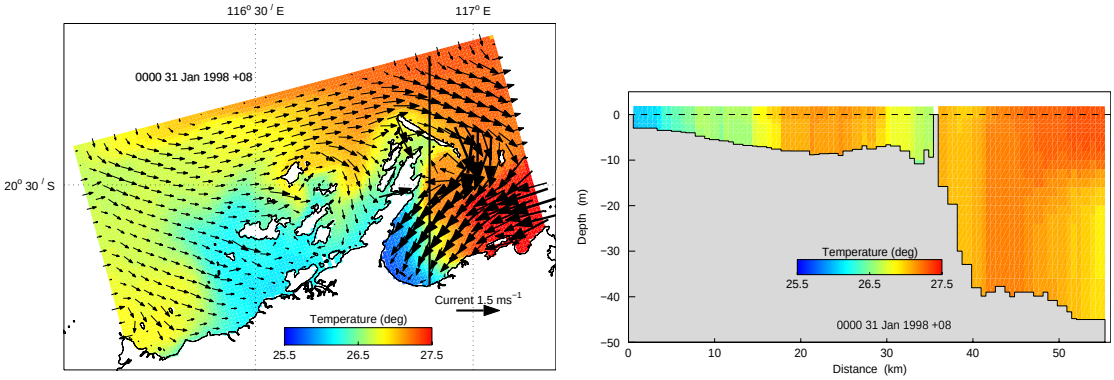

Figure 5.1.3: Current vectors in the top model cell (depth = 1.5 m) overlain on temperature close to spring tide from the Dampier model (left). Corresponding vertical section of temperature following a northerly line from Karratha (also marked on the left panel).

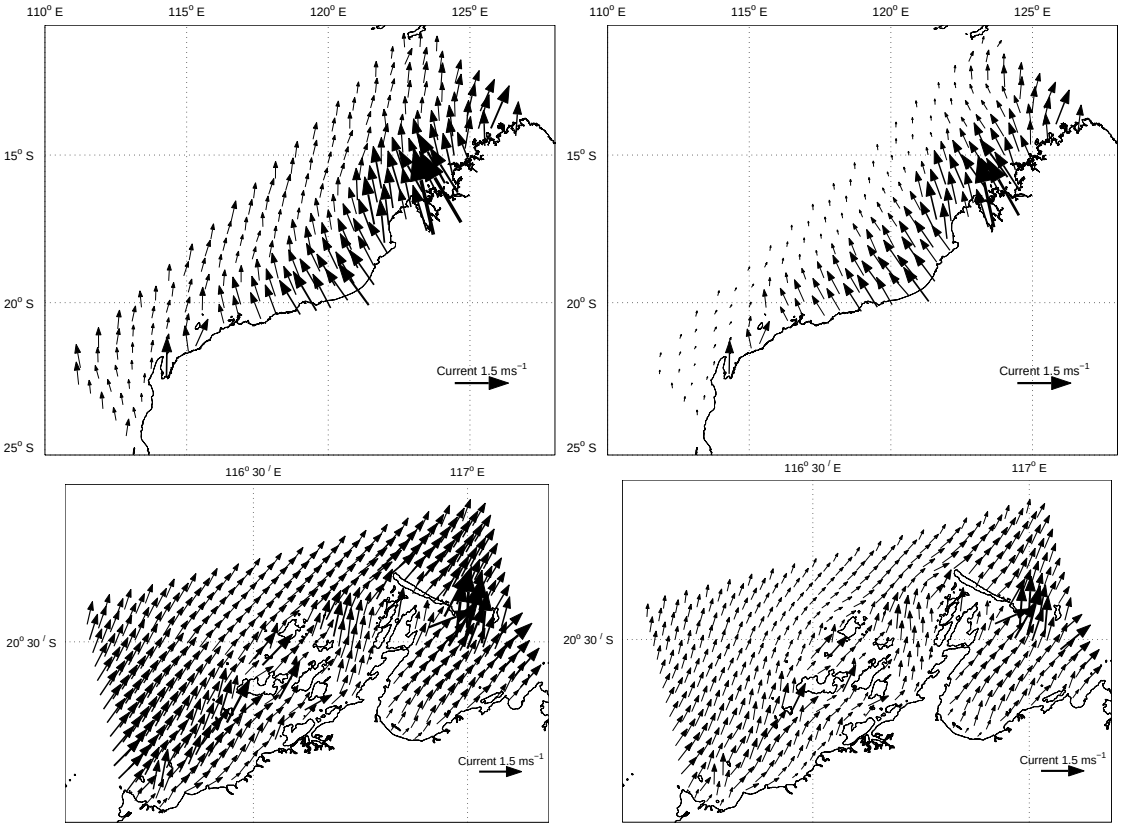

Figure 5.1.4: Maximum current (99th percentile) in the top model cell (1.5 m) (left) and maximum depth averaged current (right) from the Northwest model (upper panels) and Dampier model (lower panels). While maximum currents tended to occur when winds were aligned with the spring tidal currents, the dominance of the tidal component ensured that there was little seasonal variation in these statistics.

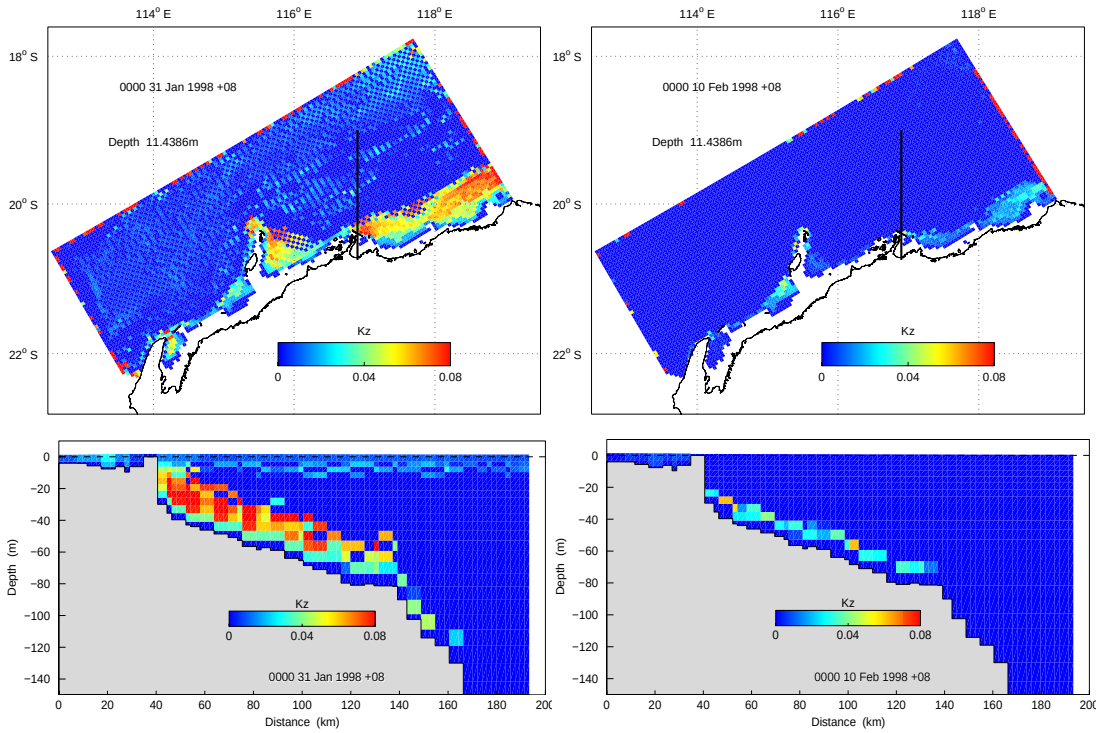

Figure 5.1.5: Upper panels show vertical diffusivity at a depth of 11.4 m close to spring tide (left) and neap tide (right) from the Pilbara model. Lower panels show the corresponding vertical sections following a northerly line from Karratha (also marked on the upper panels).

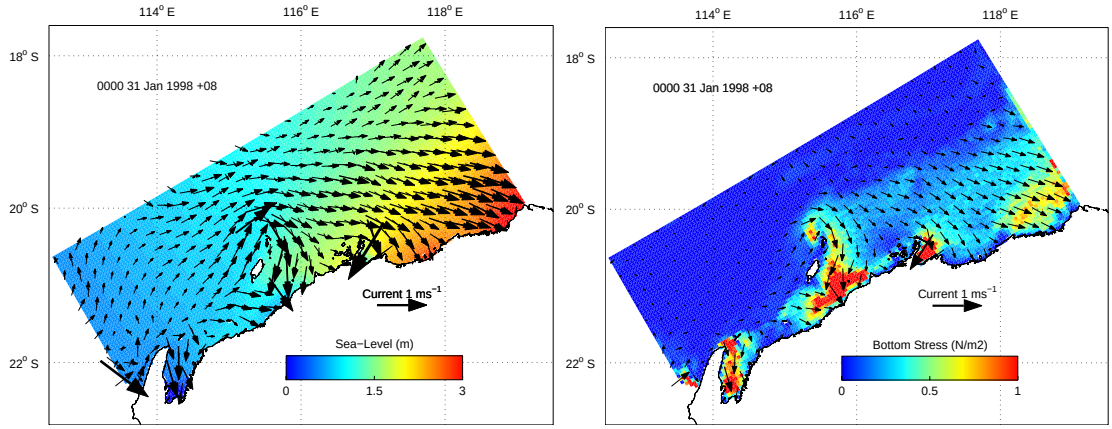

Figure 5.1.6: Current vectors in the top model cell (depth = 1.5 m) overlain on sea level (left) and current vectors in the deepest model cell overlain on bottom stress (right) from the Pilbara model.

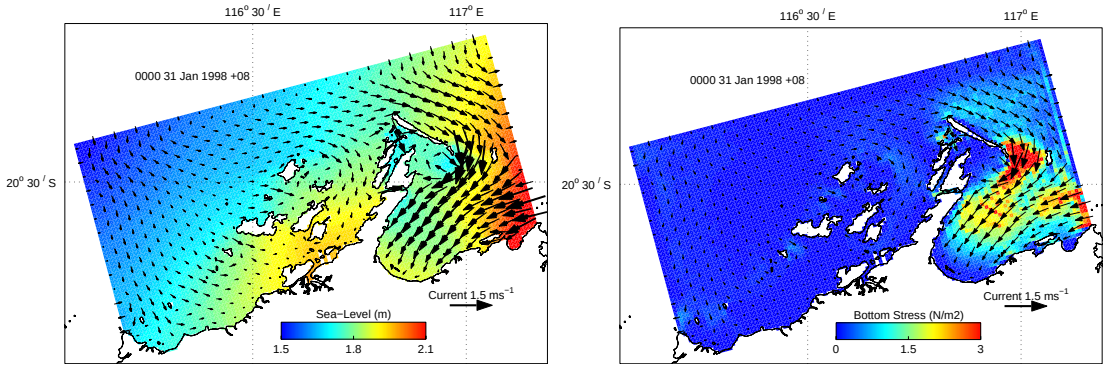

Figure 5.1.7: Current vectors in the top model cell (depth = 1.5 m) overlain on sea level (left) and current vectors in the deepest model cell overlain on bottom stress (right) from the Dampier model.

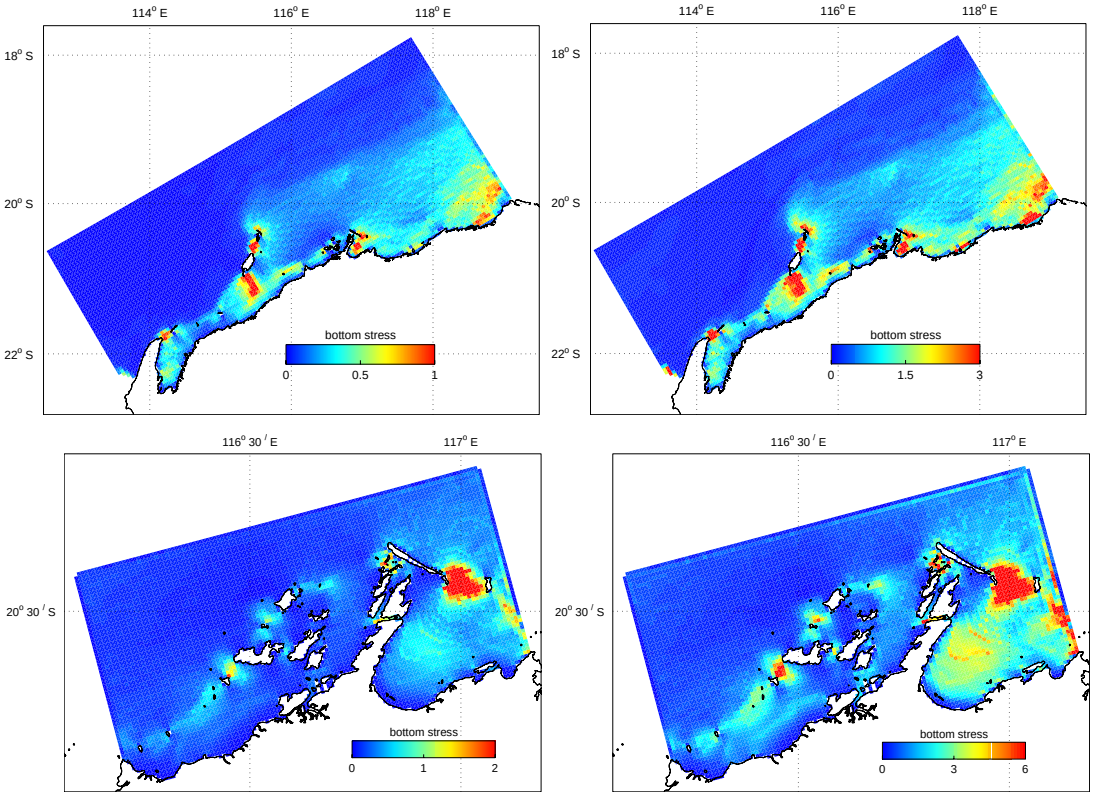

Figure 5.1.8: Mean bottom stress (left) and maximum bottom stress as indicated by the 99th percentile (right) from the Pilbara model (upper panels) and Dampier model (lower panels). These statistics showed relatively little seasonal variation.

5.2 Seasonal patterns

Mean flows determine long-term transport patterns, but on the NWS tend to be masked by the large tidal currents. Monthly mean currents have therefore been computed by averaging hourly output fields from the Northwest model over six years for each month of the year. Similar computations were made for Pilbara and Dampier models, but based only on two years of model output. While significant errors were evident in some of the

low frequency current estimates used in these calculations (section 4.4), long-term means tend to be much less sensitive to transient features such as waves and eddies.

Over the open shelf regions, flows appeared to be predominantly driven by local winds. Near surface currents were mostly in the range of 5 to 20 cm s^{-1} or a few percent of the wind speed (figures 5.2.1 and 3.1.2). They tended to be directed slightly to the left of the wind vectors, consistent with a wind-driven Ekman spiral (southern hemisphere). However, beyond the shelf break, the influences of the regional scale current patterns were more pronounced. This can be clearly seen off the west coast during autumn, when the surface flow associated with the Leeuwin Current opposed the prevailing winds (figures 5.2.1 and 3.1.2). The depth averaged currents were smaller in amplitude, but revealed northeastward transport over the slope in late autumn and winter, counter to wind direction, surface currents, and the coastal mean flow (figure 5.2.2). Quantitative comparisons with observations (section 4.4) suggest that the outer shelf and slope model currents should be viewed with some caution. However, these seasonal patterns are broadly consistent with monthly averaged currents observed in 1982 and 1983, with the exception of the 1982 to 1983 summer period when anomalous southwesterly currents were observed (Holloway & Nye, 1985). Similar anomalies were evident in the model results (e.g. 1996) and will be discussed further in section 5.3.

The observational comparisons (section 4.4) suggest that the model should provide reliable estimates of sub-tidal flow patterns around the Dampier Archipelago. The results show that the local land geometry and bathymetry had a major influence on the currents (figure 5.2.3). Complex recirculation patterns developed as the alongshore currents interacted with islands and headlands. For example, in Nichol Bay there was only a weak anticlockwise mean circulation, which reversed in winter. However, a much stronger northwestward flow persisted across the mouth of the bay, terminating in a permanent clockwise eddy centred on a bathymetric depression (figure 3.1.1) at the southeastern tip of Legendre Island (figure 5.2.3). The mean circulation on the western side of the peninsula was weakly northward over spring and summer, then reversed and strengthened over autumn.

5.3 Interannual variability

The temporal coverage of the Northwest model runs was six years, which provided some basis for examining interannual variability in the circulation of the NWS. Anomaly fields relative to the longer term (6 year) monthly average (figures 5.2.1 and 5.2.2) have been calculated for both the surface and depth averaged currents. Examples are presented from January and July for the years from 1994 to 1996 (figures 5.3.1 and 5.3.2).

Interannual variability in the surface currents was generally smaller than the mean, but exceeded it in particular locations and years (figures 5.2.1 and 5.3.1). The prevailing summertime flow to the northeast was weakened (southwesterly anomaly) during 1994, strengthened in 1995, and then reversed over much of the Pilbara shelf during 1996 when a strong a anticlockwise feature was also evident over the slope. During winter, the interannual variability over the shelf was significantly less than the mean southwesterly flow (figures 5.2.1 and 5.3.1) and also less than the summer variability. The most significant wintertime variability occurred over the slope, where the prevailing southwesterly flow was suppressed by northeasterly anomalies during 1994 and 1995. This trend was reversed in 1996 when the mean flow was enhanced and eddy like features where more prevalent near the offshore boundary of the model.

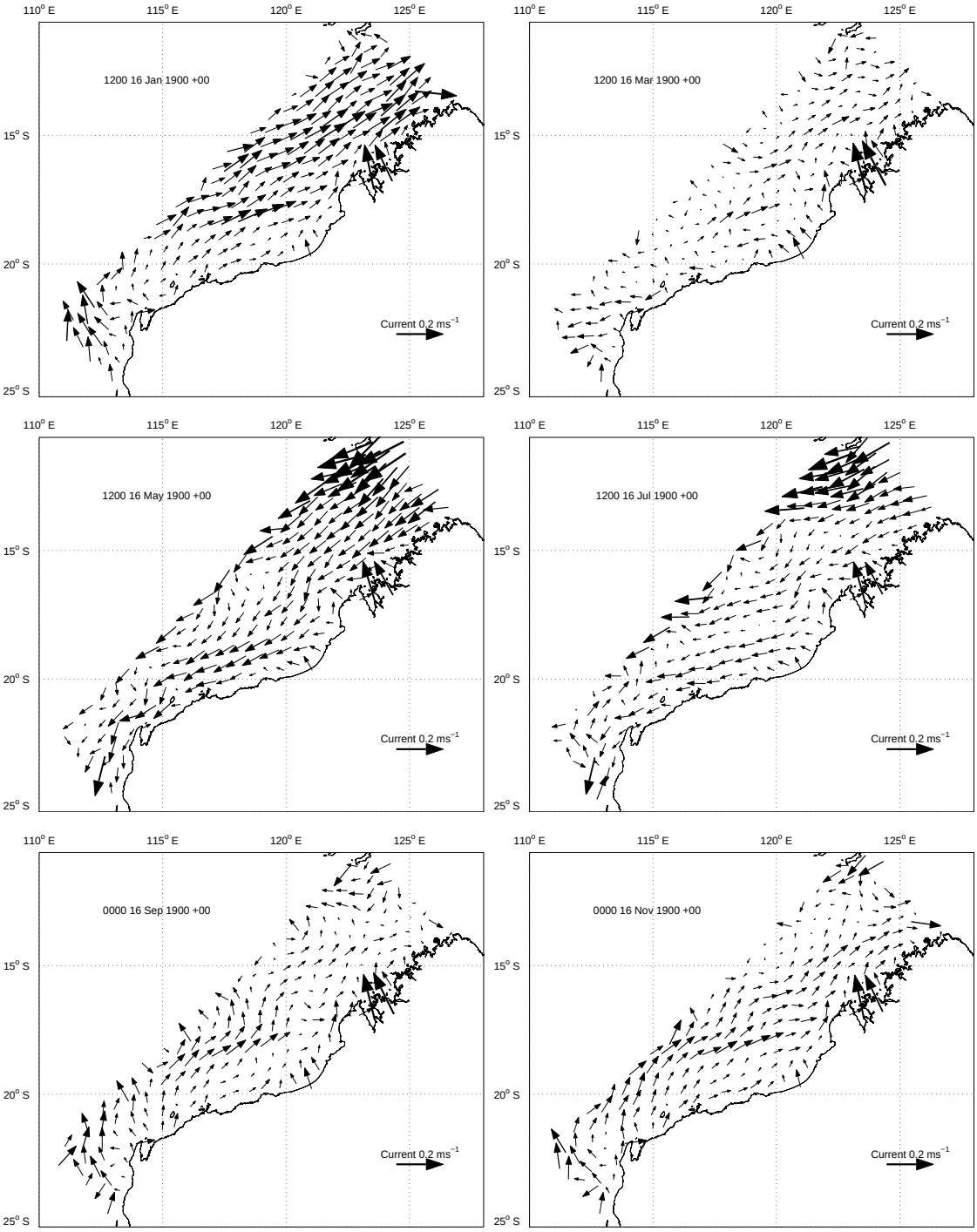

Figure 5.2.1: Monthly mean currents in the top model cell (1.5 m) based on six years of Northwest model runs covering the period 1994 to 1999.

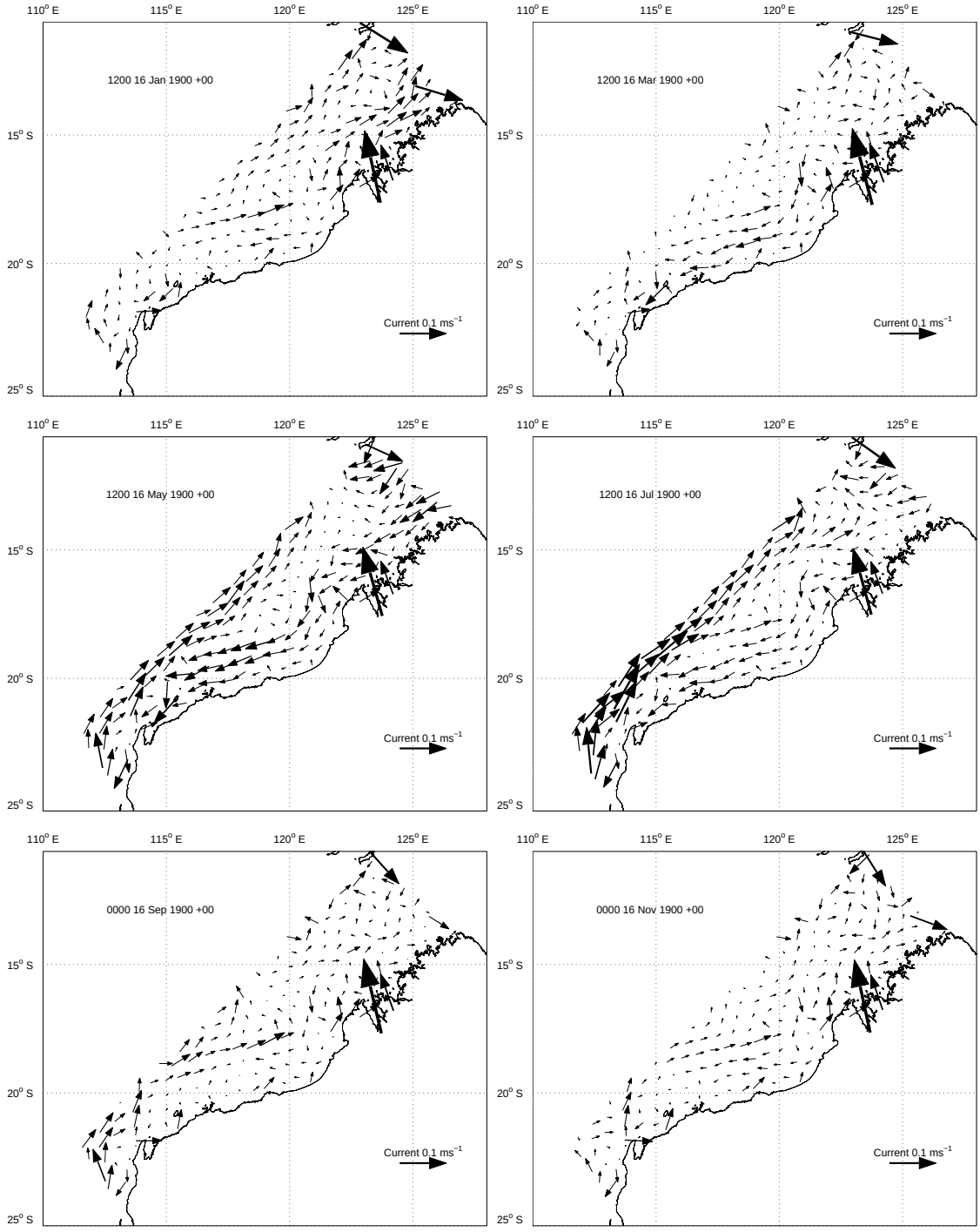

Figure 5.2.2: Monthly mean depth averaged currents based on six years of Northwest model runs covering the period 1994 to 1999.

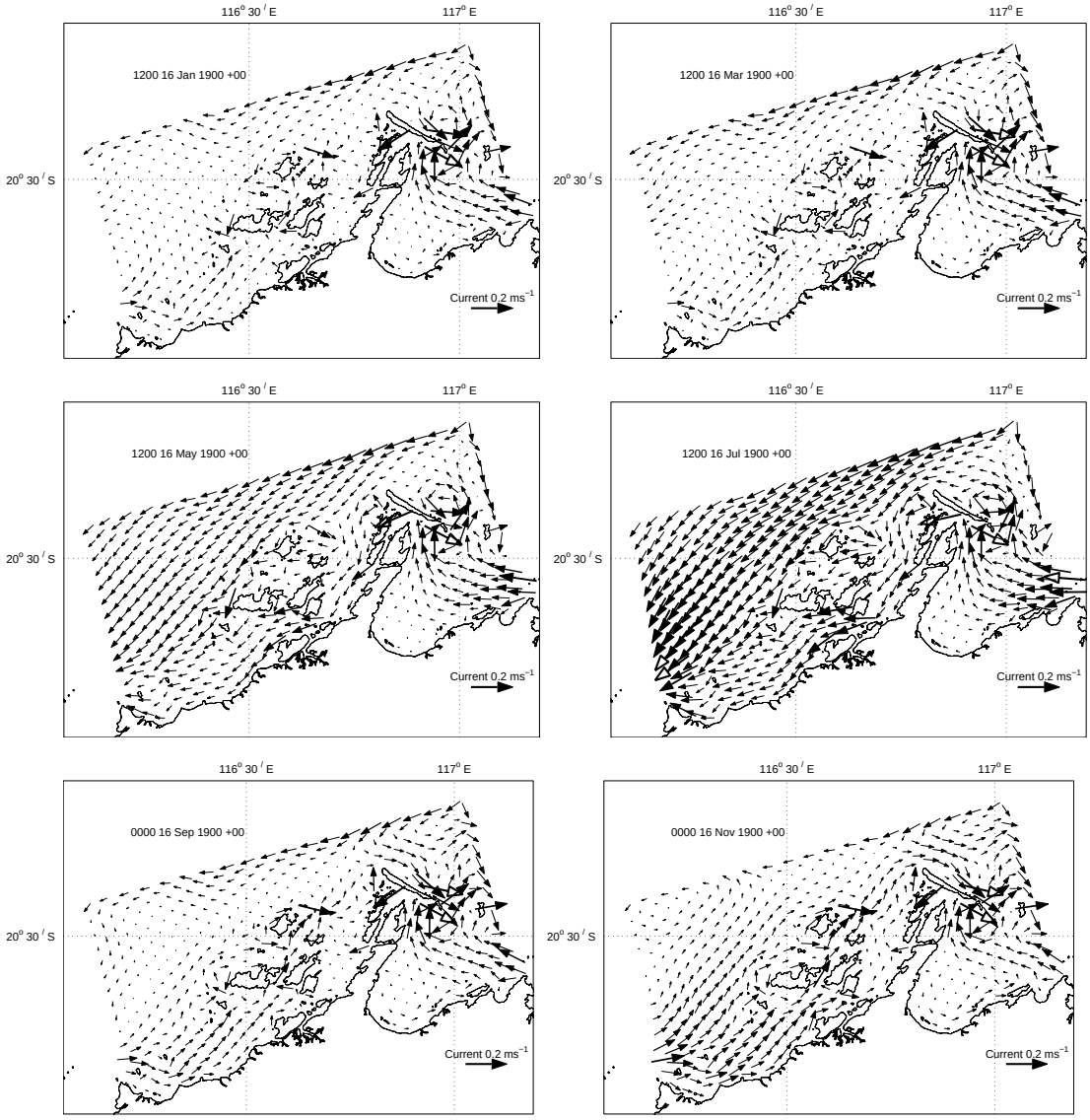

Figure 5.2.3: Monthly mean depth averaged currents based on two years of Dampier model runs from July 1996 to June 1998.

The mean summertime depth averaged currents over the Pilbara shelf were relatively weak (figure 5.2.2) and often dominated by interannual variability (figure 5.3.2), while the opposite tended to be true over the Kimberly shelf. For example, there was a significant reversal in summer flows over the Pilbara shelf between 1995 and 1996 (figure 5.3.2). Variability in the wintertime depth averaged currents was small compared to the mean currents.

In general terms, summertime interannual anomalies tended to be highest in near surface and mid shelf waters, reflecting year to year variability in wind forcing. In contrast, wintertime interannual anomalies tended to be highest off the shelf and extended through the water column, reflecting variability in the large-scale circulation patterns (ACOM) at the time when the Leeuwin Current is near its peak strength.

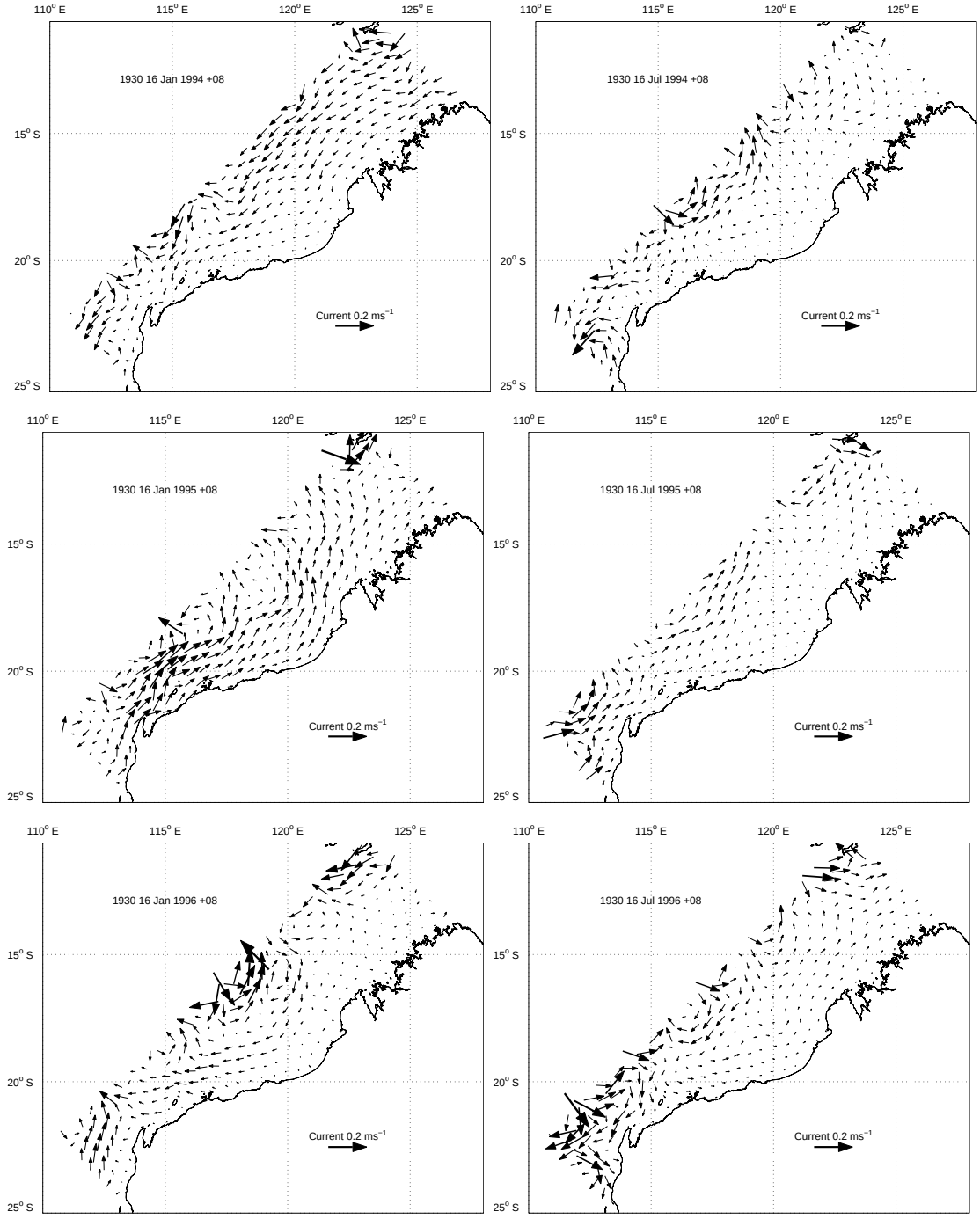

Figure 5.3.1: Current anomaly relative to the mean (figure 5.2.1) in the top model cell (1.5 m) for the years 1994, 1995, and 1996 for the months of January (left) and July (right).

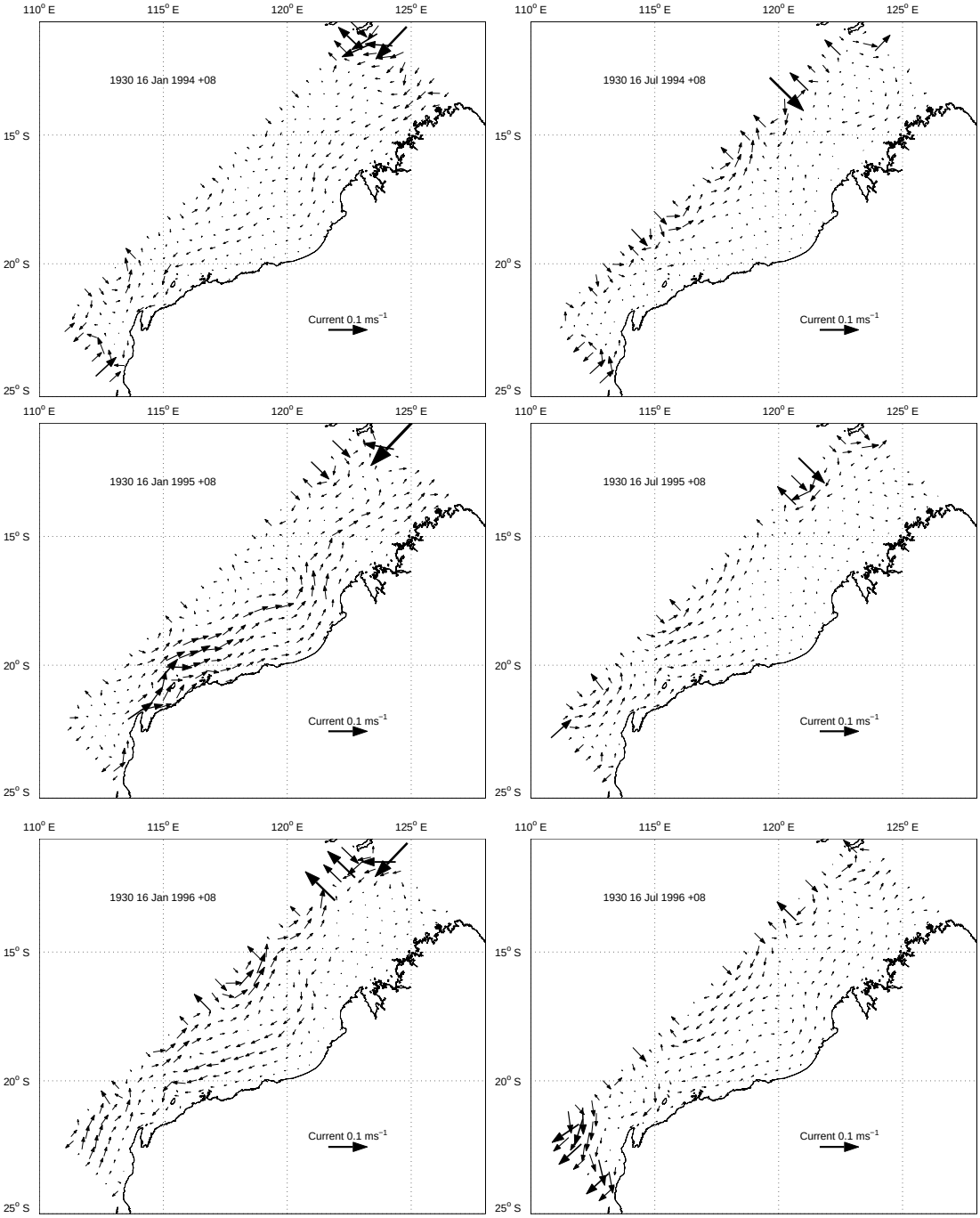

Figure 5.3.2: Depth averaged current anomaly relative to the mean (figure 5.2.2) for the years 1994, 1995, and 1996 for the months of January (left) and July (right).

5.4 Tropical cyclones

Tropical cyclones are a relatively common event over summer on the NWS, with an average of more than two per year within the study area. However, the NCEP-NCAR winds do not adequately resolve these features, so that they appear only as intense low pressure zones. A detailed case study has therefore been undertaken in which a high resolution cyclone wind field has been embedded within the existing Northwest and Pilbara models. Following previous storm-surge modelling on the NWS (Hearn & Holloway, 1990; Fandry & Steedman, 1994; Phillips & Luettich, 2000), the cyclone winds were simulated using the model of Holland (1980) with the observed track and central pressures. The case study focused on Tropical Cyclone Bobby, which crossed the Pilbara coastline near Onslow in February 1995 after tracking southwestward along the NWS.

The low pressure associated with the centre of the cyclone generated a local high in sea level. However, in the case of Tropical Cyclone Bobby, tides were close to neap conditions and the associated modelled storm surges were only comparable in amplitude to the spring tide (figures 5.4.1 and 5.4.2). A cyclonic (clockwise) circulation developed in surface waters over the outer shelf, with corresponding uplift in the thermocline below the cyclone (figure 5.4.1). As the cyclone moved onto the inner shelf, intense currents developed in water trapped against the coast with enhanced mixing to depths of at least 80 m (figure 5.4.2). The most energetic ocean currents occurred on the eastern side of the cyclone, where the presence of the cyclone impeded the southwestward propagation of coastally trapped waves.

Bottom currents also intensified in response to the cyclonic forcing, particularly where mixing extended to the bottom eliminating any thermocline capable of supporting vertical shear in the currents (figures 5.4.2 and 5.4.3). This resulted in high bottom stresses over regions such as the outer shelf (>3 N m^{-2}, figure 5.4.3), where peak stresses were normally quite low (<1 N m^{-2}, figure 5.1.8). While there was also significant enhancement in shallow water bottom stresses, these regions were routinely exposed to quite high values during spring tides, so that the implications for the disturbance of sediments and benthic communities may not be as significant. These issues are considered in more detail in accompanying reports (Margvelashvili et al. 2006; Fulton et al. 2006a).

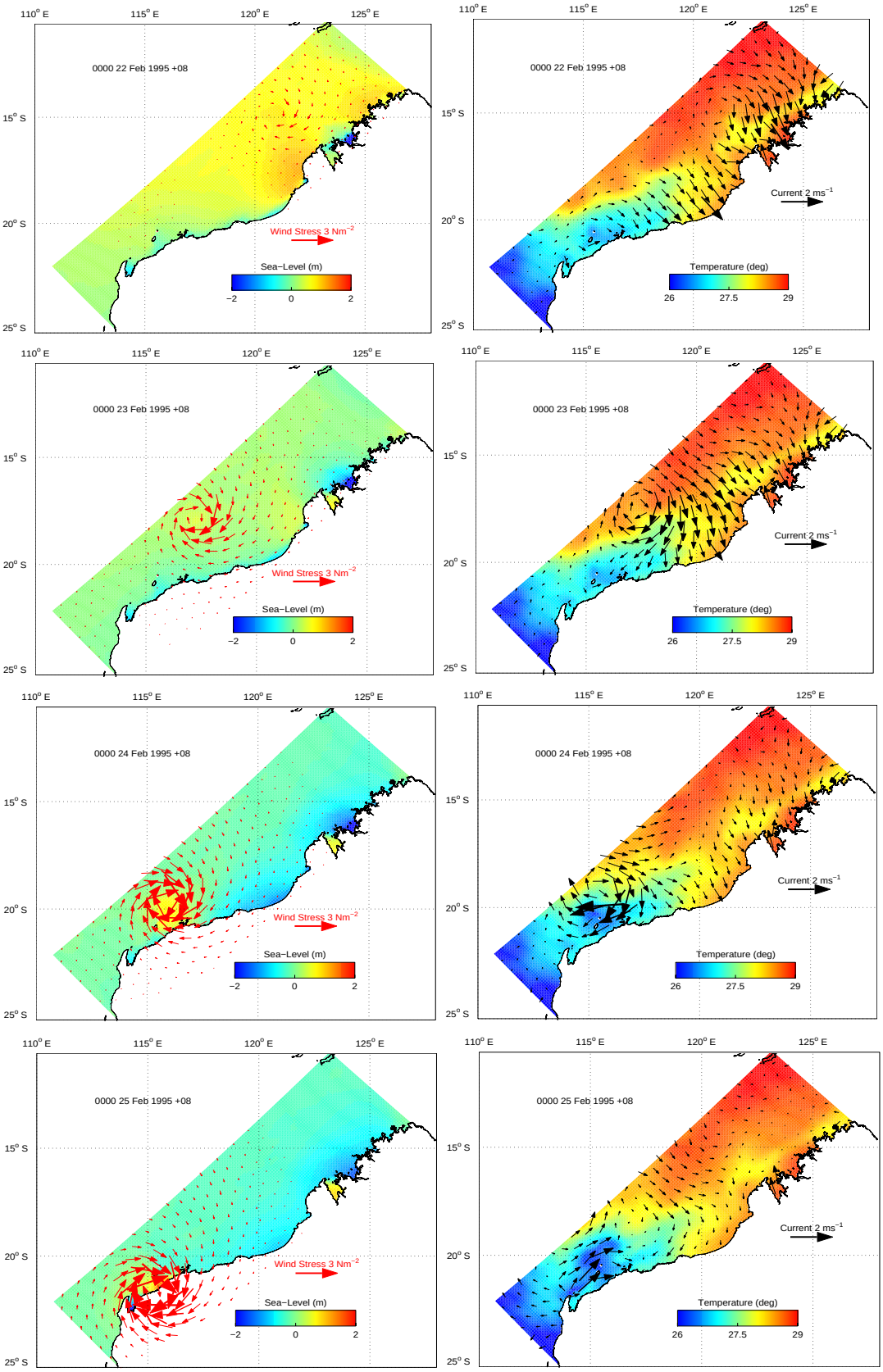

Figure 5.4.1: Wind stress vectors overlain on sea level (left) and current vectors overlain on temperature (at a depth of 1.5 m) (right), both from the Northwest model during Tropical Cyclone Bobby.

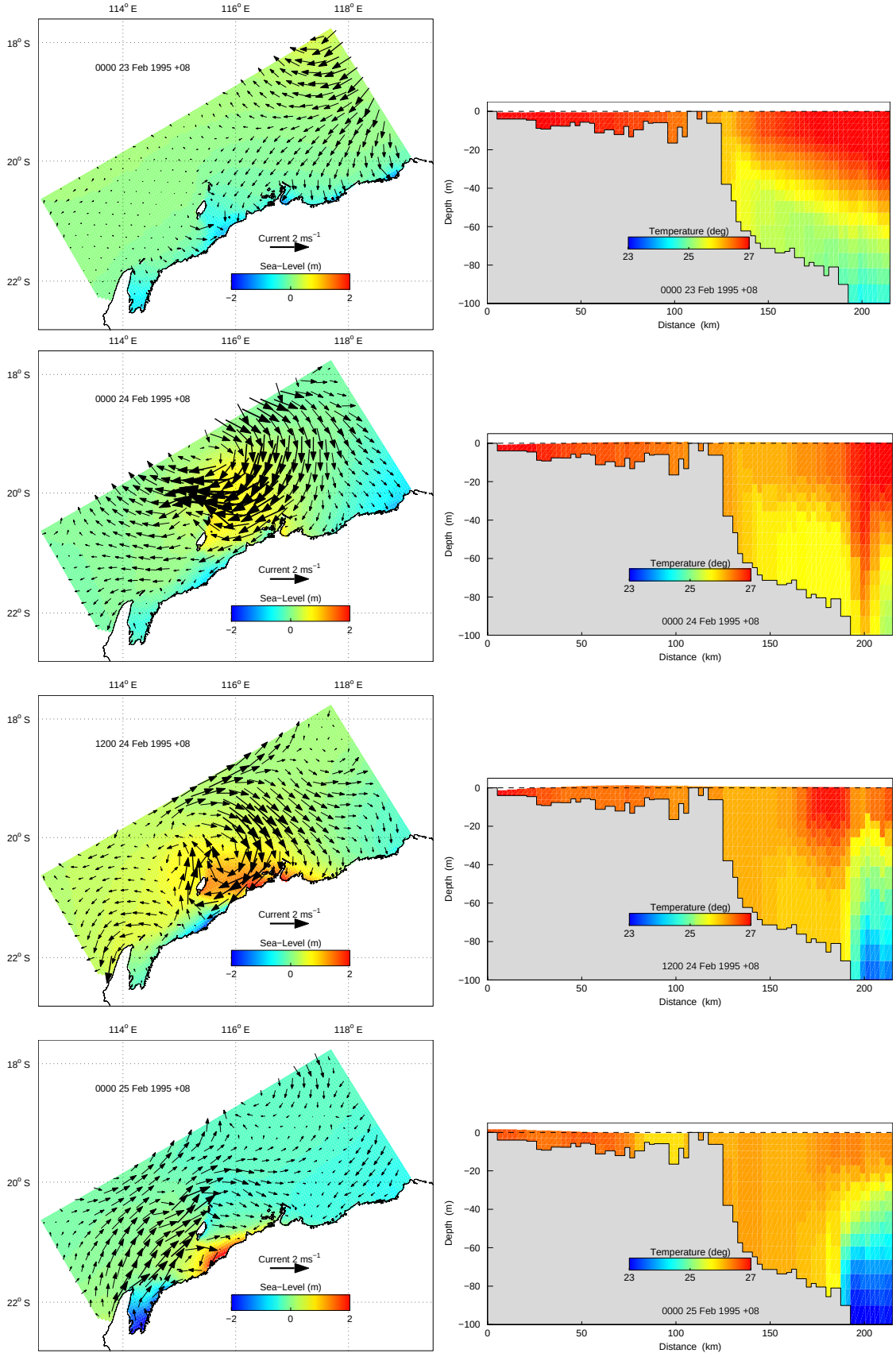

Figure 5.4.2: Current vectors (at a depth of 1.5 m) overlain on sea level from the Pilbara model during Tropical Cyclone Bobby (left). Corresponding vertical sections of temperature following the 115.5°E line from the coast to 19.5°S via the Monte Bello Islands (right).

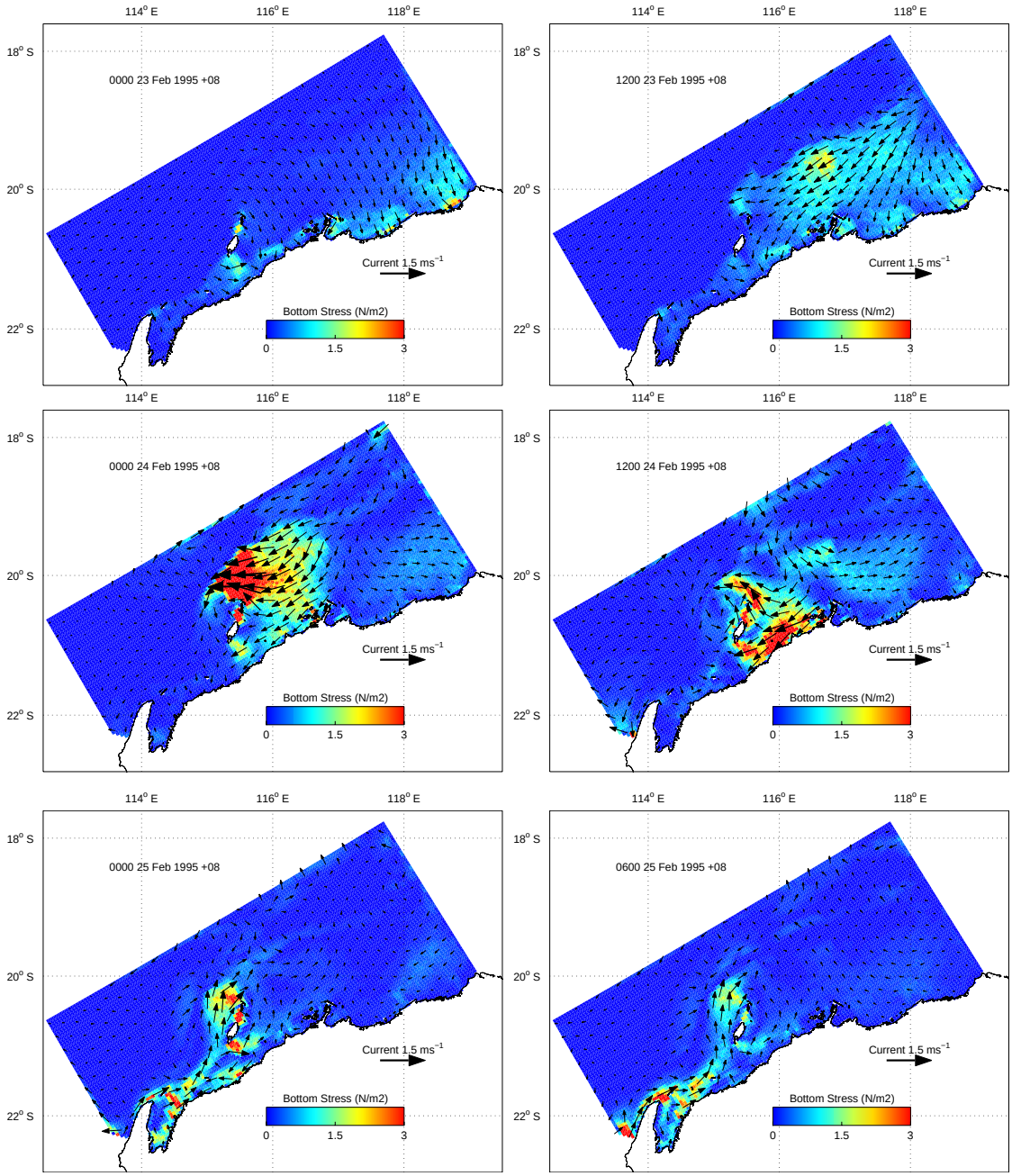

Figure 5.4.3: Current vectors in the deepest model cell overlain on bottom stress from the Pilbara model during Tropical Cyclone Bobby.

6. CHARACTERISING CONNECTIVITY PATTERNS

The modelled currents provide an indication of the instantaneous movements of dissolved or particulate material in the water column. However, additional information is required to estimate advection and dispersion patterns. Individual-based particle tracking techniques were adopted for this purpose. A comprehensive statistical summary of the results are available through a web-based interrogation tool developed as part of the project. This section provides a brief description of the methodology and some example applications.

6.1 Particle tracking

A large number (~10^5) of neutrally buoyant particles were seeded randomly through the water column across the Northwest model domain. The circulation and particle movement calculations were then conducted simultaneously, with particle positions being updated every 10 minutes by the interpolated model current velocities. A random walk component was also added to the trajectory to represent the dispersive influence of turbulent motions not resolved by the circulation model. Each particle was individually tracked and its location recorded every three hours. The model domain was re-seeded with particles every three months to counter losses through the outer edges of the domain.

Particles followed complex paths, which were sensitive to their initial location (figure 6.1.1). This suggested the need for a statistical description of the dispersion results based on large numbers of particle trajectories.

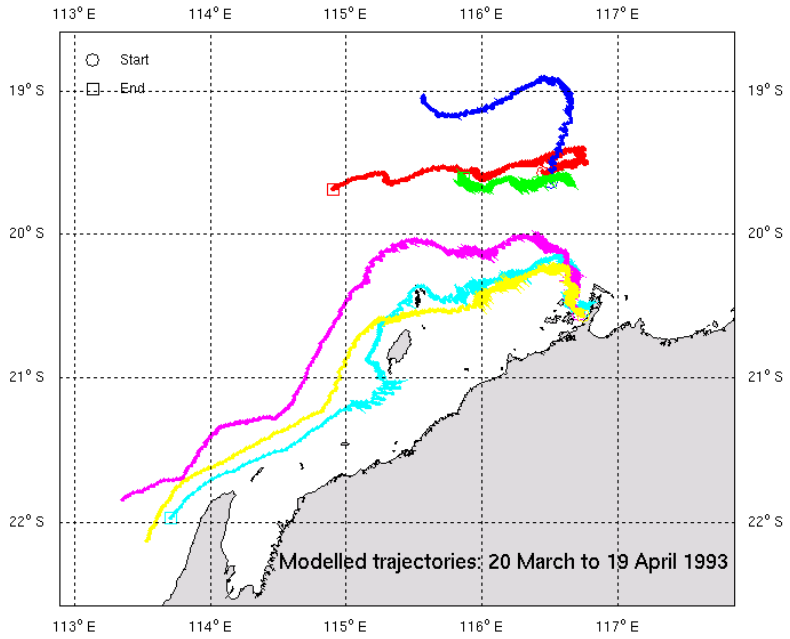

Figure 6.1.1: Sample model trajectories for three particles released on the western side of the Dampier archipelago and three more over the mid shelf. All trajectories start at midday on March 20 and end at midday on April 19. Tidal excursions are most clearly evident around spring tide.

6.2 Connectivity statistics

A statistical description was developed on the basis of all particle trajectories. The probability of any two regions within the model domain being connected by the modelled circulation was computed for a range of dispersion times on a 0.1 degree geographical grid. The following statistics were calculated for each grid cell:

- The probability that particles beginning within any specified region will be inside the grid cell at the end of the dispersion period (i.e. lifetime);
- The probability that particles beginning within any specified region will be inside the grid cell anytime before the end of the dispersion period;
- The probability that particles arriving within any specified region were inside the grid cell exactly one dispersion period previously; and
- The probability that particles arriving within any specified region were inside the grid cell anytime within the previous dispersion period.

All statistics were monthly compilations for a specified dispersion period, T. Probabilities were calculated from day 1 of the calendar month to day T, then from day 2 to day T+1, until reaching the last day of the month. The probabilities were then averaged to give a probability distribution representative of that month. Longer period dispersion probabilities (≥28 days) were similarly computed over three month quarterly periods.

Statistics were computed for each of the months (and quarters) for which the model was run (1994 to 1999). The selected dispersion times were 7, 14, and 21 days for monthly, and 28, 56, and 84 days for quarterly. These results have been further aggregated across years to provide seasonal probability distributions (i.e. averaged across all Januarys, all Februarys, etc).

6.3 A web-based interrogation tool: ConnIe

The Connectivity Interface or *ConnIe* is a web-based tool for interrogating the connectivity statistics described above and providing a graphical representation of spatial connectivity on the NWS. Outputs are in the form of estimates of the probability that any two user-specified regions are connected by modelled ocean circulation over selected dispersion periods. *ConnIe* can be most effectively explored by visiting the website: http://www.per.marine.csiro.au/connie

To operate *ConnIe* the user must select:

1. A region of interest on the map of the NWS (resolution = 0.1°).
2. Whether the selected region represents a source region from which particles disperse (probability of going to other areas) or a sink region into which particles arrive (probability of coming from other areas).
3. The year(s) and month(s) on which the connectivity statistics will be based.
4. The dispersion period (7, 14, or 21 days for monthly or 28, 56, or 84 for quarterly).

5. Whether the connectivity probabilities are based only on the particle distribution at the end of the dispersion period (*after lifetime*), or on all the particle distributions that occur within the dispersion period (*within lifetime*).

Outputs are in the form of maps of the NWS showing the probability distribution for the user specified source or sink (resolution = 0.1°).

6.4 Comparisons with drifter observations

The most direct validation of connectivity statistics might be expected through comparisons with satellite tracked drifters. Unfortunately, relatively few drifters have passed over the North West Shelf and none during the modelling period (1994 to 1999). The comparisons presented here were therefore limited to historical drifter tracks and seasonal probability distributions (i.e. averaged across all Januarys, all Februarys, etc). This may help to identify systematic errors, as well as providing a measure of how representative the seasonal statistics are of years outside the modelling period.

The comparisons used the first observed drifter position as the source cell and checked whether each subsequent position (3 day intervals) was inside the predicted connectivity envelope (probability > 0) or outside the envelope (probability = 0). In total, 72% of the observations fell within the envelope (figure 6.4.1), with monthly values varying between 50% (May) and 86% (Dec). The tracks of individual drifters (which can be viewed on the web interface) often showed larger cross shore excursions than those generated by the model.

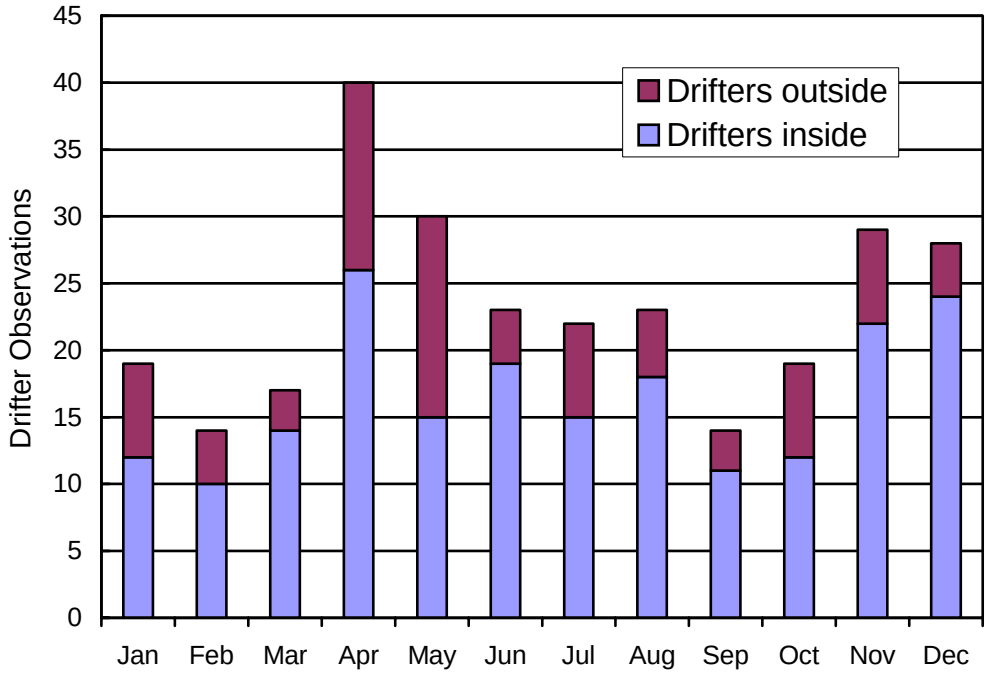

Figure 6.4.1: Number of drifter observations falling inside and outside of the predicted seasonal envelope.

There may be a number of factors contributing to drifters moving outside of the predicted envelopes, such as the mismatch between the observational and modelling periods, and the potential for drifters (with surface floats and drogues at around 10 m) to be directly influenced by offshore winds. However, most of the discrepancies occurred over the outer shelf or slope close to the lateral boundaries of the model, where significant errors in low frequency currents have already been documented (section 4.4; figure 4.4.1).

6.5 Examples

The depletion of coral communities through bleaching and other pressures has generated renewed interest in the potential for cross seeding between reef systems. While fine scale flow features and larval behaviour are likely to be critical to the level of retention around individual reefs, the connectivity modelling described here is particularly relevant to the longer term transport between reefs.

Mass coral spawnings on the NWS usually occurs after the full moon in late March or April (Simpson, 1991; Simpson et al. 1993). The spawn initially forms surface slicks, but any longer term transport occurs lower in the water column. The potential for cross seeding can be broadly represented by connectivity probability distributions averaged across all years (1994 to 1999) for April (7, 14, 21 days) and the April to June quarter (28, 56, 84 days). The viable lifetime of coral larvae in this region is not well known, although it is likely to be near the shorter end of this range of time scales.

Results from *ConnIe* (figure 6.5.1) suggest that exchanges from the Monte Bello and Barrow Island reefs to Ningaloo Reef may be relatively common, and that exchange from the Dampier Archipelago reefs to Monte Bello and Barrow may also be significant. Exchanges between the remote offshore reefs of Ashmore, Scott, and the Rowley Shoals is likely to be infrequent, although possibly sufficient to maintain genetic linkages. All exchange rates are likely to be characterised by significant interannual variability and transport of viable larvae from the offshore reefs of the Kimberly to the more coastal reefs of the Pilbara would appear to require oceanic conditions outside of those captured within the modelling period.

As a second example of the application of *ConnIe*, we consider the potential for suspended material (e.g. contaminants) to enter the conservation reserves proposed for the Dampier Archipelago/Cape Preston region and the Monte Bello/Barrow/Lowendal Islands (indicated by the hatched regions in figure 6.5.2). This has been demonstated using connectivity probability distributions averaged across all years (1994 to 1999) for January and July (21 days). During January material is most likely to enter from offshore or the southwest (figure 6.5.2), reflecting predominantly westerly and southwesterly winds. During July, winds are directed offshore, the envelope is smaller, and material is most likely to enter the reserves from the east or northeast. While only marginally resolved, there appears to be significant exchange between the Dampier Archipelago/Cape Preston reserve and the central area of Nickol Bay falling outside of the proposed reserve.

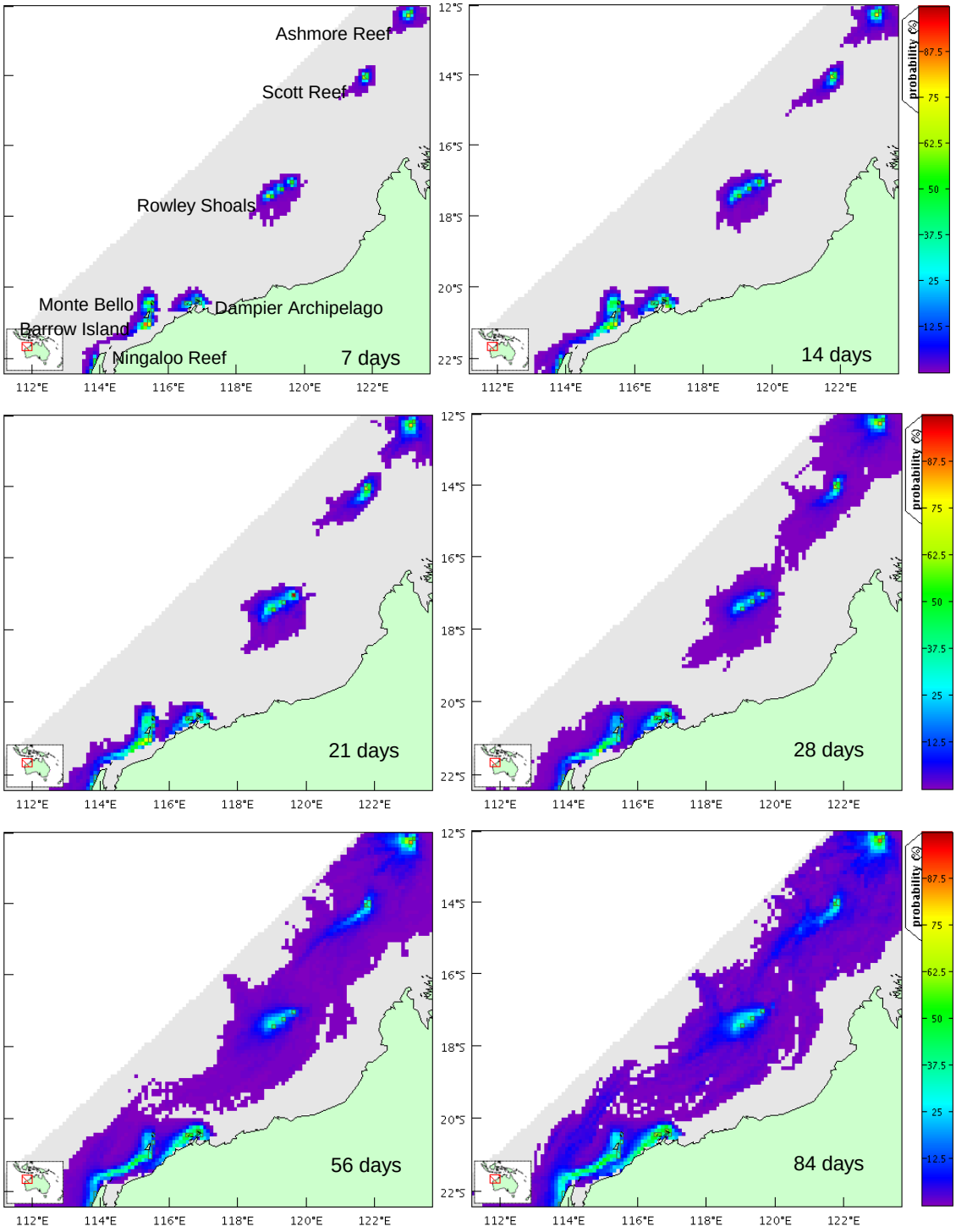

Figure 6.5.1: Connectivity probability distributions (within lifetime) from sources corresponding to coral reefs on the NWS for April (7, 14, and 21 days) and April to June (28, 56, and 84 days).

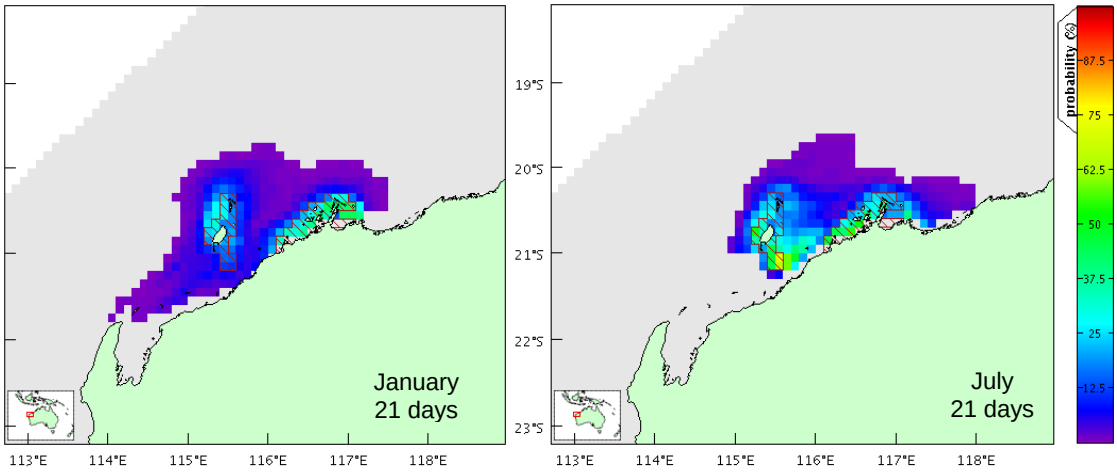

Figure 6.5.2: Connectivity probability distributions (within lifetime) to sinks corresponding to proposed protected areas (hatched) on the NWS for January and July.

7. CONCLUSION

A series of nested circulation models have been developed for the NWS to investigate aspects of the circulation at a range of scales covering aspects of regional climatic forcing and circulation, shelf scale processes, and local coastal process. This represents the first attempt to model this system using realistic forcing by winds, tides, and the large-scale regional circulation.

Simulations covering periods of more than six years have allowed the tidal, seasonal, and interannual characteristics to be investigated, as well as the response to episodic events such as tropical cyclones. Instantaneous current patterns were strongly dominated by the barotropic tide and its spring neap cycle. However, longer-term transports over the inner and mid shelf were mainly controlled by wind-driven flow, which followed the seasonal switch from summer monsoon winds to southeasterly trades in winter. Over the outer shelf and slope the large-scale regional circulation, provided by the global model, had a major influence.

Model results were shown to be relatively insensitive to adjustable model parameters and sub-model structures. However, model performance was strongly dependent on the quality of the forcing fields. For example, the prediction of low frequency inner shelf currents was improved substantially when the relatively coarse resolution NCEP-NCAR winds where replaced by locally observed winds in the Dampier model. Much lower skill in predicting low frequency currents on the outer shelf can be largely attributed to forcing from the global model. While the temperature and salinity forcing provided by ACOM was realistic, there was clearly a large component of observed mesoscale variability absent from the model. This may be improved by better resolution of eddies in the global model. However, accurate representation of local currents would also require assimilation of observed data to ensure that the location of eddies and other transient mesoscale features were reproduced.

Connectivity patterns on the NWS have been characterised by coupling a particle transport model to the Northwest model and providing access to the statistical outputs through a web-based user interface developed as part of the project (http://www.per.marine.csiro.au/connie). Skill in predicting connectivity patterns appeared to diminish towards the outer shelf, reflecting the errors documented in the low frequency currents. However, taking into account such uncertainties, *ConnIe* might be expected to find applications in areas such as larval dispersion and recruitment studies, and the development of scenarios and risk assessments for contaminant dispersion.

As part of NWSJEMS, the Pilbara model has been coupled to a sediment transport model to examine resuspension, transport, and deposition processes on the NWS (Margvelashvili et al. 2006). For this purpose, bottom stress distribution (including wave enhancement) and low frequency current patterns were particularly critical. The Pilbara model has also been coupled to a biogeochemical model and investigations made of the processes controlling nutrient cycling and primary and secondary production on the NWS (Herzfeld et al. 2004). Factors such as transports and mixed layer depths were particularly important in this context. Finally, current fields from all three models have been used in the management strategy evaluation models developed for the NWS (Condie et al. 2003; Fulton et al. 2006b), where they determined the transport of suspended material such as chemical contaminants and fish larvae.

REFERENCES

Batteen, M.L., M. J. Rutherford and E. J. Bayler (1992) A numerical study of wind- and thermal-forcing effects on the ocean circulation off Western Australia. J. Phys. Oceanogr., 22, 1406-1433.

Brainerd, K.E. and M.C. Gregg (1995) Surface mixed and mixing layer depths. Deep Sea Res. Part I, 42, 1521-1543.

Bruce, B. D., S. A. Condie, and C. A. Sutton (2001) Larval distribution of blue grenadier (Macruronus novaezelandiae Hector) in south-eastern Australia: further evidence for a second spawning area. Mar. Freshwat. Res. 52: 603-610.

Buchan, S. J. and S. A. Stroud (1993) Review of oceanography of North West Shelf and Timor Sea regions pertaining to the environmental impact of the offshore oil and gas industry. Steedman Science and Engineering Report No. R644, Perth.

Cleveland, W.S. and S. J. Devlin (1988) Locally weighted regression: An approach to regression analysis by local fitting. J. Amer. Stat. Assoc., 83, 596-610.

Condie, S. A., N. R. Loneragan and D. J. Die (1999) Modelling the recruitment of tiger prawns (Penaeus esculentus and P. semisulcatus) to nursery grounds in the Gulf of Carpentaria, northern Australia: implications for assessing stock-recruitment relationships. Mar. Ecol. Prog. Ser., 178, 55-68.

Condie, S. A. and J. Andrewartha (2002) North West Shelf Joint Environmental Management Study: Milestone Report No. 2.2: Wave Modelling. CSIRO Marine Research Report.

Condie, S., C. Fandry, D. McDonald, J. Parslow, and K. Sainsbury (2003) Linking ocean models to coastal management on Australia's North West Shelf. Eos, Transactions, American Geophysical Union, 84, 49, 53.

Craig, P. D. (1988) A numerical model study of internal tides on the Australian North West Shelf. J. Mar. Res., 46, 59-76.

Cresswell, G.R., Frische, A., Peterson, J., and Quadfasel, D. (1993) Circulation in the Timor Sea. J. Geophys. Res. 98, 14379-14389.

Dunn, J. R. and K. R. Ridgway (2002) Mapping ocean properties in regions of complex topography. Deep-Sea Res. I, 49, 591-604.

Eanes, R. and S. Bettadpur (1995) The CSR 3.0 global ocean tide model. *Center for Space Research, Technical Memorandum, CST-TM-95-06.*

Fandry, C. B. and R. K. Steedman (1994) Modelling the dynamics of the transient, barotropic response of continental shelf waters to tropical cyclones. Cont. Shelf Res., 14, 1723-1750.

Fulton, E., Hatfield, B., Althaus, F., and Sainsbury, K. (2006a). Benthic habitat dynamics and models on Australia's North West Shelf. NWSJEMS Technical Report No. 11.

Fulton, E., McDonald, D., Hayes, D., Lyne, V., Little, R., Fuller, M., Condie, S., Gray, R., Scott, R., Webb, H., Hatfield, B., Martin, M. and Sainsbury, K., (2006b). Management Strategy Evaluation specification for Australia's North West Shelf. NWSJEMS Technical Report No. 15.

Godfrey, J.S. and Ridgway, K.R. (1985) The large-scale environment of the poleward-flowing Leeuwin Current, Western Australia: Longshore steric height gradients, wind stresses and geostrophic flow. J. Phys. Oceanogr. 15, 481-495.

Grant, W. D. and O. S. Madsen (1979) Combined wave and current interaction with a rough bottom. J. Geophys. Res., 84, 1797-1808.

Hearn, C.J. and P.E. Holloway (1990) A three-dimensional barotropic model of the response of the Australian North West Shelf to tropical cyclones. J. Phys. Oceanogr., 20, 60-80.

Herzfeld, M., J. Waring, J. Parslow, N. Margvelashvili, P. Sakov and J. Andrewartha (2002) MECO, Model of Estuarine and Coastal Oceans, V4.0, Scientific Manual, CSIRO Marine Research.

Herzfeld, M., J. Parslow, P. Sakov and J. Andrewartha (2006) Biogeochemical Modelling on Australia's North West Shelf. NWSJEMS Technical Report No. 8

Holland, G.J. (1980) An analytic model of the wind and pressure profiles in Hurricanes. Mon. Weather. Rev., 108, 1212-1218.

Holloway, P.E. (1983) Tides on the Australian North-West Shelf. Aust. J. Mar. Freshwat. Res., 34, 213-230.

Holloway, P.E. (1984) On the semidiurnal internal tide at a shelf break region on the Australian North West Shelf. J. Phys. Oceanogr., 14, 1787-1799.

Holloway, P.E. (1985) A comparison of semidiurnal internal tides from different bathymetric locations on the Australian North West shelf. J. Phys. Oceanogr., 15, 240-251.

Holloway, P.E., S.E. Humphries, M. Atkinson, and J. Imberger (1985) Mechanisms for nitrogen supply to the Australian North West Shelf. Aust. J. Mar. Freshwat. Res., 36, 753-764.

Holloway, P. E. and H.C. Nye (1985) Leeuwin Current and wind distributions on the southern part of the Australian North West Shelf between January 1982 and July 1983. Aust. J. Mar. Freshwat. Res., 36, 123-137.

Holloway, P.E. (1987) Internal hydraulic jumps and solitons at a shelf break region on the Australian North West Shelf. J. Geophys. Res., 92, 5405-5416.

Holloway, P.E. (1995) Leeuwin Current observations on the Australian North West Shelf, May-June 1993. Deep Sea Res., 42, 285-305.

Holloway, P.E. (2001) A regional model of the semidiurnal internal tide on the Australian North West Shelf. J. Geophys. Res., 106, 19625-19638.

Kalnay, E., M. Kanamitsu, R. Kistler, W. Collins, D. Deaven, L. Gandin, M. Iredell, S. Saha, G. White, J. Woollen, Y. Zhu, M. Chelliah, W. Ebisuzaki, W. Higgins, J. Janowiak, K.C. Mo, C. Ropelewski, J. Wang, A. Leetmaa, R. Reynolds, R. Jenne and

D. Joseph (1996) The NCEP/NCAR 40-year reanalysis project. Bull. Amer. Meteor. Soc., 77, 437-471.

Lough, J.M. (1998) Coastal climate of northwest Australia and comparisons with the Great Barrier Reef: 1960 to 1992. Coral Reefs, 17, 351-367.

Margvelashvili, N., J. Andrewartha, S. Condie, M. Herzfeld, J. Parslow, P. Sakov and J. Waring (2006). Modelling Suspended Sediment Transport on Australia's North West Shelf. NWSJEMS Technical Report No. 7.

Meyers, G., R.J. Bailey and A.P. Worby (1995) Geostrophic transport of Indonesian throughflow. Deep Sea Res. Part I, 42, 1163-1174.

Meyers, G. (1996) Variation of Indonesian throughflow and the El Nino - Southern Oscillation. J. Geophys. Res., 101, 12255-12263.

Mills, D.A (1985) A Numerical Hydrodynamic Model Applied to Tidal Dynamics in the Dampier Archipelago. Report 190, Department of Conservation and Environment, 30pp.

Mills, D.A, D.R. Pitt and C.J. Simpson (1986) Summary of Current Meter Data from the Dampier Archipelago 1981-1984. Environmental Note 178, Department of Conservation and Environment.

Phillips, R.L. and R.A. Luettich (2000) Simulation of tide and storm surge in the Dampier Archipelago using a finite element hydrodynamic model. WNI Science and Engineering Report.

Schiller, A., J.S. Godfrey, P.C. McIntosh, G. Meyers, and R. Fiedler (2000) Interannual dynamics and thermodynamics of the Indo-Pacific Oceans. J. Phys. Oceanogr., 30, 987-1012.

Simpson, C.J. (1991) Mass spawning of corals on Western Australian reefs and comparisons with the Great Barrier Reef. J. Roy. Soc. West. Aust., 74, 85-91.

Simpson, C.J., J.L. Cary and R.J. Masini (1993) Destruction of corals and other reef animals by coral spawn slicks on Ningaloo Reef, Western Australia. Coral Reefs, 12, 185-191.

Tranter, D.J. and G.S. Leech (1987) Factors influencing the standard crop of phytoplankton on the Australian North West Shelf seaward of the 40m isobath. Cont. Shelf Res. 7, 115-133.

U.S. Army Coastal Engineering Research Center (1973) Shore Protection Manual. U.S. Government Printing Office.

U.S. Army Coastal Engineering Research Center (1984) Shore Protection Manual. U.S. Government Printing Office.

Walker, S.J. (1999) Coupled hydrodynamic and transport models of Port Phillip Bay, a semi-enclosed bay in south-eastern Australia. Mar. Freshwat. Res. 50: 469-481.

Webster, I. (1985) Wind-driven circulation on the North West Shelf of Australia. J. Phys. Oceanogr. 15, 1357-1368.

ACKNOWLEDGEMENTS

The following people and agencies have contributed significantly to the Study through the provision of technical expertise and advice, and historical data and information. The Study partners gratefully acknowledge their contribution.

Western Australian State agencies
Department of Environment and Conservation (Department of Conservation and Land Management and Department of Environment)
Department of Fisheries
Department of Industry and Resources (Department of Mineral and Petroleum Resources)
Department of Land Information
Department for Planning and Infrastructure (Department of Transport)
Pilbara Tourism Association
Shire of Roebourne
Town of Port Hedland
Tourism Western Australia
Western Australian Land Information System
Western Australian Museum

Commonwealth agencies
Australian Institute of Marine Science
Geoscience Australia (formerly Australian Geological Survey Organisation)

Consultants
Cognito Consulting
David Gordon International Risk Consultants
METOCEAN Engineers (formerly Weather News International, Perth)
Oceanica (formerly DA Lord and Associates)

Industries
Australian Petroleum Production Exploration Association (APPEA)
Apache Energy
BHP Petroleum
Chevron Australia
Dampier Salt
Hamersley Iron
Mermaid Marine
Woodside Energy

Individuals
Clay Bryce
Graham Cobby
Nick D'Adamo
Mike Forde
David Gordon
Andrew Heyward
Barry Hutchins
Bryan Jenkins

Di Jones
Ian LeProvost
Ray Masini
Mike Moran
Steve Newman
Eric Paling
Kelly Pendoley
Bob Prinz
Chris Simpson
Shirley Slack-Smith
Di Walker

Editorial and publishing
Louise Bell – Graphics/cover design
Lea Crosswell – Webpage design
Rob McKenzie – Editor
Diana Reale – Webpage design
Linda Thomas – Editorial consultant/layout and design
Helen Webb – Editorial consultant/Project Manager

Front cover photos courtesy of:
Centre – Coral reef ecosystem, WA Museum, Clay Bryce
Aquaculture pearls, Department of Fisheries WA
Recreational fishing, Department of Fisheries WA, Jirri Lockman
Offshore petroleum platform, Woodside Energy Ltd
Commercial Fishing, Department of Fisheries WA
Tourism, CSIRO
Coastal development aerial photos, Hamersley Iron Pty Ltd